FINAL REPORT

Flood Risk Modelling for the North and Central Malawi

This report was produced with financial support from the European Union, in the framework of the ACP-EU Africa Disaster Risk Financing Program, managed by the Global Facility for Disaster Reduction and Recovery. The sole responsibility of this publication lies with the author(s). The European Union is not responsible for any use that may be made of the information contained therein.

1 Table of Contents

2 Background

This activity was financed under the framework of the Africa Disaster Risk Financing (ADRF) initiative, which is part of the overall European Union (EU) – Africa, Caribbean, Pacific (ACP) cooperation program "*Building Disaster Resilience in Sub-Saharan Africa*" managed by several partners, including the African Union Commission (AUC), the African Development Bank (AfDB), the United Nations International Strategy for Disaster Risk Reduction (UNISDR) and the Global Facility for Disaster Reduction and Recovery (GFDRR) with the World Bank (WB)..

In recent years, the EU has put a strong effort in improving the understanding of risks related to natural hazards in Africa. This effort has been catalysed by the increasing risks that the region is facing, materializing through several natural hazards. These natural risks are hampering the development of many African countries that see GDP and investments impaired by the impact of such natural hazards. Specifically, in January 2015 and continuing through February, southern Malawi was hit by severe floods caused by a large low-pressure system that continued to generate heavy rains over the area. The Shire River south of Lake Malawi and tributaries flooded large parts of the country in several flood waves. More than 170 people lost their lives, thousands were displaced and crops were lost.

The objective of the activity financed under the framework of the Africa Disaster Risk Financing (ADRF) initiative is to produce flood hazard maps that form the basis for a preliminary risk assessment. This assessment ultimately produces risk figures that can be primarily used to increase scientifically-supported awareness of flood risk at the national and sub-national levels. This can help to protect people and properties of Malawi against future floods. Risk financing could play a key role in protecting the financial investments and can lead

the way to a future where such risk is understood, reduced and controlled. The first step along this path is to understand the underlying risk that Malawi faces.

While assessing the post-disaster needs and trying to recover from the floods it was found that the existing flood hazard map for Malawi was not adequate. This map is based on the SRTM90m and covers only part of the country. GFDRR, on behalf of the Government of Malawi, has therefore put forward a request to compute improved flood hazard maps covering the Northern part of Malawi on a higher resolution.

The flood hazard maps have been produced by a consortium of three partners from EU-funded FP7 project for Rapid Analysis and Spatialisation of Risk (RASOR)[1], which is building a platform for worldwide rapid risk analysis. RASOR offers a single work environment that generates new risk information across hazards, data types (satellite EO, in-situ), user communities (global, local, climate, civil protection, insurance, etc.) and across the world. RASOR uses the 12m TanDEM-X Digital Elevation Model as a base layer, and then adds archived and near-real time very-high resolution optical and radar satellite data, combined with in-situ data. A scenario-driven query system allows users to model multi-hazard risk both before and during an event.

The RASOR partners, CIMA and Deltares, have extensive experience both on the global level and local level in flood risk assessment. . In particular, CIMA developed a global probabilistic flood risk assessment that used cutting edge hazard modelling that can be used as an asset for this assignment in order to provide benchmark results (Rudari et al., 2015) in present climate. Deltares has developed the "Global Flood Risk with IMAGE Scenarios" river flood risk framework (GLOFRIS) (Winsemius et al., 2013; Ward et al., 2013) that has been employed successfully in previous GFDRR projects (Ward et al., 2014) similar to the current Flood Risk

[1] http://www.rasor-project.eu/

Modelling project in Malawi and has been used as the main building block for developing the required data.

In order to achieve these results, global open data, such as globally available forcing data, and exposure datasets, if possible complemented by open local data sets, have been used so that the obtained results can be shared publicly after the project has been completed. Concerning GDP data, GFDRR provided the most appropriate and updated dataset, while for the other assets, including critical infrastructure have been taken from available exposure datasets.

3 Objectives

In this section, we list the objectives of this project (taken from the ToR) and provide our interpretation of what is required by GFDRR. Unless otherwise mentioned, all work described refers to phase 1 of the project, conducted from July 2015 to July 2016.

With respect to hazard assessment:

- Provide pluvial and fluvial flood hazard maps for the Northern part of Malawi with focus on hotspots concentrated on the shoreline of Lake Malawi at a resolution of 15m or less, for a set of predefined recurrence periods;
- Provide modeled pluvial and fluvial flood maps for the Northern part of Malawi with focus on hotspots concentrated on the shoreline of Lake Malawi related to at least 3 historical events
- Provide modeled pluvial and fluvial flood maps for the Northern part of Malawi with focus on hotspots concentrated on the shoreline of Lake Malawi related to at least 3 stochastic events

With respect to risk assessment:

Provide pluvial and fluvial flood loss metrics for Northern Malawi and the Hotspots in tabular format as they are listed in the ToR including the Loss Exceedance Curve both for the Northern Malawi and the identified Hotspots.

a. Tabulated record of historic disaster events, with associated losses
b. Year Loss Table (YLT), this solution is preferred to the event loss table
c. National-level loss exceedance curve and tabulated return period losses

d. Tabulated Annual Average Loss (AAL) at the national level and at the level of first administration boundaries

e. Tabulated vulnerability functions showing the mapping of hazard parameter to impact

f. In addition to the required deliverables other useful indicators have been delivered (e.g. affected population, number of critical infrastructures)

In addition to the tabulated deliverables, hazard footprints and loss footprints a well as the exposure data used for the loss calculations have been provided in GIS-compatible spatial datasets, standard data formats have been used to ensure sharing and usability. Such maps have been put in the local RASOR Geonode and are ready to be transfer into a local Geonode installation (e.g. the masdap.org installation) for the benefit of the End Users and stakeholders.

Our approach follows the exact order as provided in the ToR. First we establish YLTs for each risk indicator proposed. The YLT consists of a 40-year reanalysis period (1960-1999). The national-level loss exceedance curve and tabulated return period losses have been based upon the YLT, through an extreme value analysis. By performing the extreme value analysis upon the losses per year over a given area, the limits in spatial correlation between extreme events is implicitly taken into account (described further in detail below). Furthermore, the AAL tables at national and sub-national scale have been established by integration of the return period losses. Finally, the above mentioned layers of information have been put into GIS-compatible spatial datasets to ensure a smooth use by the client. Hazard layers have been delivered as gridded data so that further analysis may be performed with them in future projects.

4 Scope of work

Our interpretation of the required end products is as follows:

Hazard Computations: the hazard computation analyzing pluvial and fluvial flood hazard separately and in a combined manner have been simulated on a 12.5 m grid resolution using the post processed Tandem-X DTM.

Type of risk estimates: In line with a scenario-based approach we produced a Year Loss Table reporting the loss in each simulated year. By applying Extreme Value statistics we then computed estimates of annual expected impacts, derived from impact-exceedance curves for a selected number of return periods. We used the return periods selected in the ToR being 2, 5, 10, 25, 50, 100, 250, 500 and 1000 year. From the YLT and its statistical characterization it is then possible to derive the AAL expressed in several indicators. In the same manner metrics other than the ones expressed in economic terms can be derived (e.g., expected number of critical infrastructures damaged).

Scenarios: Historical events have been simulated for the 40 years provided by the EU-Watch reanalysis (www.euwatch.org) and by the 12 year CMORPH series (http://www.cpc.ncep.noaa.gov/products/janowiak/cmorph.html). Design scenarios have also been provided for a range of return periods based on estimated extreme values statistics.

Indicators: the indicators that computed are affected population, physical damage, and impact on GDP (for given return periods and per year).

Level of detail: the World Bank requires risk estimates over Northern Malawi, at the district level. Shape files with the administrative boundaries of each district have been provided by the World Bank. The Analysis have been conducted at two different levels of detail: the full Northern Malawi areas and at higher resolution the Hotspots identified with the Client, as

described in this report. The specific approach for the Northern Malawi and the hotspots will be detailed in the approach Section.

Integration in a visualization system: the Consortium made the RASOR platform available to the Government of Malawi and made products generated through the project available through the platform, allowing for a comprehensive risk assessment approach that allows for flexible simulations and fine tuning as the platform compares modeling outputs to satellite data records, for example

5 Technical Approach

5.1 General approach

The worldwide availability of historical information on catastrophic natural hazard events is very limited, and data on the economic consequences is even less available. Considering the likelihood of highly destructive events in the future, risk assessments of natural hazards need to focus on probabilistic methods that use available information to best predict future scenarios, and consider the spatial and temporal uncertainties involved in the analysis process. Therefore, risk assessments are needed for the present-day conditions, anticipating scientifically credible events that may happen in the future. For a realistic and structured assessment of risk, it is necessary to estimate a) the probability and severity of hazard; b) the exposed people, assets or other elements that are susceptible to the peril; and c) the vulnerability of the exposed units, i.e. their susceptibility to the considered hazard.

In general terms, probabilistic risk assessment is performed by evaluating the loss, expressed as an indicator of impact on a certain group of exposed units due to the occurrence of several hazard conditions with different probabilities of occurrence, which collectively describe the natural hazard, and then integrating the results in risk indices (Melchers 1999).

Based on such approach a schematic of our proposed workflow for this assignment is provided below. The Terms of Reference for this assignment requests to develop a flood hazard modeling framework based on a DEM resolution of at least 15 m and starting from that to develop a probabilistic national-level hazard models for Malawi, comprising the perils: a) fluvial flood; b) pluvial flood.

The following schema describes the proposed approach to the assignment.

Figure 1 Flow diagram of the proposed approach

We propose to use a globally applicable model cascade. The cascade consists of:

- reanalysis or GCM-based weather forcing used as a source for the analysed perils in the study. A 40-year period have been considered for the fluvial flooding simulations (1960-1999). The CMORPH series (2002-now, 3-hourly rainfall) have been used to analyse the relevant recent events and pluvial flooding.
- a number of hydrological, hydraulic models to translate the meteo forcing into hydrological parameters that are at the basis of the hazard footprint computations;
- a number of impact models, combining hazard footprints and socio-economic parameters to assess impacts and integration into risk.

A frequency analysis and extreme value analysis have been applied to the streamflow simulations obtained from hydrologic model so to compute the boundary conditions for the detailed 2D flood models that computed the hazard maps for fluvial flood hazard. For the pluvial flood hazard, a frequency analysis have been done on the rainfall data to calculate the probability of runoff excess as computed by the hydrological model, which can be linked to pluvial or surface water flooding.

The impacts have been computed on a yearly basis computing the sequence of the maximum loss that can be suffered in each year considered. In this way a Year Loss Table (YLT) is compiled aggregating the loss in each year on the identified sub-national spatial units and at the country level. Extreme values statistics on yearly losses are derived from the YLT using Extreme Value theory to estimate the frequency of occurrence of the Loss Indicator considered.

In earlier studies, impacts occurring with different return periods at different locations were assumed to be fully correlated. We recognize that correlation between annual extreme events reduces, as the region over which the analysis is aggregated grows. This needs to be taken into account as we aggregate results to state, and country level. Highly sophisticated methods can be employed to account for all correlations during events, including pre-event conditions, spatial correlations and others. These require a very large amount of synthetic event simulations

across the domain of interest. We feel that this is beyond the scope of this project. Our understanding is that a rapid assessment is required, and therefore we suggest using the state level and country level YLTs to estimate return period losses and Annual Average Losses at the state and country level. In this way the covariance between events at different locations is implicitly included in the return period and annual average losses.

The following table presents an overview of the set of indicators. The return period considered are: 2, 5, 10, 25, 50, 100, 250, 500, 1000 years. The approach for the hazard and impact computation is described in further detail in later sections.

PERIL (all indicators are presented for both Pluvial and Fluvial Flooding as well as for their combination)	TYPE	INDICATOR	UNIT	COMMENT
Flood	HAZARD	Water depth maps (fluvial flood) or flood extent maps (pluvial flood) for different return periods (at 12m and 100 m resolution)	[m]	The product is a raster.
Flood	RISK	Affected population for different return periods	[#]	
Flood	RISK	Annual average affected population	[#/yr]	
Flood	RISK	GDP affected / and as fraction of total GDP for different return periods	[$], [%]	GDP in US equivalent dollars and percentage of the total GDP
Flood	RISK	Annual average GDP affected (absolute and as fraction of total GDP)	[$/yr], [%/yr]	GDP in US equivalent dollars and percentage of the total GDP
Flood	RISK	Exposed physical assets for different return periods	[#]	Number of affected buildings, number of affected critical infrastructure elements
Flood	RISK	Annual average exposed physical assets	[#/yr]	Number of affected buildings, number of affected critical infrastructure elements
Flood	RISK	Direct physical property damage to human settlements	[$]	Damage to buildings based on exposure data provided
Flood	RISK	Annual average loss of human settlements (AAL)	[$/yr]	
Flood	RISK	Damage to agriculture	[$]	Based on value added lost due to flooding
Flood	RISK	Annual average loss of agriculture (AAL)	[$/yr]	

The above-mentioned indicators have been summarized as requested by the ToR in graphic and tabular formats (e.g. PML Curves, Yearly Loss Tables)

The steps suggested in Figure 1 are in principle not unique for natural hazard risk assessments. In fact many if not most probabilistic risk assessments follow such an approach. However, the way in which we follow these steps are unique as follows:

a) We make use of global and open datasets, and global (applicable) models so that the approach can be replicated in other regions and countries. This is important given the fact that the ToR suggests that the approach may be applied on other regions after this study.
b) We make use of open and free SW models so that no license would be needed if the stakeholders decide to repeat computations.
c) EU-WATCH is one of the most comprehensive global scale forcing datasets based upon a fusion of meteorological model outputs and global measurements from both ground and satellite observations.
d) Our consortium has extensive experience in national level probabilistic risk assessment and that have 2 suites of global hydrological/hydraulic models (outputs) available (GAR and GLOFRIS).
e) We realize that the correlation of events in space is important to consider when assessing risk over a large area. We are including the correlation in our risk assessment procedure.
f) The partnership has a unique experience in utilizing the Tandem-X Global DEM at 12 m horizontal resolution and 1m vertical resolution that represents the state of the art in satellite-derived DTM with unmatched accuracy performance. The partnership has secured approval in writing from Airbus Defence and Space to extend the RASOR Phase 1 agreement to Malawi and make the DEM available free of charge to the RASOR team as in other RASOR Case Study areas. The DEM required editing (smoothing, removal of obstacles, removal of noise) to be useful for the flood modelling work and this editing work have been performed by Airbus and is included in the project budget. The DEM tiles over Malawi have been processed and the team is awaiting the go-ahead from GFDRR on the Malawi project to make the tiles available. After the project, the

DEM will remain the property of Airbus Defence and Space but can be accessed via the free and open RASOR platform for flood calculations using the RASOR platform.

g) All results have been delivered on the RASOR Platform and connected Geonode to facilitate access computation and further analysis to the end users and the GFDRR. Specifically, the RASOR Platform enables smart and easy visualization of the results both in terms of Hazard and Risk, providing a play space for the user for further analysis. The platform is open source and has been profiled to be compliant with the Malawi Geonode installed already in the Country. The files can be easily moved onto the masdap geonode installation.

5.2 Flood hazard and risk profiling

In order to produce the flood hazard maps, hydrologic (WFLOW-HBV) and hydraulic (SOBEK-FM) models have been employed. Airbus/Infoterra supplied 12m resolution digital elevation maps based on their TanDEM-X remote sensing product. The models were driven by and calibrated on global open data sets, such as globally available EU-WATCH meteorological forcing data. No local (in situ) data sets of sufficient quality and coverage could be found within the time frame of this project. The models could therefore contain biases caused by errors in the global data sets, although the most critical data sets (e.g. the EU-WATCH data set for meteorological input) have been used in several previous studies with good results.

5.2.1 General modeling framework

In order to produce flood risk maps (flood extent, water depth and impact maps), a flood modelling framework have been developed that consists of three components:

- A hydrological model WFLOW, to calculate surface flow in the region of interest;
- A simplified Flood volume redistribution scheme to mimic the flood distribution in the flood plain called HAND applied to the larger domain here in this document referred to as Norther Malawi that comprises all of Malawi north of the city of Liwonde (coordinates: -15.0687604, 35.2288728) see Figure 2

- 2D hydraulic flood models based on FM software, to calculate flood extents and water depths in the hotspot sites (Karonga, Salima, Mangochi) see Figure 2 for the localization of the hotspot domains;
- A flood impact model based on Delft-FIAT.

Figure 2Domain for the flood maps in Norther Malawi and identification of the Hotspot domains.

5.3 Hazard Modeling Framework

The flood mapping framework is depicted in Figure 3. This flow chart shows there are two main branches of calculations. The first branch starts off with a hydrologic modelling task resulting in 32 years of simulated flows, using the EU WATCH data as meteorological forcing. The results of this simulation are processed in three ways to produce design discharges at locations of interest and annual maxima fluvial and pluvial flood maps. The second branch starts off with

a statistical analysis of the EU-WATCH rainfall and derivation of design events before the hydrologic modelling is done. The second branch also produces design discharges, fluvial and pluvial flood maps, but for specified return periods.

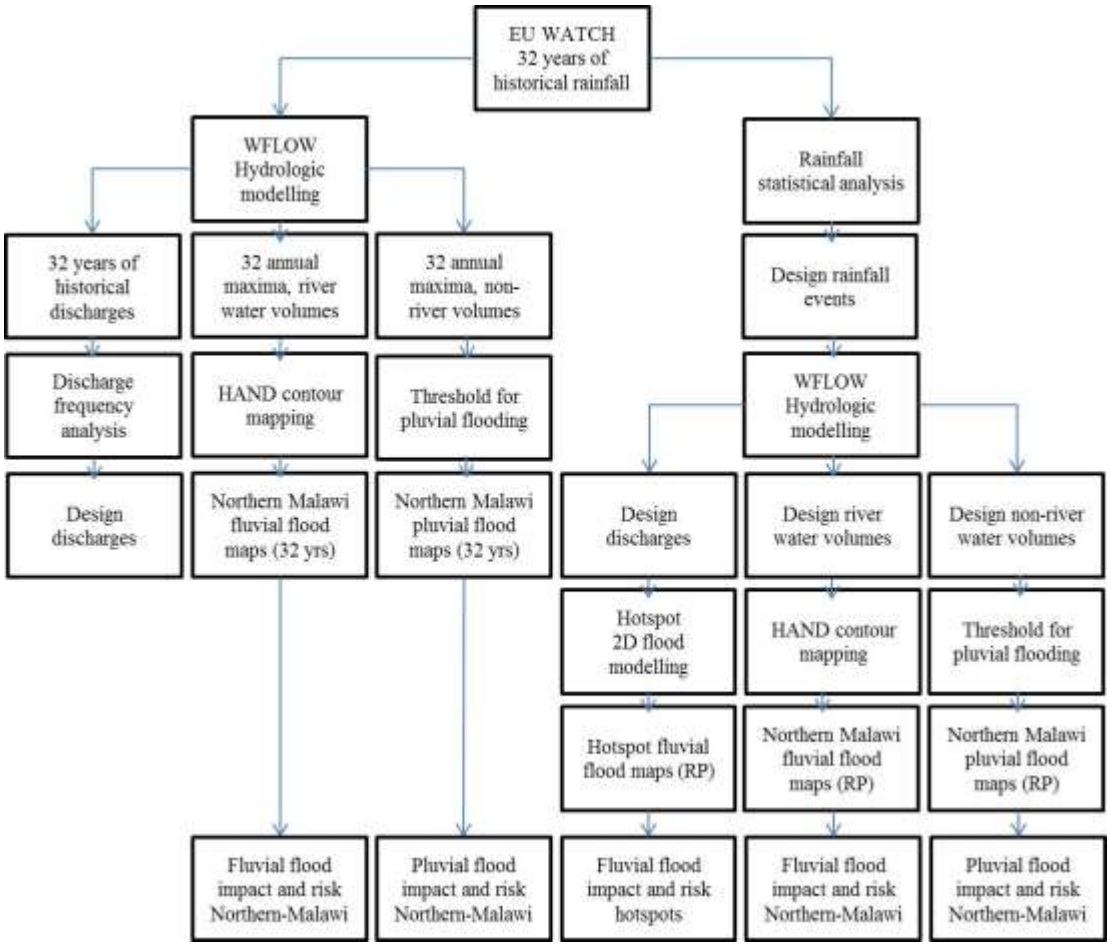

Figure 3: Flood mapping flow chart.

The double approach offers several opportunities for cross-validation and uncertainty assessment. For example, the design discharges are computed in both branches.

The results can be compared as a validation of the design rainfall event approach. The hotspot models allow for a validation of the HAND contour mapping and the pluvial flood mapping.

In the remainder of this chapter, we describe a number of components of the computational framework in more detail. These are:

- EU WATCH Meteorological forcing data;
- WFLOW hydrologic model;
- HAND contour mapping method;
- Rainfall statistical analysis and derivation of design events;
- 2D flood models for the hotspots;
- Pluvial vs fluvial flooding.

5.3.1 Meteorological forcing

Rainfall and (potential) evapo-transpiration (PET) are the two main driving forces for the hydrologic model to simulate surface runoff and river discharge. The rainfall input was obtained from the freely available EU-WATCH dataset (Weedon et al., 2011; Haddeland et al, 2011). This set was produced as part of the EU FP6 'WATCH' project for regional and global studies of climate and water. The EU-WATCH dataset describes rainfall at 3 hour temporal and ~50km spatial resolution for the full 20th century (1900-2001). However, a test run of the hydrological model revealed that the pre-1970 rainfall over Malawi has a different distribution with higher average flows (see Figure 4). Probably, the post-1970 rainfall was bias-corrected by using a data source that was not available before 1970. The pre-1970 data was therefore excluded from the analyses.

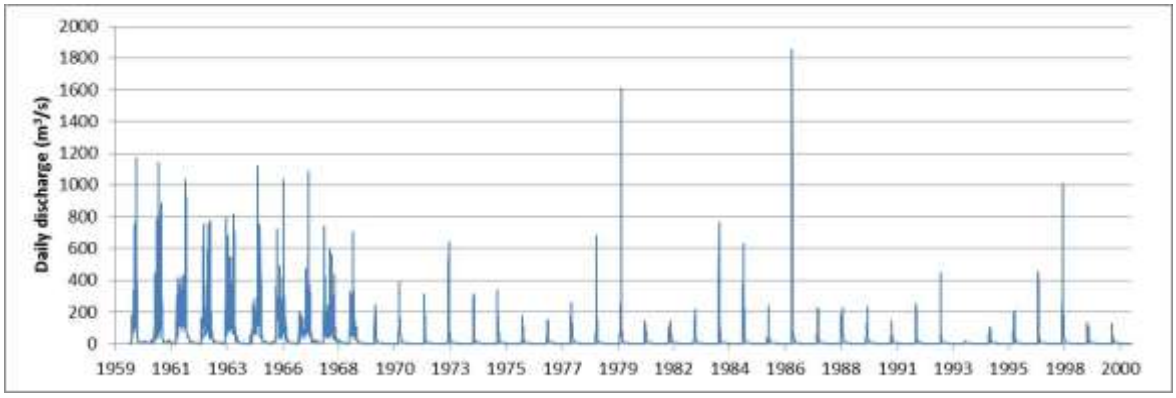

Figure 4: Karonga daily discharges (WFLOW-HBV modeling using EU-WATCH rainfall as input. There is a clear crossover from pre- to post 1970 flow regime.

The EU-WATCH annual rainfall between 1970 and 2001 (32 years) was validated against rainfall measurements at ground gauges. The gauge stations at Lilongwe, the capital of Malawi, and Mzuzu were considered most reliable and were selected for this validation. For Lilongwe, the average EU-WATCH annual rainfall between 1970 and 2000 was 899 mm/yr (Figure 5). For Mzuzu the average is 1159 mm/yr. These values correspond reasonably well with the 900 mm/yr for Lilongwe and 1289 for Mzuzu as reported by the Malawi Department of Climate Change and Meteorological Services (http://www.metmalawi.com/).

The Malawi Department of Climate Change and Meteorological Services also posts a map of spatial distribution of average rainfall on their web site (see Figure 5). This map indicates that, in general, the area close to the shores of Lake Malawi receives more rain than locations farther inland. However, there are exceptions to this rule. Just south of Karonga the shores of Lake Malawi seem to be dryer than the inland region north of Bolero.

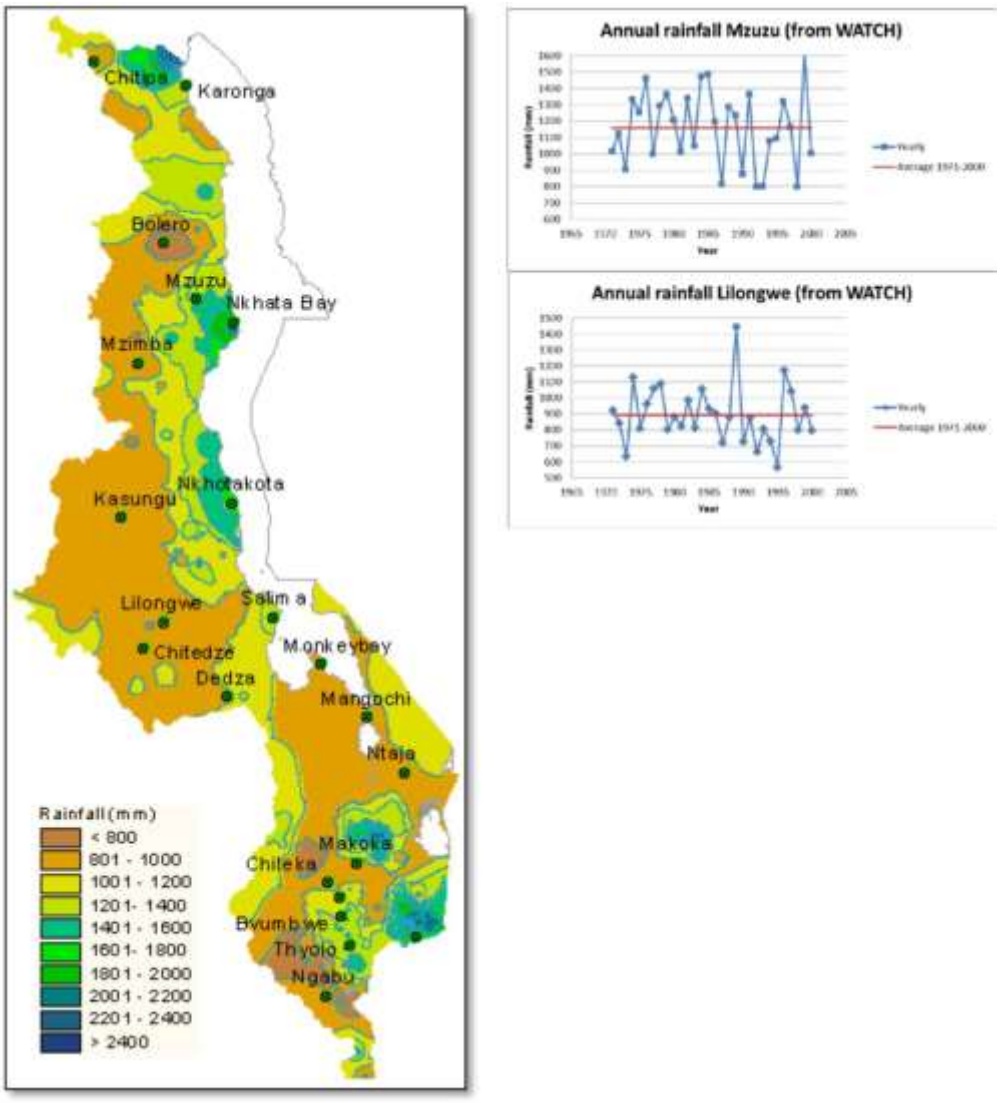

Figure 5: Lilongwe and Mzuzu annual rainfall from EU-WATCH. Average annual rainfall over Malawi (source: http://www.metmalawi.com/)

The Potential Evaporation-Transpiration (PET) for Malawi was taken from Ngongondo et al (2015), who derived an average PET of 2.9 mm/day, based on a 30-year surface water balance study.

5.3.2 Hydrologic modelling

The hydrologic modelling was done using the open-source WFLOW-HBV software that is developed by Deltares (http://www.openstreams.nl). The WFLOW-HBV model is a fully distributed version of the HBV-96 model, where the original routing function (MAXBAS) was traded for a kinematic wave function (Schellekens, 2013). The workflow is shown in Figure 6. More information and documentation can be found on http://www.openstreams.nl.

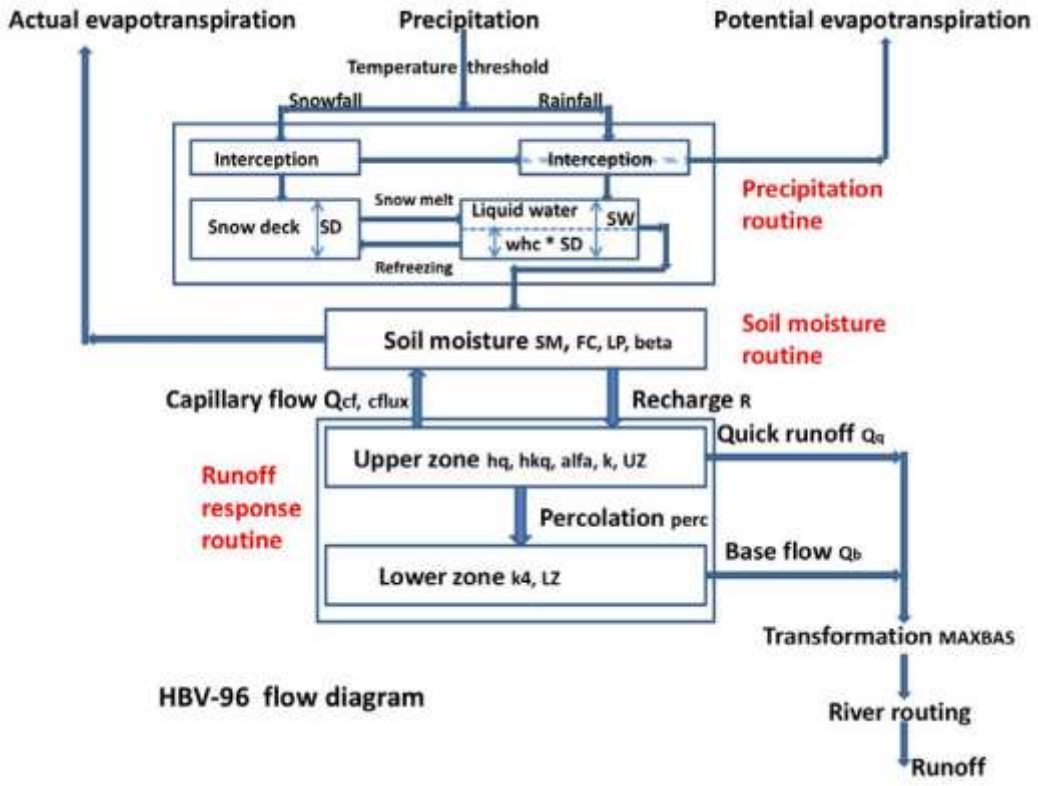

Figure 6: General representation of the distributed WFLOW rainfall runoff model (from WFLOW documentation).

The required WFLOW model parameters were taken from freely available global data sources, such as the GlobCover land cover database of the European Spatial Agency (ESA)[1] for land use and the FAO Harmonized World Soil Database (HWSD) and Soil Map[2] for soil type. Results

from earlier studies show that WFLOW produces very reasonable results by using model parameters based on these global data, without further calibration to local gauge data.

Based on the Digital Elevation Model (DEM), which was derived from TanDEM-X by a resampling to 1km, the local drainage direction (LDD) and sub-basins map were derived. Figure 7 shows examples of sub-basins for the hotspots Karonga and Salima. The North Rukuru River that flows north of Karonga has one drainage basin (magenta-coloured area in Figure 7). The Lilongwe River in Salima has a confluence just upstream of Salima. The 2D model thus has two inflows, connected to two drainage basins in WFLOW (green and brown areas in Figure 7).

In very flat areas, the direction of flow is often not well-defined, which may lead to incorrect course of rivers in the model. This was solved by 'burning in' the main rivers into the DEM, i.e. artificially lowering grid points along the course of the rivers to lead the water in the right direction. The river courses were initially derived from the DEM and then corrected by hand (comparison to Google Maps). Figure 11 shows a map of the main rivers that was obtained this way.

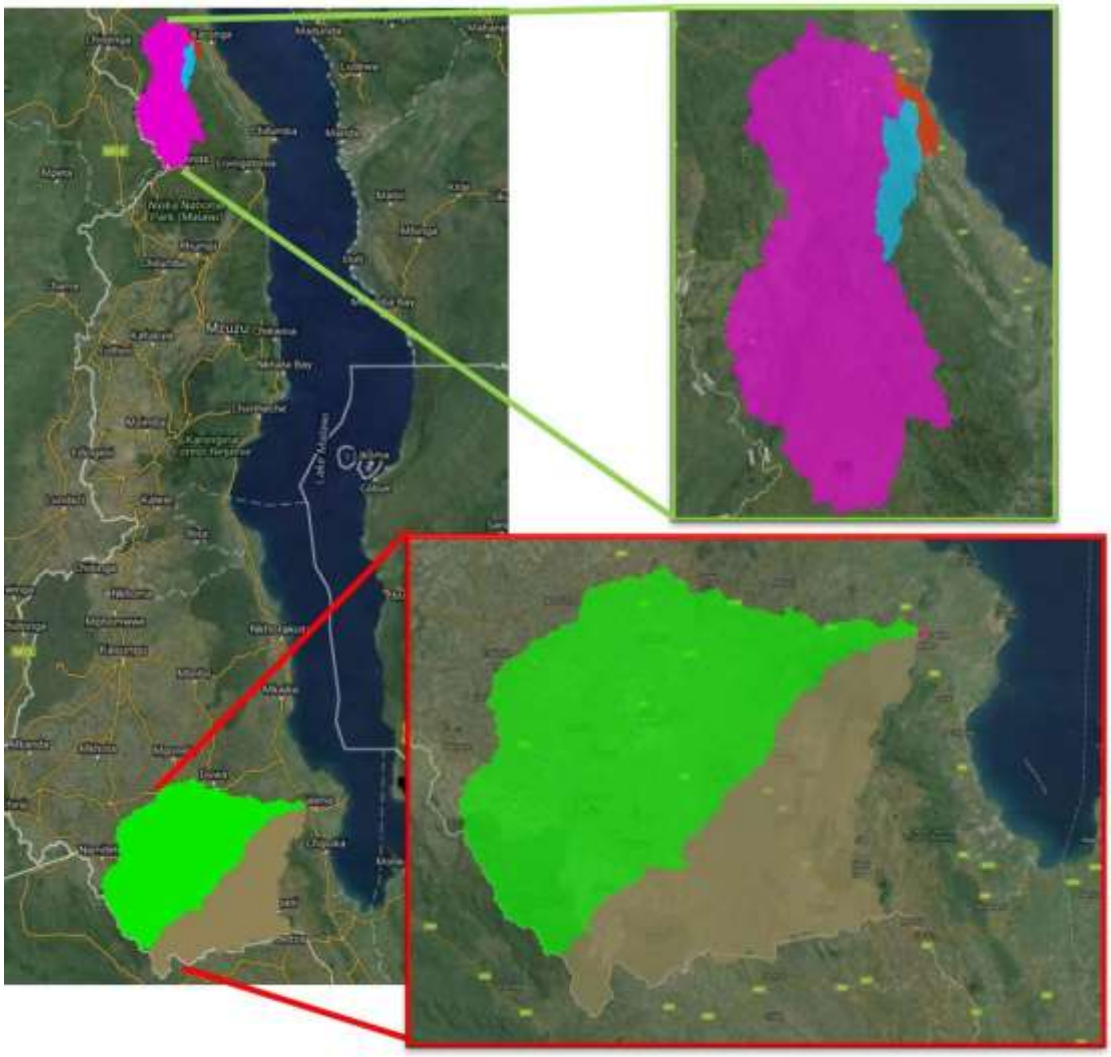

Figure 7: WFLOW sub-catchments for Karonga and Salima.

The Malawi WFLOW-HBV model was used for two sets of simulations:

- 32 years of historical rainfall runoff (1969-2000), using EU-WATCH rainfall input;

- Design rainfall events for a range of return periods (2-1000 years).

Basin-averaged rainfall for 6-month period from the 32-year historical rainfall is shown in Figure 8. The simulated discharge time series are shown in Figure 9. The three basins show a typical hydrological response to rainfall, with a rise in flow after a period of rain and subsequently a slow decay.

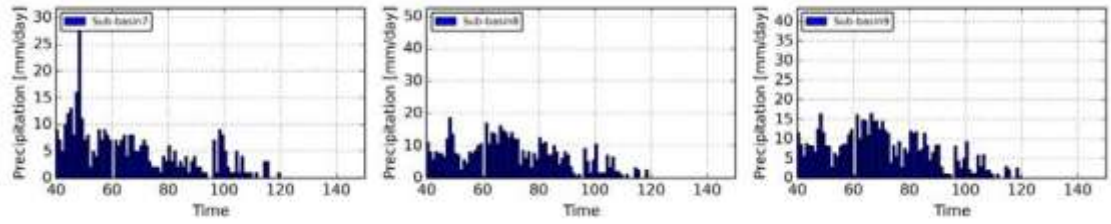

Figure 8: Historical basin-averaged rainfall for three example basins in northern Malawi (time in days).

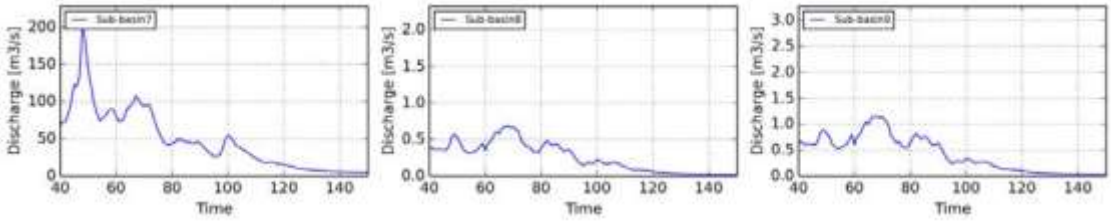

Figure 9: Simulated discharge (basin outlet) for the same historical period and basins (time in days).

The average monthly flows for three locations of interest (because they are at the upstream boundaries of the hotspot areas) is shown in Figure 10. The dry (May-October) and wet (December-March) seasons are clearly visible.

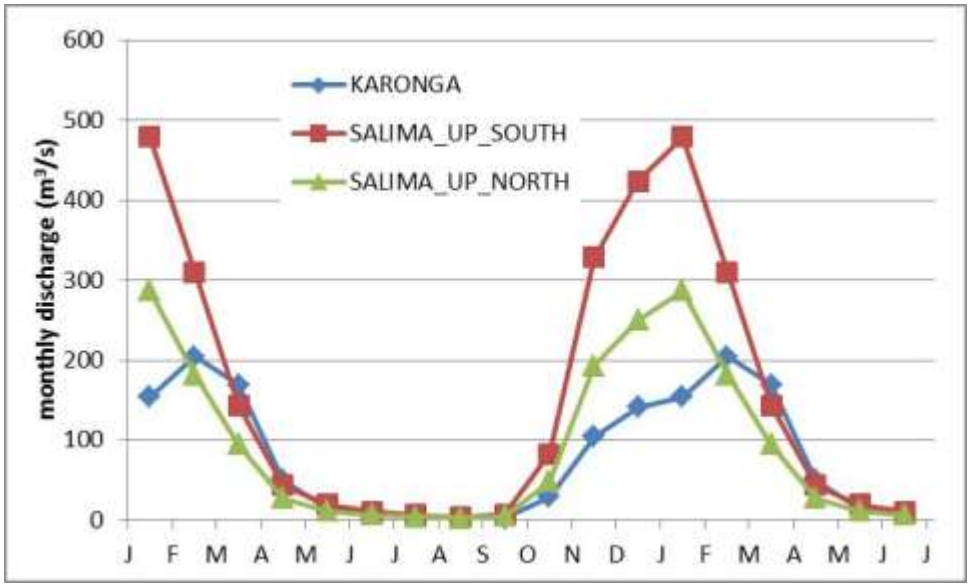

Figure 10 : Average monthly flow at three test locations.

An attempt was made to compare these simulated discharges to observed flow in some main rivers from GRDC (http://www.bafg.de/GRDC/EN/Home/homepage_node.html). However, most stations have limited data sets of poor quality (gaps) and the location of the gauge station is often ambiguous. The GRDC data was therefore not considered suitable for calibration of the model and it was decided to use the model as is, without further calibration to local gauge data.

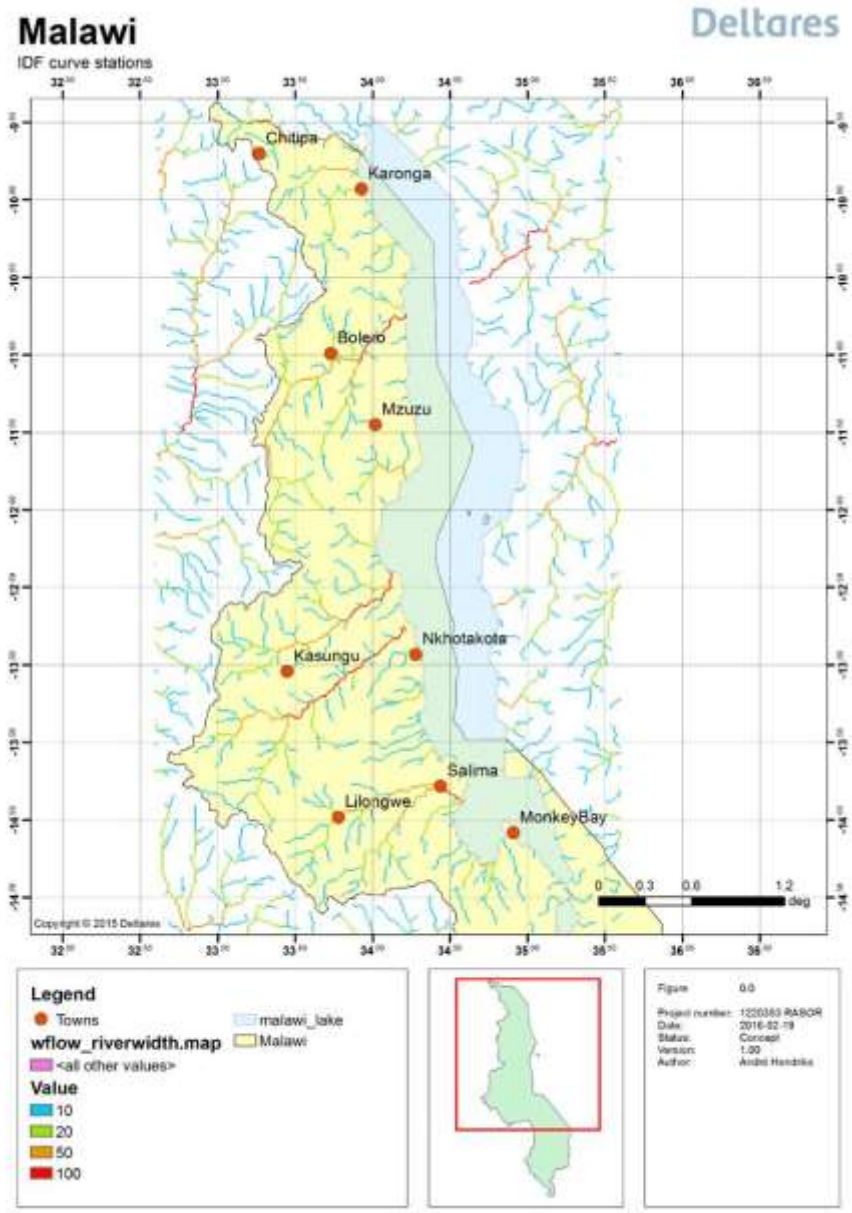

Figure 11: Main rivers in the WFLOW model

5.3.3 HAND contour mapping

For the whole of northern Malawi, a detailed 2D hydraulic modelling is computationally unfeasible. To produce the larger area flood maps, the surface water as calculated by the

relatively coarse WFLOW hydrologic model was scaled down to the target 12m resolution by using a water volume distribution scheme that is based on the Height Above Nearest Drainage (HAND). To calculate a HAND map, the difference is taken between the elevation of a given pixel and the elevation of the nearest drainage or watercourse. These watercourses are derived from the Local Drainage Direction (LDD) map using a minimum Strahler stream order threshold (see Figure 12), so that only the main rivers are defined as watercourses.

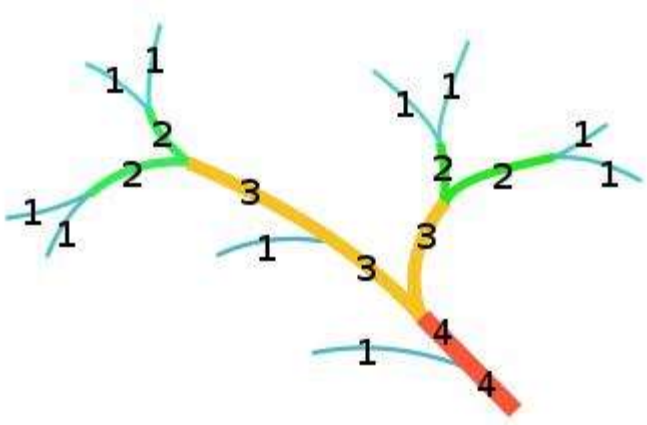

Figure 12: Strahler stream order (from Wikipedia).

HAND contour mapping is a static approach for mapping the potential extent of inundation that extends beyond simple mapping low-lying areas. The method does not require hydrodynamic modelling of water flow which makes it much less computationally demanding. The HAND-delineated relative height is directly related to the river stage height (Nobre, et al., 2011) and an effective predictor of flood potential.

The volume of surface water in 1km computation cells that are part of the river network (see Figure 11) in the WFLOW model is redistributed over 12m cells of the TanDEM-X as follows:

- First the riverine water volume as calculated by WFLOW (Figure 2.12) is reduced by the riverine water volume as calculated for the T=2 yr rainfall event. The T=2 yr situation is often considered the bank-full level, i.e. no flooding occurs (Dunne and

Leopold, 1978). The excess water volume above the T=2 level is thus the water that will flood the land.

- This excess water volume is used to 'fill up' the terrain, starting from the lowest HAND contours until the mapped water volume equals the target volume.

The results of this HAND contour mapping method were compared to conventional flood mapping (using 2D hydraulic models) for two hotspot areas Karonga and Salima. Results will be discussed in section 5.3.3

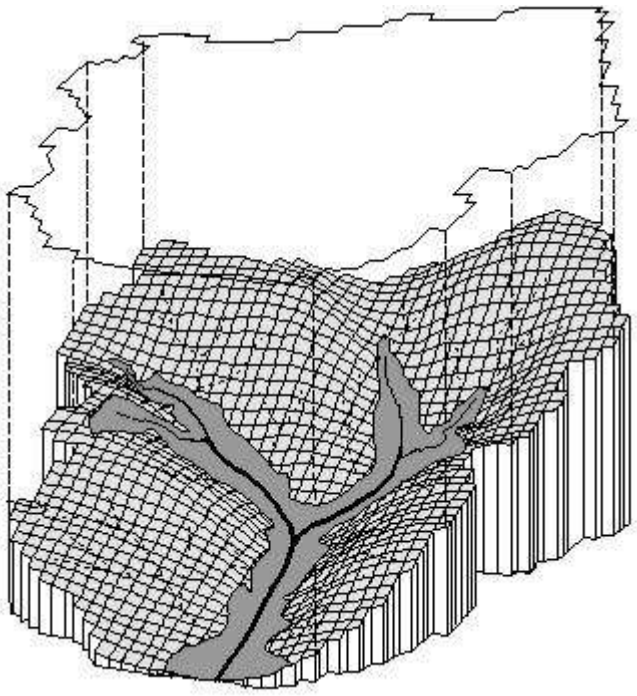

Figure 13: Schematic drawing of HAND contour surface water mapping. The areas that have the least elevation difference to a nearby drain are inundated first.

5.3.4 Rainfall statistical analysis

To force the hydrologic model, a design rainfall event for every return period is needed. This was derived from Intensity-Duration-Frequency (IDF) rainfall statistics. The IDF-table or IDF-curve is a common representation of the probability of exceedance of rainfall thresholds over a

given duration. The 32-year EU-WATCH data at 3-hour temporal resolution were used to derive IDF curves for northern Malawi.

The IDF curves were obtained for several locations spread over northern Malawi (all cities in Figure 5) and mutually compared. The average over all stations was taken to obtain an average location IDF (Figure 14).

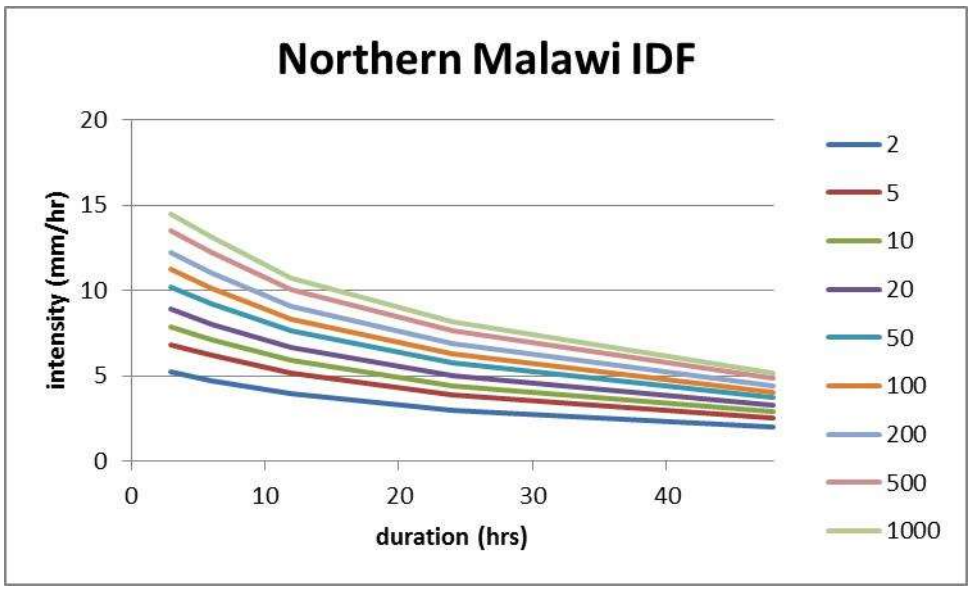

Figure 14: Average IDF curves for all stations over northern Malawi. Each graph represents a return period (shown in the legend in years).

All locations produced comparable IDF curves except for Karonga and Nkhotakota, which seem to be wetter than the other stations (

Figure 15). This is possibly due to their vicinity to the shore of Lake Malawi (see Figure 5) or to orographic effects. This could, in principle, be taken into account in the design rainfall events. However, to differentiate between several regions within northern Malawi would require an in-depth analysis of the climatic zones and orography, using data from many locations and knowledge from Malawi meteorologists. Such a study was considered beyond the scope of the current project. It was therefore decided to use the average IDF curves (Figure 14) for all of

northern Malawi. It is possible though that this will lead to an underestimation of rainfall runoff and flood maps for some of the coastal stations, such as Karonga.

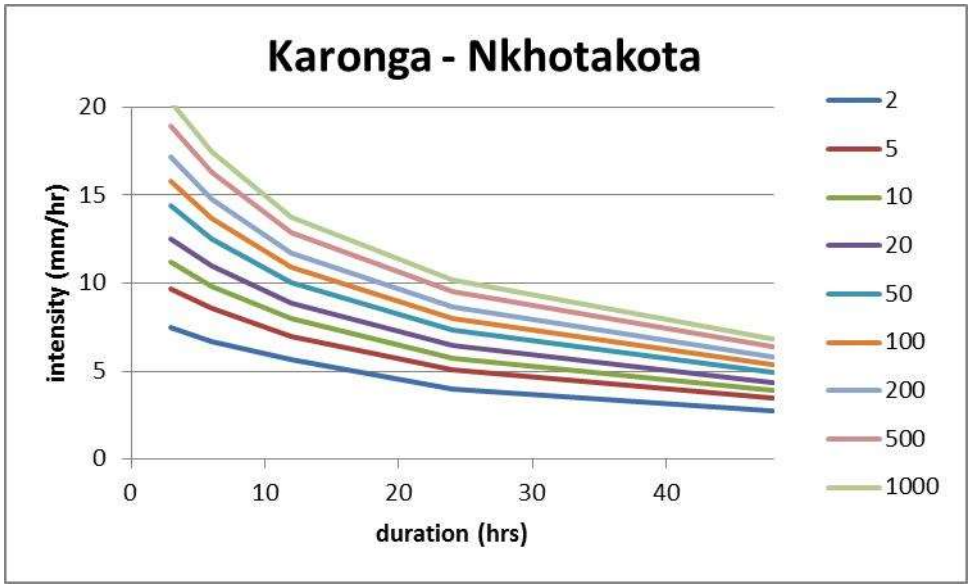

Figure 15*: IDF curves for the two 'wet' stations Karonga and Nkhotakota. Each graph represents a return period (shown in the legend in years).*

An empirical formula (known as Wisner's formula) was fitted to the IDF table data:

$$i = \frac{a}{(t_d + b)^c}$$

where,

t_d = duration (minutes)

i = average intensity in period t_d (mm/hr)

a, b, c = parameters, depending on the return period T

Next, a design rainfall event, or hyetograph, was derived from the IDF curves using the 'alternating block method', as described in Chow et al. (1988). Contiguous blocks of rainfall

are added on alternating sides of the storm peak such that the total rainfall depth always matches the average intensity over the total duration given by the IDF. The temporal resolution of the hyetograph is 1 hour and the total duration is 100 days, so the IDF curves were extrapolated to shorter and longer time scales. A typical result is given in Figure 16.

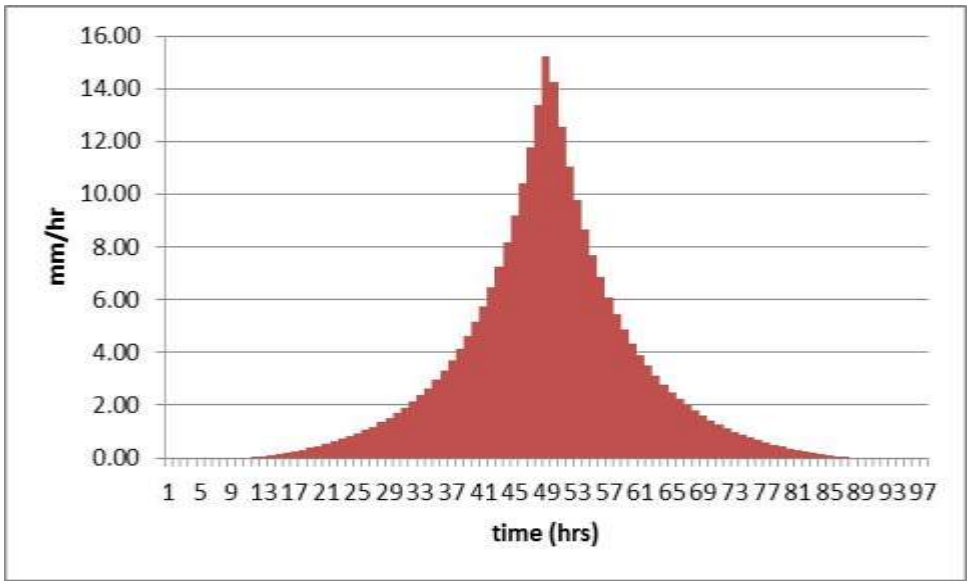

Figure 16: Design hyetograph obtained from the IDF and 'alternating block' method.

This design hyetograph was applied as uniform rainfall over the total area (northern Malawi). No Areal Reduction Factor (ARF) was applied, since the simulation should produce flood maps for both smaller and larger (fast and slow responding) catchments in a single run. Neglecting the ARF is expected to have a relatively small effect, because the ARF is typically around 0.9 for rainfall of longer duration (>24 hrs).

5.3.5 2D flood modelling

The flood maps for three hotspot areas were calculated using a model called D-Flow Flexible Mesh (D-Flow FM) [3]. This open source software engine for hydrodynamic simulations is being

developed by Deltares. D-Flow FM is a shallow-water solver based on the finite-volume method applied on unstructured grids.

It solves the full Saint-Venant equations and thus guarantees conservation of mass and momentum, while also accurately representing the drying and flooding of grid cells (Kernkamp et al., 2011; Verwey et al., 2011).

D-Flow FM uses a flexible mesh and a variable grid resolution. This enables the modeler to use a higher resolution and more accurately simulation of the flow of water in topographically complex areas, while keeping the rest of the model at a lower resolution for optimal computational performance. A small piece of a computational grid with varying cell size and triangular elements is shown in Figure 17.

[3] *http://oss.deltares.nl/web/delft3d/d-flow-flexible-mesh*

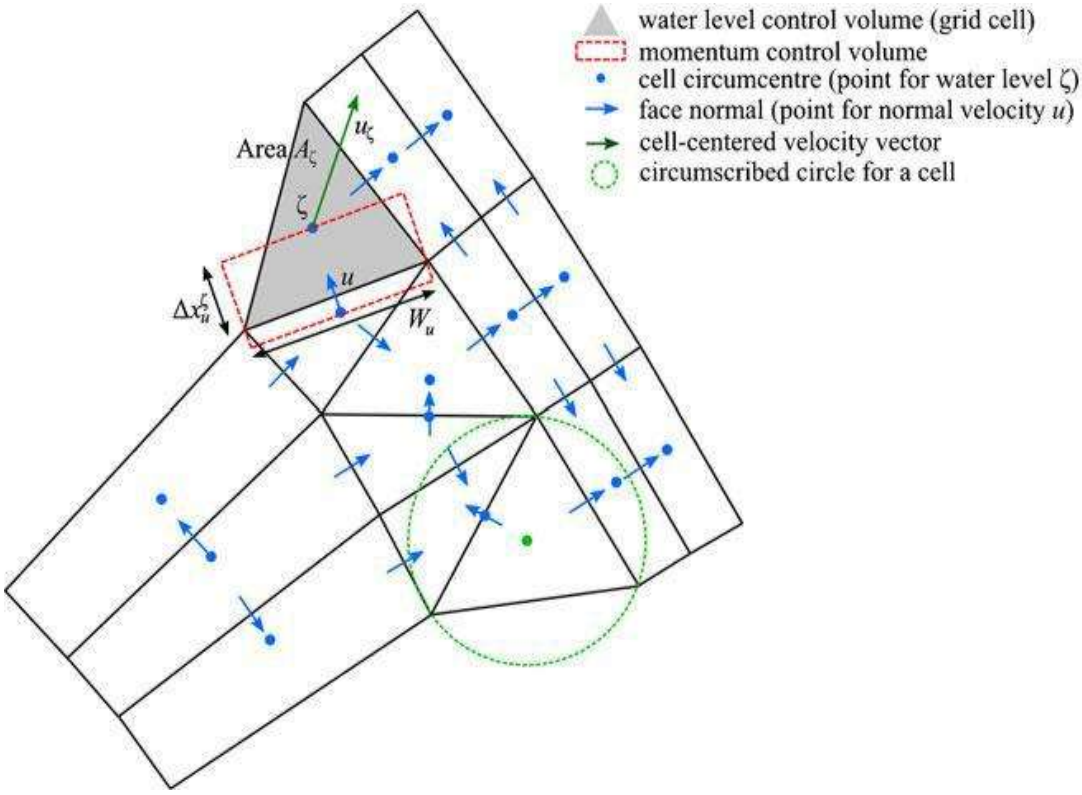

Figure 17:D-Flow FM grid and computational elements.

The general setup of the 2D hydraulic models is as follows:

- The terrain model is taken from the WorldDEM TanDEM-X.
- The river course (drawn by hand) is dug into the terrain, such that the T=2 year discharge is just conveyed without bank overflow. Bankfull discharge is generally associated with

a momentary maximum flow that has an average recurrence interval of 2 years (Dunne and Leopold, 1978).

The upstream boundary conditions are derived as follows:

- Peak discharges are derived from WFLOW simulations of design rainfall events for several return periods;
- The shape of the inflow hydrograph is taken as the average shape of the four highest discharge peaks in the 32-year historical WFLOW simulations. This shape is then scaled up or down to the target peak discharge.

The downstream boundary condition is a fixed water level (Lake Malawi, or for the Salima model a location several km downstream)

More details of the FM models for the hotspot areas Karonga, Salima and Mangochi will be given in the following chapters.

5.3.6 Pluvial versus fluvial flooding

Whereas fluvial flooding is clearly defined as flooding caused by river bank overflow, the definition of pluvial flooding requires some clarification. According to the UK Environment Agency, "pluvial flooding is defined as flooding that results from rainfall-generated overland flow, before the runoff enters any watercourse or sewer." What we call pluvial flooding thus depends on our definition of a watercourse.

In this study, the watercourses that cause fluvial flooding were defined as the rivers in the WFLOW model (see Figure 11). Water from these rivers is distributed over the flood plains by the HAND contour mapping method. To be consistent, pluvial flooding is defined here as flooding caused by surface water that has not yet entered into these watercourses, or the 'non-riverine surface water'. This is the surface water over the saturated zone in the WFLOW model, except for the water in the main rivers (see Figure 11). The non-riverine water includes direct

overland flow as well as water in small streams and ditches that were not resolved as rivers in the WFLOW model.

In order to distinguish between a more or less normal situation after rainfall and actual flooding, the non-riverine surface water in the T=2 design event was subtracted from the simulated surface water for historical years and longer return periods (negative outcomes are put to zero). By applying this 'threshold', only the most severe cases of pluvial flooding are selected. A non-riverine surface water volume of less than that for T=2 is not seen as pluvial flooding, because, up to T=2, the surface water volume is assumed to be collected in natural or urban drainage (e.g. small streams, ditches and sewers), which is not typically seen as pluvial flooding. Beyond T=2, the small streams and urban drainage systems can no longer convey the water and flooding occurs. The spatial distribution of the surface water in excess of the T=2 value thus gives an indication of the pluvial flood hazard. However, pluvial flooding is largely a local effect and the actual water depths will depend on the terrain features on smaller scales than the 1km WFLOW grid. To account for this, a spatial smoothing was applied that reflects the uncertainty in the water depths and actual location of the flooding.

5.4 Hazard Results

5.4.1 Design discharges

The design hyetographs and uniform PET of 2.9 mm/day were used as input to the WFLOW-HBV hydrologic model to produce surface runoff and discharges at three test locations. These locations are the upstream inflow boundaries of the two hotspots Karonga and Salima. The results from the direct frequency analysis of the 32 years of EU-WATCH-based discharges and the peak discharges from design hyetographs offer the opportunity for a cross-check.

Figure 18, Figure 19 and Figure 20 show results from both the direct frequency analysis and the design event approach in the same graphs. In general, the frequency curves correspond well. For the two Salima stations, the design event discharges are clearly larger than those from the

direct frequency analysis for longer return periods, although the deviations are no more than a factor of two. A partial explanation for this could be the neglect of the areal reduction factor (ARF). The catchment size for the Salima stations is larger than for Karonga and the overestimation of the areal rainfall would therefore be larger at Salima.

The design event method underestimates the discharges for the shortest return periods for all three stations. This could be related to an underestimation of the effect of pre-event rainfall in the design event simulations. The design event simulations start from average initial conditions.

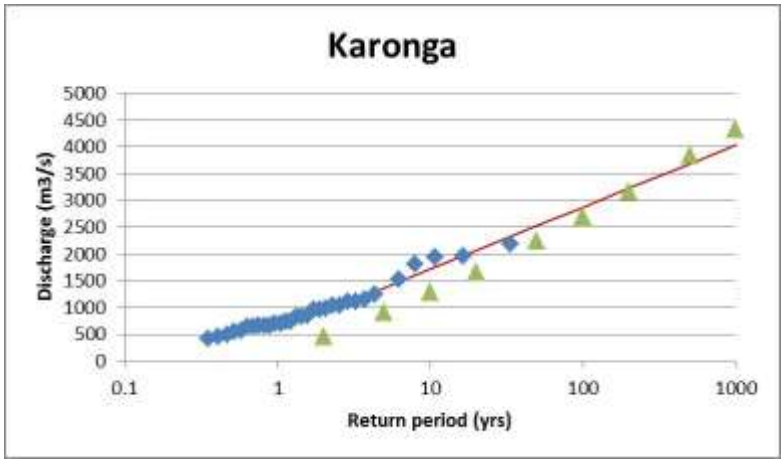

Figure 18: Results from frequency analysis and design hyetograph for Karonga. The red line is a fitted exponential distribution.

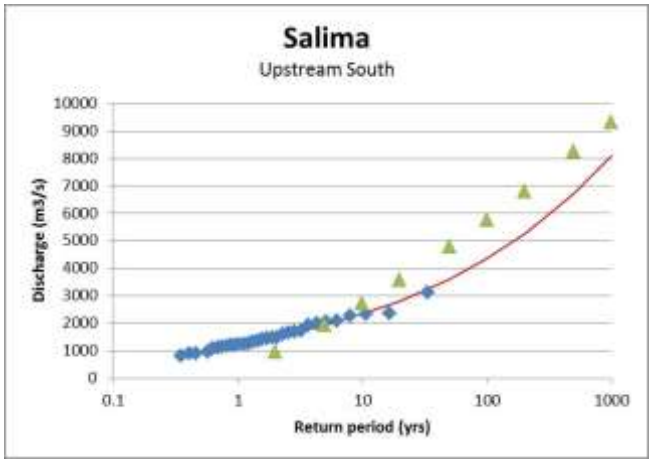

Figure 19: Results from frequency analysis and design hyetograph for Salima-South. The red line is a fitted Pareto distribution.

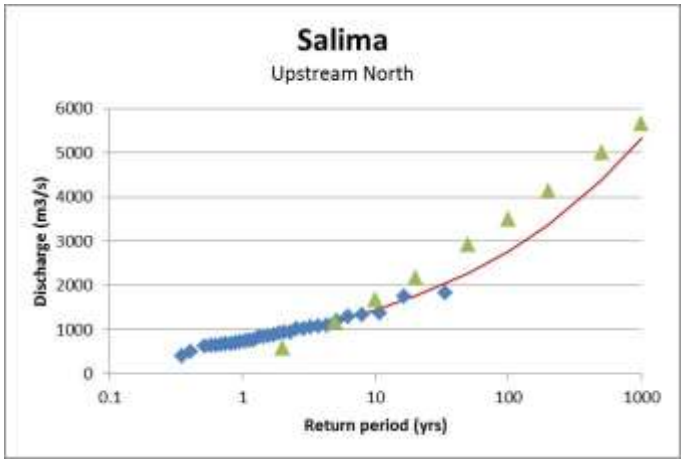

Figure 20: Results from frequency analysis and design hyetograph for Salima-North. The red line is a fitted Pareto distribution.

5.4.2 Fluvial flood maps

Fluvial flood maps were produced for a range of return periods, using WFLOW riverine water volumes and the HAND contour mapping algorithm described in previous sections.

Figure 22 shows a smaller area of about 100 km by 70 km with more details of the inundation map. Figure 23 shows a smaller subarea with even more detail. This series of Figures shows the scale of the total area relative to the resolution of the flood maps.

Figure 21 Fluvial inundation map for 100-yr return period inundation

Figure 22: Zoom in example

Figure 23: Zoomed in further

Detailed inspection of the fluvial flood maps revealed that, in general, the flood maps are realistic (see e.g.Figure 23). However, there are a few limitations and shortcomings that need to be mentioned:

1. **Fluvial flood maps account for flooding from major rivers only**

The HAND contour mapping method considers only water from the larger rivers that are defined in the relatively course hydrologic model (see Figure 11). Smaller streams and ditches that may flood during extreme rainfall events are not included in the fluvial flood mapping method. This 'non-riverine' surface water is taken into account in the pluvial flood maps (see next section), however at a coarser resolution than the 12m that is used for the fluvial flood maps.

2. **Flood level for T=2 is zero by definition**

The bank full situation is defined as the T=2 yr flow volume. Therefore, by definition, no fluvial flooding occurs for this return period.

3. **Overestimation of inundation depths on elevated plateaus**

The HAND mapping routine uses an automated identification of rivers and streams that is derived from the LDD (local drainage direction) map. This procedure occasionally identifies a headwater as a stream. If this headwater has a local drainage area, the HAND map recognizes

this as a floodable area and part of the water volume is attributed to that local drainage area. An example is given in Figure 24.A small plateau on a hillslope is recognized as a drainage area of a tributary to the larger river that runs through the valley. Part of the water volume from the larger river is attributed to the plateau. Although such areas are indeed floodable, the inundation depth is probably overestimated by the HAND mapping.

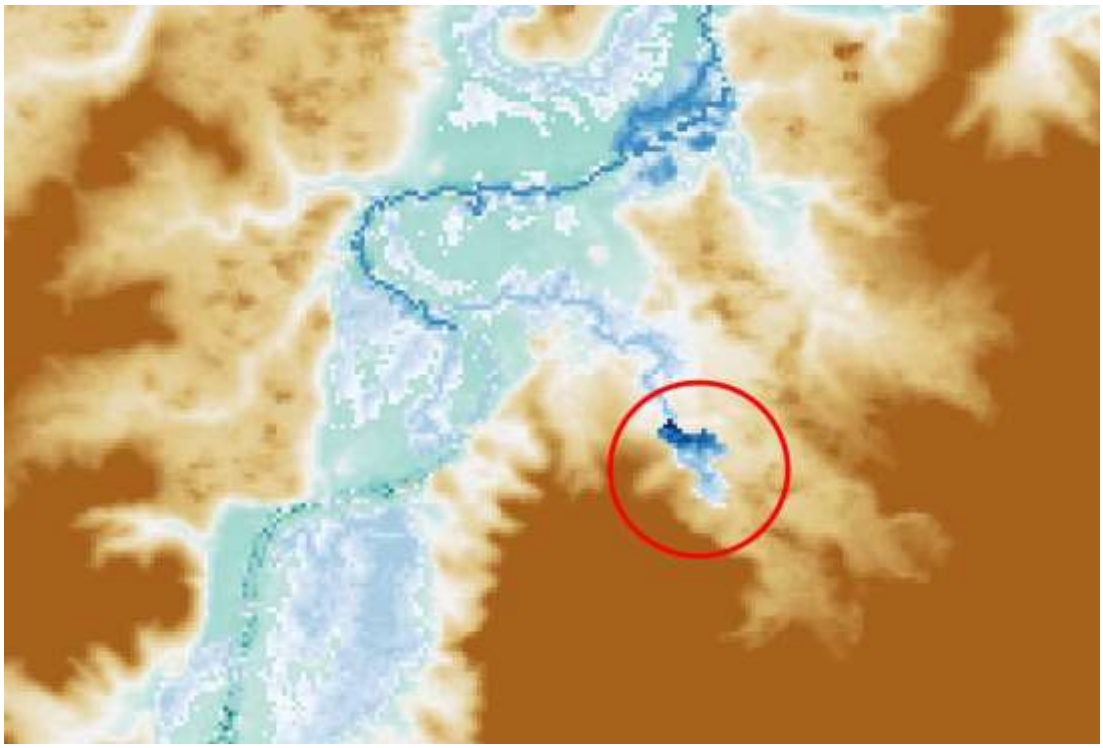

Figure 24: Local drainage area (encircled) on an elevated plateau where the inundation depth is overestimated.

4. HAND mapping cannot reproduce complex flow patterns

Another limitation of the HAND contour mapping is that it cannot reproduce complex flow patterns including the effect of levees. The contour mapping simply fills up the lowest areas, without considering the direction of flow. The implications of this are not that large, because most rivers and streams are natural streams and there are not that many levees. An exception is the city of Karonga, where a levee protects part of the city from flooding by the North Rukuru River. The flood map (see Figure 25) shows flooded areas on either side of the levee (drawn in red). The HAND contour mapping fills up areas on both sides of the levee, because both sides

have a low elevation. In reality, the levee will hold back the water that is coming from the west and the east side will stay dry until the levee overflows.

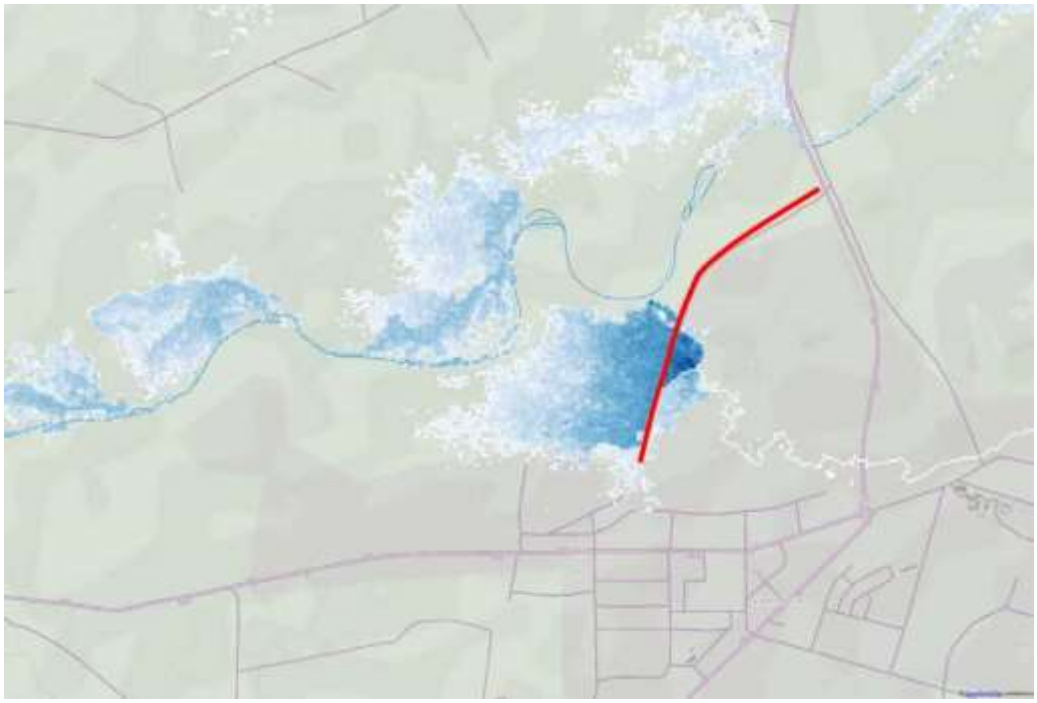

Figure 25: T=100 flood map of Karonga. The levee is drawn in red.

5. Erroneous flooding near lake shores

Lake Malawi was masked out from the inundation maps because the TandDEM-X is very noisy over open water. This causes issues at the lake shores. In some cases, water that is likely to flow

into the lake is forced back onto the terrain and therefore causes unlikely flood patterns near the lake shore. An example is given in Figure 26.

Figure 26: Erroneous inundations on the lake shore.

6. Elevation offsets due to forests and urban areas

Although TanDEM-X has a very high horizontal resolution, the DEM contains signals from objects in the field. A typical elevated feature is a forest. Examples of this effect on the flood maps is shown in Figure 27, where a patch of commercial forest (encircled in red) is causing a dry patch of land that in reality would be inundated. Another artefact is buildings and urban areas (encircled in yellow). These offsets are hard to remove from the DEM without sophisticated correction algorithms.

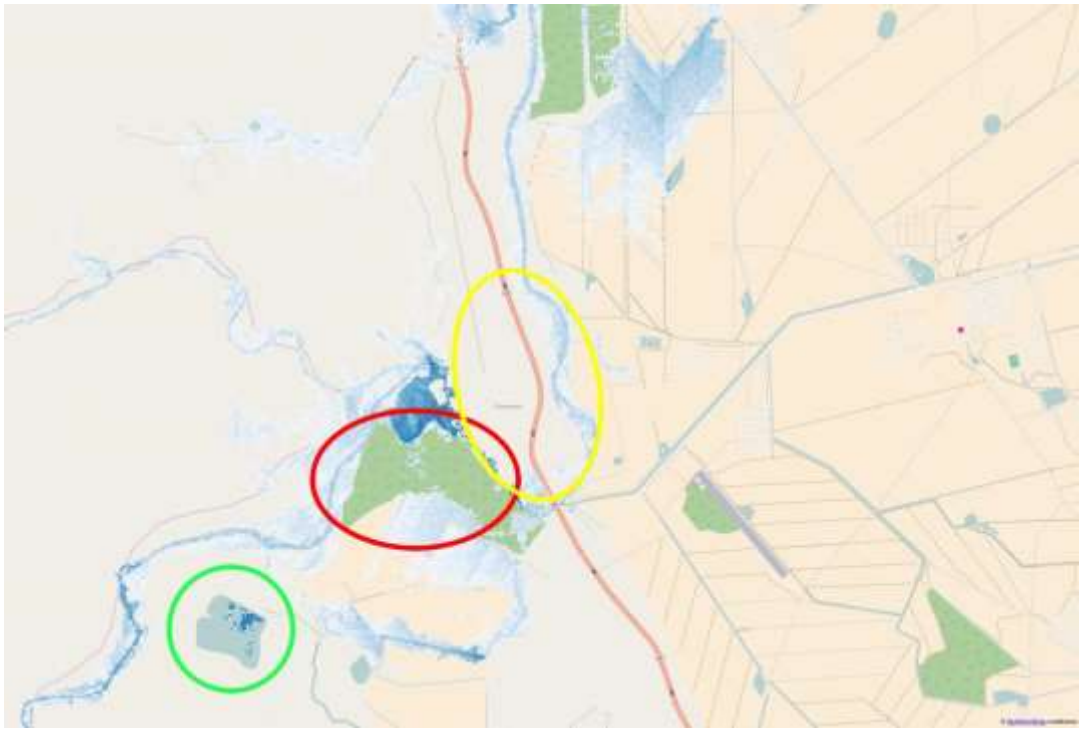

Figure 27 Effect of forest (red circle) and built-up areas (yellow circle). An open water body (indicated by a green circle) gives a noisy signal.

7. Noise in open water bodies

Permanent surface water gives a noisy signal in the raw TanDEM-X product, causing high and low peaks in the DEM. The effect of this can be seen in Figure 27. A small open water body shows scattered pixels with large differences in inundation depth over the pond. These water bodies are masked out in the processed DTM product, but this DTM is only available for the hotspot areas. Deltares is developing algorithms to mask out permanent surface water at 30m resolution with LandSAT 8 imagery. However, these algorithms are not ready and cannot be applied to these flood maps yet. Moreover, the 30m resolution water mask does not match the

12m TanDEM-X resolution and will probably cause problems near the boundaries of these water bodies.

5.4.3 Fluvial flood maps validation - hotspots Karonga and Salima

The fluvial flood maps were validated by using a more traditional approach, i.e. by a 2D hydraulic model with an upstream boundary condition of water inflow for a given return period. Two models were developed for smaller (10x10km) hotspot areas near Karonga and Salima. Post-processed TanDEM-X digital terrain models (DTM) were used that were manually corrected by Airbus to remove elevated objects from the terrain (forests, buildings). A water mask was also applied in the case of Salima to suppress the noise from the open water of the river.

The Karonga 2D hydraulic model has a single inflow boundary condition (North Rukuru River). The Salima model has two upstream inflows (named Salima North and Salima South). The peak discharges for these inflows were derived from the annual maxima of the WFLOW model simulation with 32 years of EU-WATCH rainfall. The peak discharges for a range of return periods are given in

Table 1.

Table 1: Peak discharges for upstream boundary conditions of Karonga and Salima models.

T	Karonga	Salima (south)	Salima (north)
2	111	95	61
5	226	191	123
10	318	270	174
20	414	352	226
50	555	472	303
100	668	569	365
200	788	672	431
500	945	815	522
1000	1075	924	591

The shapes of the normalized hydrographs are shown in Figure 28. It was derived by averaging the four highest discharge peak hydrographs in the historical series. The design hydrograph for

Karonga has a sharp peak of only a few days, because of the smaller catchment size (fast response).

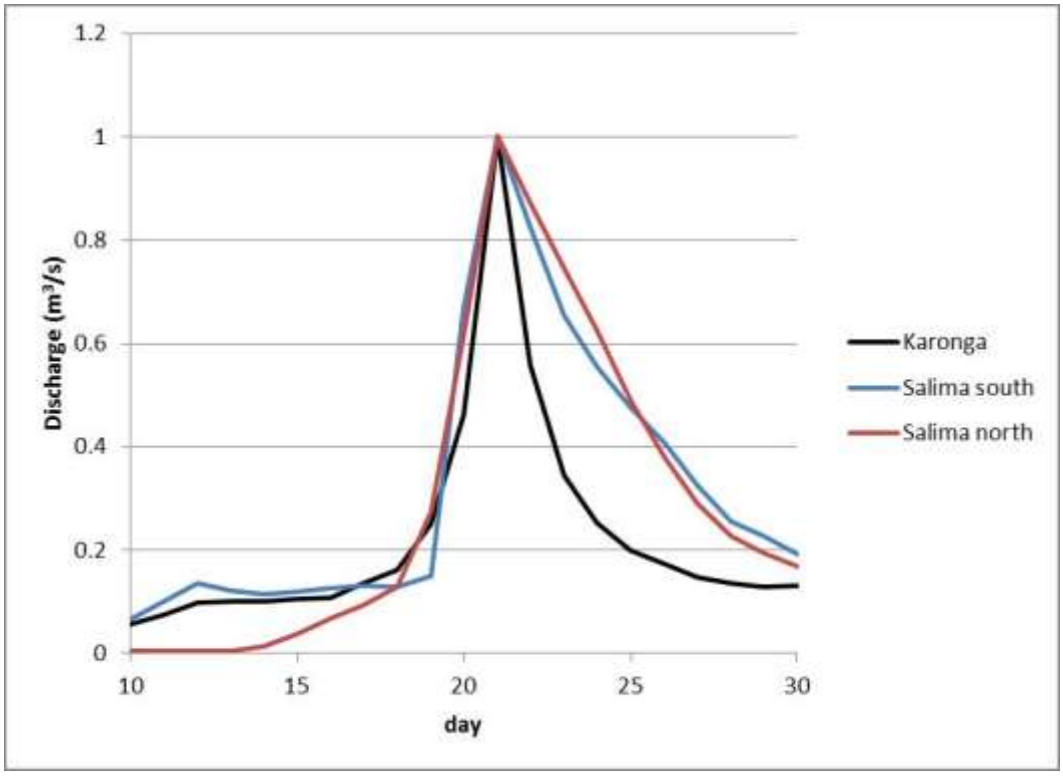

Figure 28: Normalized hydrograph for inflow boundary conditions of Karonga and Salima models.

The correlation between the two inflows of the Salima model was investigated in the 32-year EU-WATCH series. Figure 29 shows a scatter plot of the discharges at the two stations. It was found that the correlation is rather high (correlation coefficient of 0.98 for all data and 0.82 for the discharges above a 100m^3/s threshold). The two inflows were therefore assumed fully correlated in the flood mapping simulations, although this is somewhat conservative.

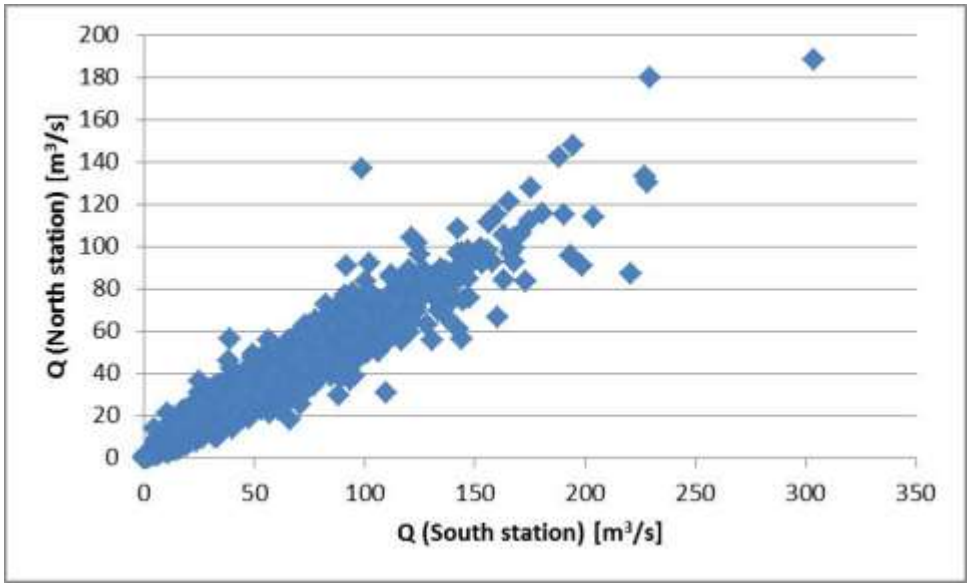

Figure 29: Scatter plot of discharges at the two Salima model inflow stations.

The Karonga flood maps for T=10 yr return period are shown in Figure 30. Both methods indicate that several areas north of the river will be flooded, although the HAND mapping method indicates smaller extents of flooding. Most of the inundations on the south bank are not reproduced by the HAND mapping method. The 2D hydraulic model predicts a diversion of the North Rukuru River towards the south, which connects to an existing stream that flows into Lake Malawi (on the right edge of the map). In the HAND mapping method this stream belongs to a different catchment, and because surface water cannot be redistributed from one catchment to another, the extent of the inundation on the southern bank is much smaller. The diversion of the North Rukuru River is an example of a complex flow pattern that cannot be reproduced by the HAND mapping method as already discussed. The small isolated flood in the north is also an artefact of the HAND mapping method.

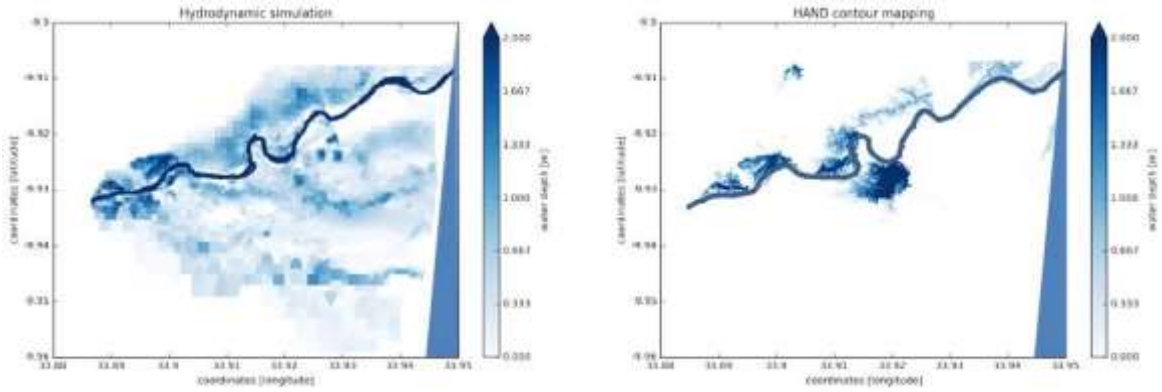

Figure 30: T=10 flood maps for Karonga from 2D hydraulic model (left) and HAND contour mapping (right).

The Salima flood maps for T=10 yr return period are shown in Figure 31. Several flooded areas match between the two maps, but there are also some important differences:

- The southern river branch just before the confluence is missing in the HAND map. This is due to the fact that the river is very shallow here and the TanDEM-X is very noisy. In the 2D model, the DTM is artificially lowered by the water mask.
- The shapes of the inundations on the south bank differ between the 2D model and the HAND map. In the 2D model, the water fills the flood plains just south of the main river. In the HAND map, the inundation follows the floodplains of a tributary. This is due to water being redistributed from the main river to flood plains of nearby tributaries.
- The isolated inundation in the North West corner of the HAND map is an artefact. Although this area is certainly floodable, the water depth for T=10 is overestimated

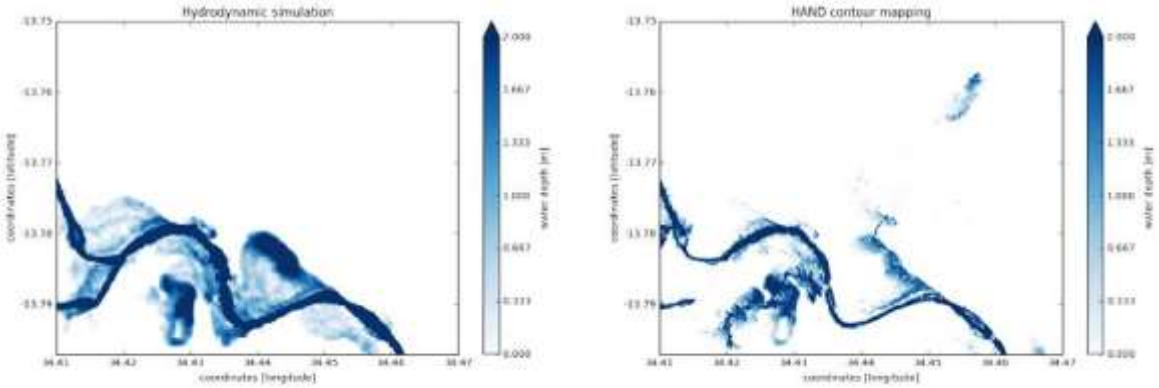

Figure 31: T=10 yr flood maps for Salima from 2D hydraulic model (left) and HAND contour mapping (right).

Maps for other return periods are included in Appendix A. In general, the flood maps show similarities, but also some differences, which can be explained by one of the shortcomings of the HAND mapping method that were described in section 5.4.2.

5.4.4 Pluvial flood maps

Pluvial flood maps for northern Malawi were computed following the procedure described in section 5.3.6.The maps are based on the non-riverine water in the 1km WFLOW grid cells for a range of return periods, derived from design rainfall events. The T=2 yr non-riverine water was subtracted as a threshold, to discriminate between surface water in natural and urban drainage after heavy rain and true flooding. A spatial smoothing was applied to remove the hard boundaries of the 1km grid cells and to obtain a gradually varying pluvial flood hazard that in a way reflects the uncertainty of the actual flood locations and depths. We stress that these pluvial flood maps give only an indication of the pluvial flood hazard. Pluvial flooding is very much a local effect and the actual flood depths will depend on the terrain features on smaller scales than the 1km WFLOW grid.

A 40x25km excerpt of the pluvial flood map for T=10 yr is shown in Figure 32. The map shows the 1km grid cells and water depths ranging between 0 and 10cm. Several ‘streams’ can be identified that were (apparently) too small to be recognized as one of the main rivers in the WFLOW model (Figure 11). This surface water is defined as non-riverine water and thus regarded as pluvial flooding. Some of these streams flow directly into Lake Malawi. Others

flow into one of the larger rivers of Figure 11. In the center of the figure, a pluvial stream gradually increases and then turns into a river with associated fluvial flooding. This illustrates the difficulty in discriminating between pluvial and fluvial flooding. When pluvial surface water enters a small stream it turns into a fluvial flow, but even a 12m high resolution DEM is not able to identify these small streams and will treat them as pluvial water until it reaches a larger river.

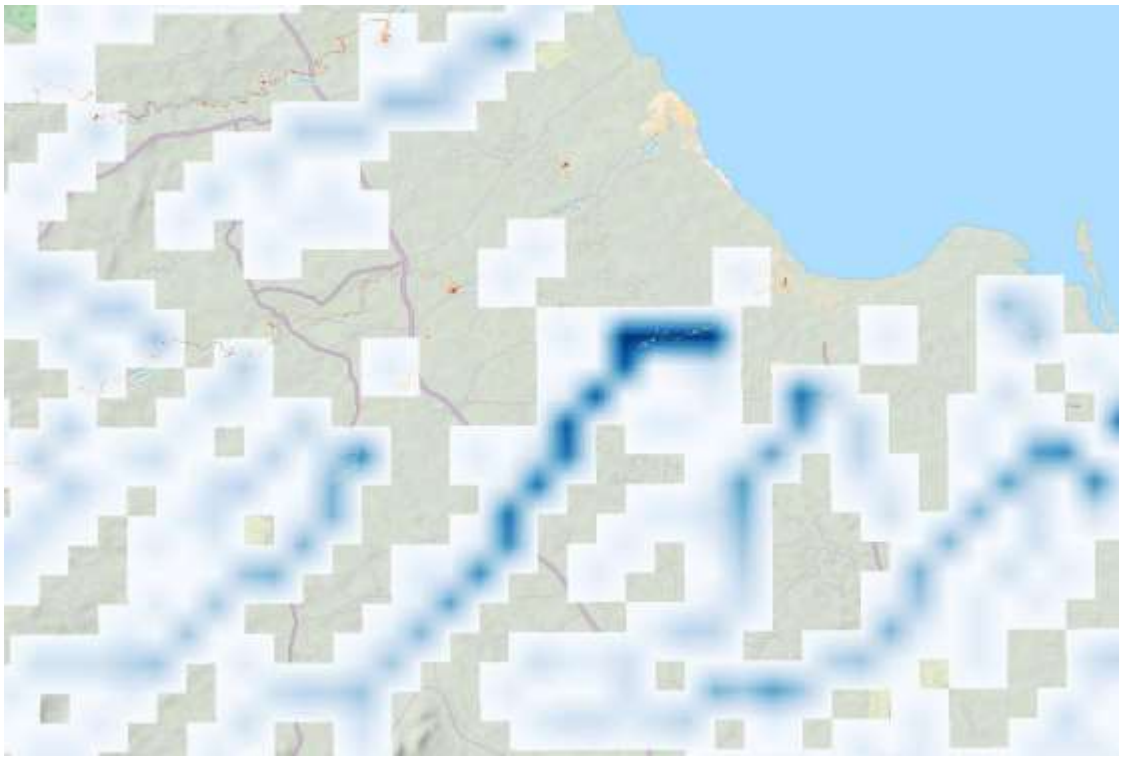

Figure 32: Excerpt from the pluvial flood map (T=10) for northern Malawi. Water depths (in blue) are up to 10cm. The fluvial flood map for the same return period is shown in orange-red colour.

5.4.5 Pluvial flood maps validation - hotspot Mangochi

The pluvial flood maps were validated by using a different approach, i.e. by employing a 2D hydraulic model to a hotspot area, near the city of Mangochi. This area has no large rivers except for the Shire River that flows from Lake Malawi past Mangochi into Lake Malombe. Flooding from the Shire River (or from Lake Malawi) was not included in this study. There is

however, a possible pluvial flood hazard in this area, especially to the north and south of the city.

The Mangochi model has no inflow boundary condition but only direct rainfall. The streams that flow north and south of Mangochi town into Lake Malawi and the Shire River are dry most of the year, except after excessive rainfall. The SOBEK-FM model simulates the rainfall runoff and ponding of low terrain. Figure 33 shows the T=10 yr return period pluvial flood map of the city of Mangochi and surroundings. Distinct areas can be identified where water depths reach a few dm. The rest of the area is inundated by a few cm at most.

The post-processed TanDEM-X DTM was used for most of the terrain in this model. However, part of an important drainage basin on the south side was missing from the DTM. Therefore, the terrain map was extended using the raw TanDEM-X DEM. This DEM product contains more noise, as can be seen in Figure 33.

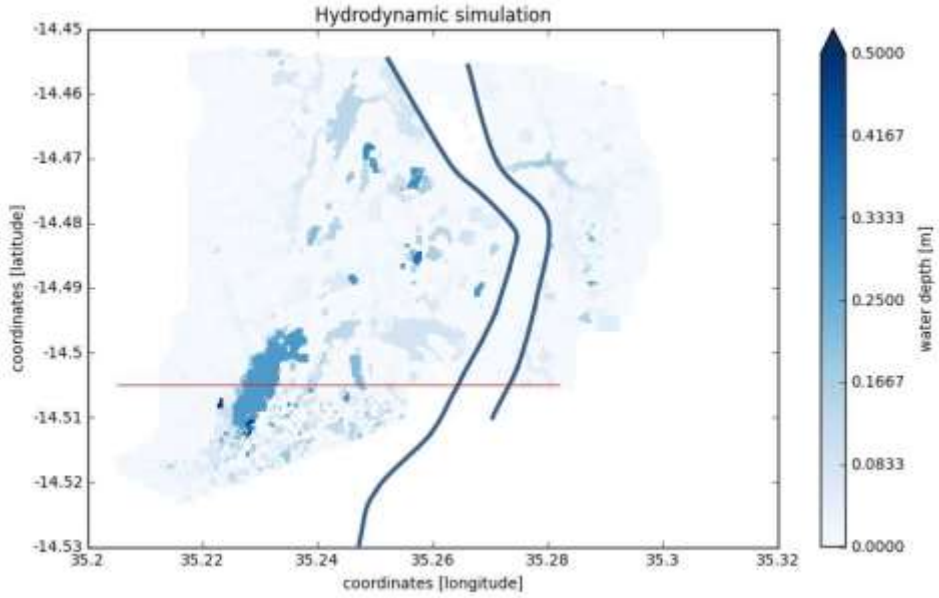

Figure 33 Pluvial flood map for the city of Mangochi and surrounding area, T=10 yr return period. The Shire River runs north-south (indicated by thick blue lines). South of the red dashed line the terrain model was derived from the unprocessed DEM, which causes more noise here

An excerpt of the larger flood map for the whole of northern Malawi is shown in Figure 34. The areas that are indicated as flood prone in Figure 33 are not resolved by this map, except for a stream on the east bank of the Shire River. This illustrates that pluvial flooding is very much a local effect and that the 1km grid is too course to resolve many of the smaller features in the pluvial flood map.

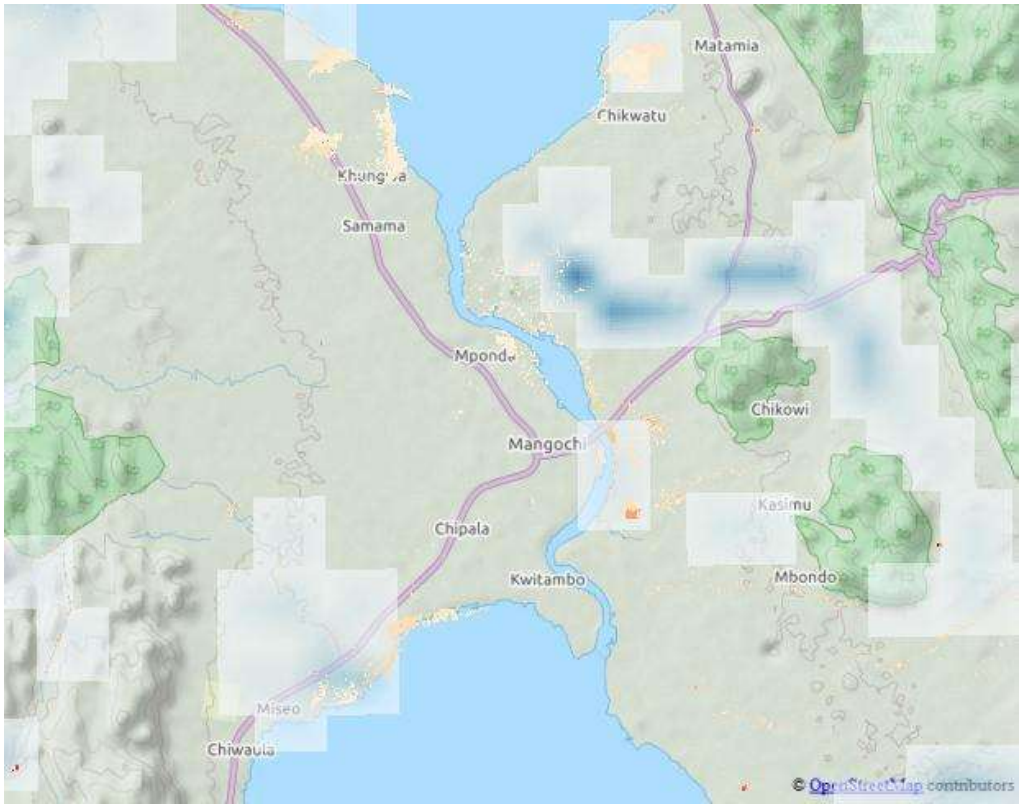

Figure 34 Pluvial flood hazard for Mangochi and surroundings according to the larger map for northern Malawi.

5.5 Discussion

Fluvial and pluvial flood maps have been computed for northern Malawi using TanDEM-X elevation maps, a combination of hydrologic and hydraulic modelling and an innovative HAND contour mapping method. A validation of this HAND mapping method was done for a number of hotspots to assess the accuracy of the maps.

The conclusion is that, in general, the flood maps are realistic. However, the HAND contour mapping method has a number of limitations that need to be taken into account:

- Complex flow patterns cannot be reproduced by the HAND mapping method. Examples of complex flow patterns are river diversions, such as upstream of Karonga, and the blocking effect of levees or natural elevations in the landscape. In the first case, certain areas will stay dry in the fluvial flood map that are actually flooded. In the second case, the opposite happens.
- The accuracy of the HAND contour mapping strongly depends on the accuracy of the DEM. Elevation offsets due to forests and buildings cause an underestimation of flood depth. Wherever a patch of urban or forest area stays dry while the surrounding land is inundated in the flood map, this is probably an artefact.
- Isolated inundations of small, elevated plateaus in the HAND flood maps are suspicious. The water depth for these areas is probably overestimated.
- Flooded areas on the shores of Lake Malawi are artefacts of the HAND mapping method due to the high level of noise in the DEM caused by the lake water.

The fluvial maps should thus be used with consideration of these limitations.

Pluvial flooding was defined as flooding by surface water that is not part of the fluvial flood analysis. This includes small streams. Pluvial flood maps were derived directly from the WFLOW surface runoff over the saturated soil. The resolution of the WFLOW hydrologic model is much lower than the 12m DEM resolution. The pluvial flood maps are therefore only

an indication of where the pluvial flooding might occur. The actual flood depths will depend on the terrain features on smaller scales than the 1km WFLOW grid.

5.6 Flood impact model

The third component of the flood risk framework combines the hazard maps with flood impact models at the same resolution to generate indicators for flood risk, including annual expected damage, affected GDP and affected population. The impact module can use the current population and GDP estimates, but also future population and GDP. The model framework is further described in Winsemius et al. (Winsemius et al., 2013) and Ward et al. (Ward et al., 2013).

The impact module is based on a mix between RASOR libraries and the Delft-FIAT Flood Impact Assessment Tool. Delft-FIAT has been developed by Deltares in the last three years and was applied in several flood risk studies around the world. The tool enables the assessment of flood impacts and risks for different flood scenarios in a flexible and efficient manner. The following figure shows the schematics of Delft-FIAT, which can handle various types of input data and formats and is compliant to geotiff, QGIS and other open (spatial) standards.

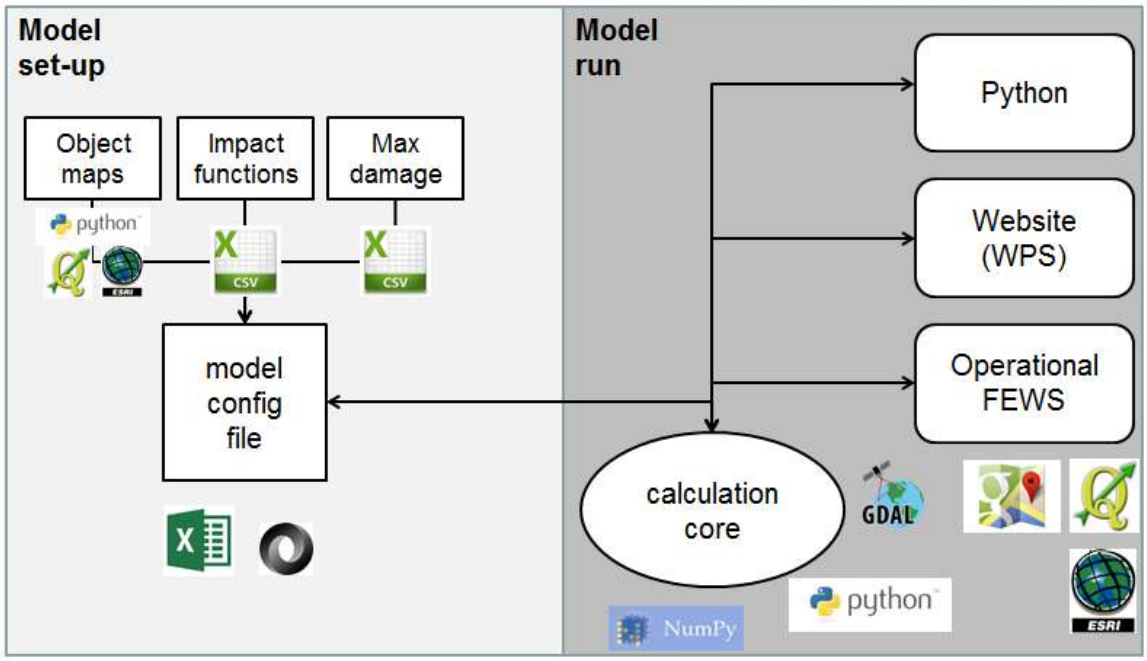

Figure 4: Delft-FIAT schematics for the flood impact assessment.

Flood impacts have been assessed with Delft-FIAT in two ways: i) by calculating the affected exposure for various exposure classes, and a subsequent quantification of monetary damage for some classes; and ii) for point/line/polygon information for critical facilities and transportation network. In both cases, impacts have been assessed using inundation maps of the entire time series (i.e. maximum inundation during each year), and for the inundation maps corresponding to the return periods of interest. Calculations have been performed at raster level using the exposure data prepared within this assignment starting from open available information, and aggregated to the national level (admin level 0) and for sub-nation administrative regions (admin level 1); according to the boundaries provided by the World Bank. We split the results into maps (raster/vector layers) and indicators (see table below), which can be used for the in-depth dialogue with World Bank and local authorities on the impact that hazards have on their economies and population.

Table 2: Results of the flood impact analysis.

Indicator	*Data type*	*Data Source*	*required information from sub-project on "Exposure analysis"*	*Results*
Human settlements (towns, cities, villages)	Raster layer	Combination of the LEO based Land Cover, GHSL at landsat resolution and the World Pop and statistics based on GEM developed study from USAid	Number of buildings per grid cell, Average footprint area per building, Average number of stories, total value, per building category	monetary damage on residential buildings (raster layer), No of buildings affected (indicator)
Transport networks - Highways - Other paved roads - Unpaved roads - Railroads	Vector layer (line elements)	Local Data from MASDAP if available, Vmap0	Transport network type	monetary damage on transportation infrastructure (vector layer), No of streets affected (indicator)
Critical facilities - Schools - Hospitals - Energy generation facilities	Vector layer (point elements)	Local Data from MASDAP if available, Vmap0	- Units, classified by infrastructure type - Dollar value per unit	Map with location of critical facilities affected (vector layer), No of critical facilities affected (indicator)

Population density	Raster layer	Afripop	Population density (people per grid cell)	Affected population (raster layer), affected population (indicator)
GDP density	Raster layer	WB Global GDP distribution	GDP density (GDP per grid cell)	Affected GDP (raster layer), affected GDP (indicator)
Crop distribution	Raster Layer	MapSPAM (Spatial Production Allocation Model) database	Crop type, crop productivity, crop yield	monetary damage on Agriculture (raster layer), Total crop Damage

Direct damage in monetary terms has been calculated for property damage in human settlements, and for losses in commercial agriculture.

The calculation of physical property damage is done using the classical approach of stage-damage functions (i.e. a specific family of vulnerability functions). These consist of a set of curves and values at risk for different land use classes. The curves relate the inundation depth found in a grid cell to the fraction of total value at risk that can be inflicted by a flood for that

specific land use. This fraction multiplied with the value at risk results in the flood damage for that grid cell (see figure below for an example).

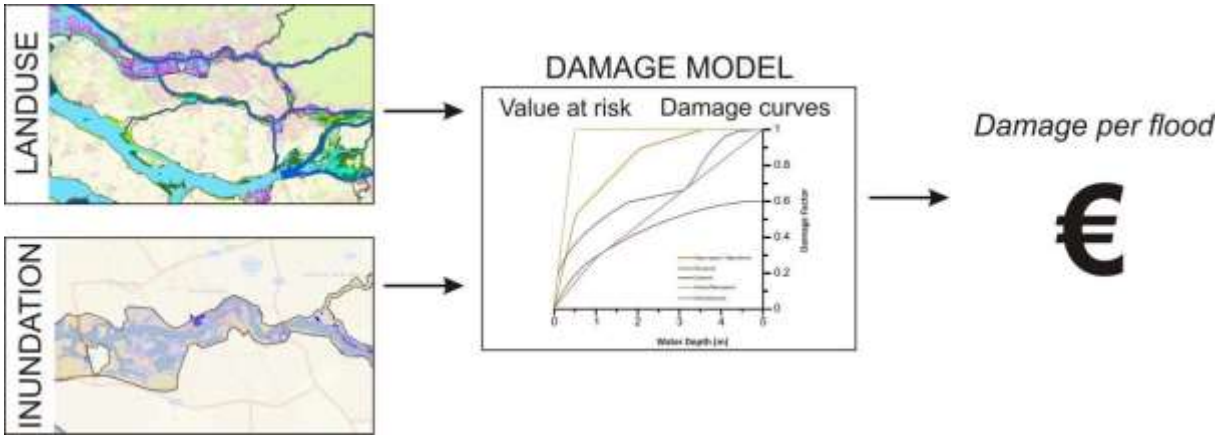

For this approach, it is crucial that the stage-damage functions are well aligned with the exposure information. Exposure and vulnerability functions for Malawi will be detailed in the following sections. Stage-damage functions usually relate to buildings itself, where the exposure data differentiate between three classes of human settlement (Traditional, semi-permanent, permanent settlements)).

There are no specific functions in the literature developed for Malawi and few reference studies that used Vulnerability curves in the African context (e.g. World Bank, 2000; Villiers, 2007). As a starting point the large literature search developed by VU-IVM with the scope of creating globally consistent damage functions for the Joint Research Centre (JRC) have been used as a starting point.

On the basis of the consultant experience some internationally available stage-damage curves proved appropriate to be applied in developing countries. This is the case of Capra curves that have been adapted to the African region within the context of GAR (Global Assessment Report) (CIMNE and INGENIAR, 2015 *CIMNE and INGENIAR, 2015. World Summarized Catastrophe Risk Profiles. Summary by Country on the Results from the Global Risk Model*) and are referred to main types of buildings commonly found in these areas. However, specific building typologies are found in

Malawi; thanks to the cooperation with local experts such typologies have been isolated and describe so that it has been possible to better adapt the Capra curves to the Malawi context (see, vulnerability analysis in the following)

For agriculture, a first assumption that catastrophic flooding will result in a loss of the yield of that year. This is estimated by first calculating the agricultural area affected per flood simulation. However, a crop can be replanted if the flood occurs in the period of possible plantation, and if the soil dries in the same period. Thus, the loss function can be modified by taking into account an initial and a final planting dates if those pieces of information are available allowing for a more accurate estimate. The agricultural has been derived from the MapSPAM (Spatial Production Allocation Model) database, which is also the basis of the agricultural risk assessment. This database provides maps for various crop types at a resolution of 10km (You et al., 2014), including the crop area.

Losses to human settlements and commercial agriculture of the individual years and the seven return periods have been used as input for post-process statistical analyses in order to derive average annual losses (AAL) for the admin 0 and admin 1 regions.

5.7 Exposure data for Malawi

This chapter provides background information about the elaboration of exposure data of built-up area, population and annual crops for Malawi.

5.7.1 Population

Population data for North and Central Malawi are expressed in terms of number of people per pixel. Reference layer is the population layer developed by WorldPop (http://www.worldpop.org.uk/), a raster which represents the predicted number of people per ~100 m pixel, obtained using as input census/population count datasets and mapping of settlements and applying the random forest (RF) model as described in Stevens, et al. (In Press). The result is then obtained adjusting the national total in order to match UN population division estimates (2012 revision).

All the details are reported at:

http://www.worldpop.org.uk/data/WorldPop_data/AllContinents/MWI-POP_metadata.html

Figure 35 Overview of the WorldPop population layer in QGis.

5.7.2 Built-up area

Built-up area for North and Central Malawi has been obtained merging information from 3 distinct layers:

- WorldPop population layer
- 2010 Land cover from MASDAP
- Global Human Settlement Layer

5.7.2.1 WorldPop population layer

WorldPop population layer is the same population layer described in paragraph 5.7.1.

5.7.2.2 2010 Land cover from MASDAP

Malawi Landcover 2010 Scheme II has been developed from Landsat Imagery (30m by 30m) resolution using supervised classification. Classification Scheme II is such that it meets the

country specific mapping standards and can be rolled back to the six IPCC land over categories for Scheme I: Forestland, Grassland, Wetland, Cropland, Settlement and Other land. Further details can be found at:

http://www.masdap.mw/layers/geonode:malawi_landcover_2010_schema_2

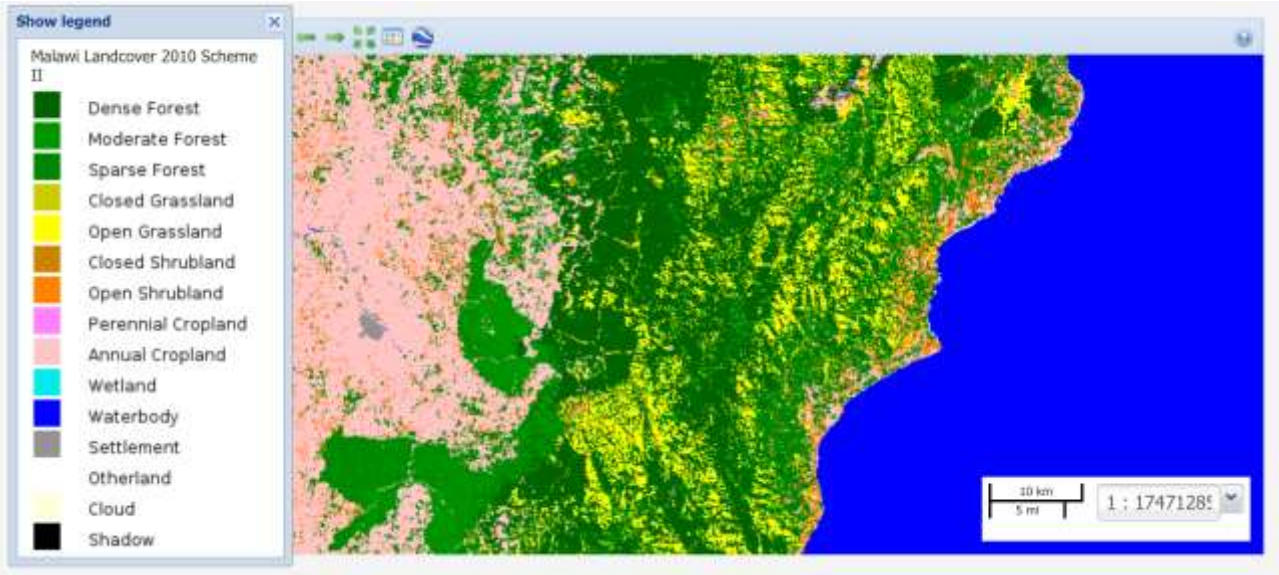

Figure 36 Overview of the Malawi Landcover 2010 Scheme II layer on www.masdap.mw

5.7.2.3 Global Human Settlement Layer (GHSL)

The Global Human Settlement Layer (GHSL) is a product developed and maintained by the Joint Research Centre, the European Commission's in house science service, born with the aim to detect and initially characterize built-up areas based on average size (scale) of built-up structures. GHSL is derived from HR and VHR optical remotely sensed data through an automatic image classification. This product identifies the built-up areas, intended as any given area or geographical space where buildings can be found.

Further details can be found at: http://ghslsys.jrc.ec.europa.eu

The GHSL mask used as input to create the final built-up area layer for Malawi has been obtained from different GHSL layers at around 30 meters of resolution, which have been merged to obtain the built-up area from 1975 till nowadays.

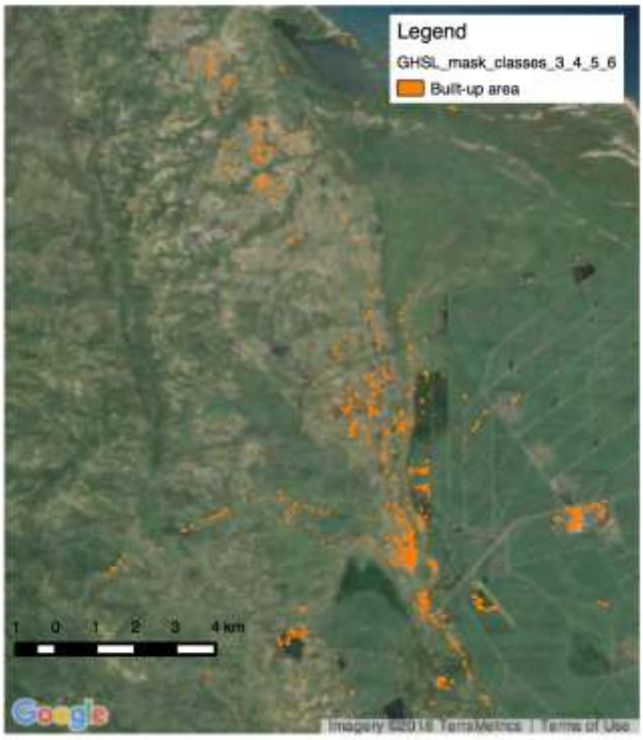

Figure 37 Overview of the GHSL in QGis

5.7.2.4 Creation of the built-up area layer

Sampling the information reported from these three layers together and comparing it with optical satellite imagery, the following considerations can be pointed out:

- class 12 of the Land Cover layer, representing the settlements, covers with a high accuracy urban and big rural settlements, while in is lacking in the coverage of small rural settlements and the scattered houses.
- The GHSL is quite inaccurate. There are many cases in which an area is indicated as built-up while in reality it is inhabited and vice versa. The point of strength of this layer is that is able in some cases to identify with a high accuracy small rural settlements and the scattered houses, which are ignored by the Land Cover layer.
- The population layer from WordPop distributes population with a good level of accuracy, covering both urban and rural areas. Very low values of population per pixel (lower then 3 people) are sometimes assigned in inhabited areas.

As a final result of this analysis, a comprehensive built-up area layer has been built merging the following pieces:

- Class 12 (settlement) of the Land Cover layer
- Areas where are simultaneously present both population with a density higher than 5 people per cell and the classes 8 and 9 (perennial/annual cropland) of the land cover. This is done to identify urban settlement not reported in class 12 of the Land Cover.
- Areas where are simultaneously present both population with a density higher than 3 people per cell and the GHSL, apart from those which coincide with the classes 1,2,10,11 (dense forest, moderate forest, wetland, waterbody) of the Land Cover layer. This third element is added to consider also very small rural settlements and the scattered houses, which are ignored by the Land Cover layer, but well captured by the GHSL. The population mask is used as a control to avoid incorporating areas that the GHSL indicates as built-up while in reality are inhabited.

5.7.2.5 Distribution of different building typologies

The built-up area layer has been further characterized in terms of the number of buildings belonging to the different building typologies present in North and Central Malawi. The reference building typologies are those introduced by the 2008 Population and Housing Census of Malawi (Lindstrom et al., 2014):

- PERMANENT: roof made of iron sheets, tiles, concrete or asbestos, and walls made of burnt bricks, concrete or stones.; these include caravans and tinned structures.
- SEMI-PERMANENT: lacking construction materials of a permanent structure for wall or roof.; these are structures, which are built of non-permanent walls such as sun-dried bricks or non-permanent roofing materials such as thatch.
- TRADITIONAL: both thatched roof and mud walls.

A survey on building stock in the three regions of Malawi (namely, North, Centre and South) has been conducted by the Global Earthquake Model inside the SSAHARA project. In this study, buildings are subdivided according the following construction materials:

- burnt bricks;
- unburnt bricks;

- concrete;
- mud/wattle;
- reed/straw;
- wood/plank;
- other.

For these categories, the number of housing in the three regions is available. The correspondence between these seven building stock material classes and the GEM taxonomy for building classification is reported in Table 3 Correspondence between the three housing typologies (permanent, semi-permanent, traditional) and the building stock material classes from GEM.

A correspondence between the three housing typologies an the classes of the census conducted by GEM has been identified and reported in Table 3.

Table 3 Correspondence between the three housing typologies (permanent, semi-permanent, traditional) and the building stock material classes from GEM.

Housing typologies	**Corresponding building stock material**
Traditional	Mud/wattle, Reed/straw, Wood/plank
Permanent	Burnt bricks, Concrete
Semi-permanent	Unburnt bricks

Table 4 Correspondence between GEM building stock material classes and the GEM taxonomy for urban settlements in Malawi.

GEM Taxonomy	Burnt bricks	Unburnt bricks	Concrete	Mud/Wattle/Dung	Reed/Straw	Wood/Planks	Other
CR/LFINF/H:1,2	10%		25%				
CR/LFINF/H:3,4	15%		25%				
CU/LFINF/H:1,2							
ER+ETR+RW+MOC/H:1,2				20%			
ER+ETR+RW+MOM/H:1,2				20%			
EU+ETC/H:1				30%			
EU+ETR/H:1				30%			
MCF+CBS/H:1,2			20%				
MCF+CLBRS/H:1,2	30%	20%					
MR+ADO+RW+MOC/H:1,2							
MR+ADO+RW+MOM/H:1,2							
MUR+ADO/H:1,2	10%	40%					
MUR+CBS/H:1,2			30%				
MUR+CLBRS/H:1,2	35%	40%					
MUR+STDRE/H:1,2							
MUR+STRUB/H:1,2							
W+WBB/H:1						20%	
W+WLI/H:1						20%	
W+WS/H:1,2						50%	
W+WWD/H:1					80%	10%	
UNK					20%		100%

Using this correspondence, the number of permanent, semi-permanent and traditional housing typologies for both North and Central Malawi has been computed and downscaled. Then, these

buildings have been redistributed on the built-up areas of the two regions proportionally to the number of people.

The final result is a series of 6 raster files, a series of three (one for each housing typology) layers per region (North and Center), with a resolution of 30 meters, which represent the expected number of buildings of a certain typology per pixel, in one of the two considered areas.

5.7.3 Agricultural production

Exposure data on the agricultural production have been based on layers publicly available at: http://www.masdap.mw/

Agricultural sites exposure has been characterized with the following attributes:

- localization (at 30m by 30m resolution);
- annual production (tons);
- production price (USD/tons).

Agricultural production layers provide information on the annual production (tons) for the following different annual crops:

- cassava
- cotton
- groundnuts
- maize
- pigeon peas
- potatoes
- rice
- sorghum
- tobacco

The choice of crops typology to consider in the analysis has been made partially considering the relevance of the single crop in the Malawian production, and partially on the basis of data availability (not only for exposure characterization, but also for vulnerability description).

Data availability concerns 3 different types of information, which are all necessary in order to carry out a complete economic damage assessment for crops:

- annual production
- production price
- damage curves

For Malawi, all these three pieces of information are available only for a series of crops, which are those highlighted in yellow in the following table:

	PRICES		PRODUCTION	CURVES
	Producer price	Retail price		
Beans	**1**	**5**		
Bananas	**1**	**6**		
Cassava	**1**	**5**		
Cotton	**2**			
Groundnuts	**1**	**5**		
Maize	**1**	**5**		
Pigeon peas	**1**			
Potatoes		**6**		
Rice	**1**	**5,6**		
Sorghum	**1**			
Sugar cane	**3**			
Sweet potatoes				
Tempered fruit				
Tobacco	**4**	**4**		
Tropical fruit				
Wheat				

LEGEND

1	Source: http://faostat.fao.org
2	Source: FAO. Technical note: Analysis of price incentives for cotton in Malawi 2005-2013. April 2015.
3	Source: Average of ex-factory prices of sugar cane in Kenya, South Africa, Tanzania, Zambia in 2012 – African Competition Forum, Competition in the regional sugar sector: the case of Kenya, South Africa, Tanzania and Zambia – 2014.

4	Source: FAO – Issues in the global tobacco economy.
5	Source: WB
6	Source: http://www.numbeo.com/cost-of-living/country_result.jsp?country=Malawi
	available data

Table 5 Availability of data on prices, pruduction and damage curves for a series of crops in Malawi.

NOTE: Producer prices are available for cassava, cotton, groundnuts, maize, pigeon peas, rice, sorghum and tobacco. The only exception is potato, for which only retail prices can be found.

As already mentioned, availability has been considered together with the relevance of the crops, which has been estimated through the list of the top agricultural products published by FAO.[2] This list reports the top 10 agricultural products by gross production value for Malawi for the period 2005-2012. The list of the provided layers cover 7 over 10 of these products. In particular, it covers the top 6 of the list. The three products which are not covered are:

[2] http://www.fao.org/fileadmin/templates/mafap/documents/Malawi/MCR_May2015.pdf

- bananas
- meat of indigenous cattle
- beans

Bananas are not taken into account because they are not particularly vulnerable to flood. Meat is not considered because it is not a crop. Beans are the only significant product for which complete data are not available. Nevertheless, they cover the 8th position in the FAO list.

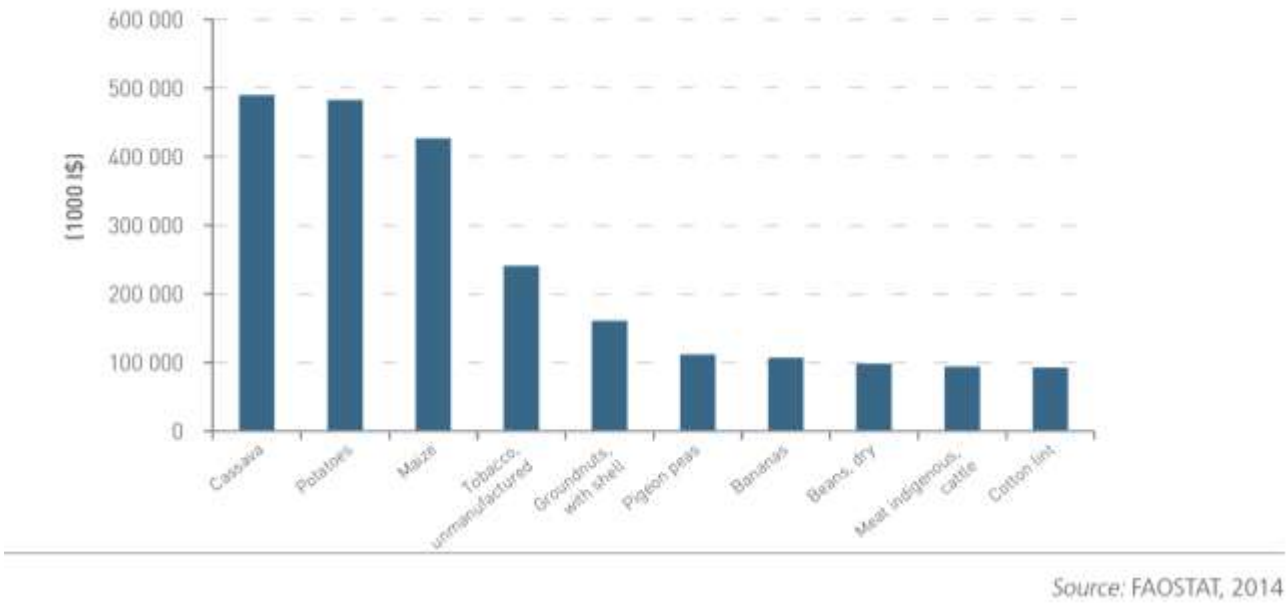

Figure 38 Top agricultural products by gross production value, average 2005 – 2012. Source: FAOSTAT, 2014.

Layers resolution is about 9km x 9km. Those data have been downscaled taking into account the areas actually covered by annual crops at a much finer resolution of 30m, which have been extracted from the "Malawi Landcover 2010 Scheme II". The Land Cover maps have been developed from Landsat Imagery (30m by 30m) resolution using supervised classification.

Image interpretation was done per scene. Images used for classification were selected based on seasonality, dry season images preferred.

With the downscaling procedure, the total amount of crop production of 9km x 9km cell has been homogenously distributed in 30m x30m annual crop cells. The 30m x30m non-annual crop cells do not contribute to the production. Due to the complexity of the domain and the fine resolution of the analysis, it has been computed using raster layers. Vector analysis is in principle possible, but strongly discouraged due to the complexity of the polygons considered, unless the domains is split in many sub-domains.

Instead raster analysis allows the implementation of this procedure, at the same time for the whole territory of Malawi.

The result is of these two procedures is a 2-band raster file (geotiff), with the following information for each crop type:

- annual production of the crop in tons (in the 1st band)
- price in USD/tons (in the 2nd band)

The file contains necessary metadata to correctly interpret the data such as type of crop and unit of measurement. Example of information contained in the file header is reported in Annex 1.

5.8 Vulnerability data for Malawi

This chapter provides background information about the elaboration of vulnerability data of built-up area and annual crop for Malawi.

5.8.1 Crops vulnerability

Examples of vulnerability functions for crops depending on flood intensity (e.g., water level) for crop areas exist in literature, see for instance Dutta et al. 2003[3]. These functions are usually defined for specific geographical areas and for a limited number of cultivation types.

In this context, another approach has been chosen, deriving crop loss functions by a loss estimation model based on the moment of the year in which the flood occurs. This choice is justified by the necessity of defining a model that could be applied to a specific area, without requiring an extensive amount of data.

The model that has been initially considered is the one adopted by the HAZUS Flood model, that is in turn based on the crop loss (damage) functions described in the AGDAM User's Manual (1985). Such functions describe the course of crop losses (expressed as difference among investment and net revenue) in the different periods of cultivation cycle, identifying 5 topic moments, namely: the beginning of cultivation, the end of cultivation, the crop maturity, the beginning of harvest and the end of harvest (see Figure 39). On the basis of these dates, four intervals are identified, in which crop loss (D(t) crop loss at day t of the year - % of maximum net revenue) is computed according to the specificity of the actions performed on the crop area:

- in a first period, only production costs are considered;
- in a second period, between the end of cultivation and the crop maturity, production costs, constant costs and net revenue are considered;
- in a third period, the potential loss is evaluated as the difference between gross value and harvest cost;
- in a fourth period, no crop loss is considered, the area is not cultivated (at least, non with the considered crop).

[3] Dutta, D., Herath, S., Musiake, H.: A mathematical model for flood loss estimation, Journal of Hydrology, 277(1–2), 24, 49, 2003. doi:10.1016/S0022F1694(03)00084F2

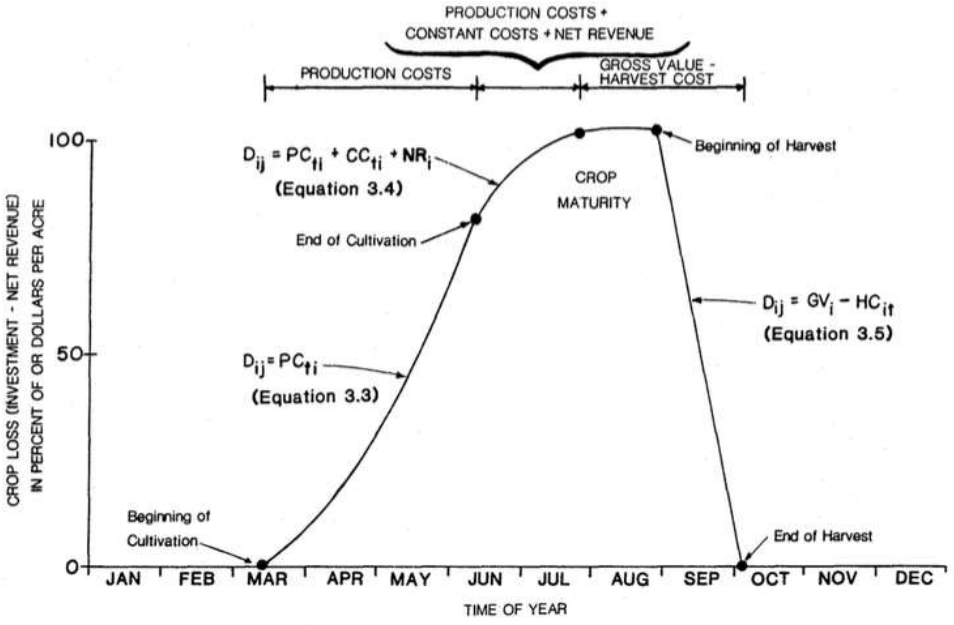

Figure 39. Crop loss function according to AGDAM (1985)

A crop can be replanted if the flood occurs in the period of possible plantation, and if the soil dries in the same period. Thus, sometimes the previous function is modified by taking into account initial and final planting dates (see HEC-FIA 2012). The Initial Plant Loss Function represents the damage incurred on any given date if the crop did not have to be replanted due to flooding, and if planting was not delayed due to previous flooding. The Last Plant Loss

Function represents the damage incurred, given the crop would not reach its full-yield potential because of late planting or re-planting. The two functions are depicted in Figure 40.

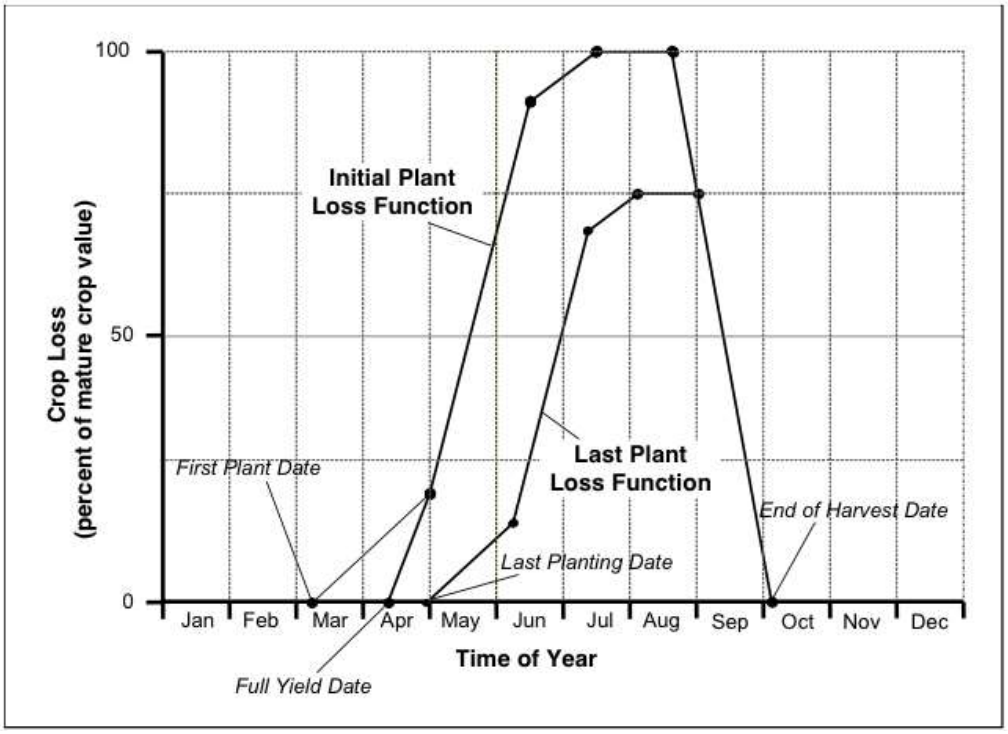

Figure 40. Initial and last plant crop loss function functions according to HEC-FIA (2012)

Then, a simple loss model can be applied:

$$L=A*(pY_0-H)*D(t)*R(t)$$

where:

L loss

A cultivated area

P price

Y_0 normal annual yeld

H harvest cost

D(t) crop loss at day t of year

R(t) a crop loss modifier for flood duration (percentage of maximum potential loss)

D(t) is evaluated on the basis of the functions previously introduced; to this end, in addition to the four cultivation milestones, some other information useful for the estimation of production and constant costs, of net revenue, of gross value and harvest cost must be known.

In addition, all the other information previously listed must be provided in order to compute damage to crops in case of flood event.

This amount and variety of information makes the approach well adjustable to the specific crop and to the specific geographic area; at the same time, the objective of defining a model usable with a limited amount of specialized information is not reached.

Focusing on information on food crops, FAO provides country-level information on some specific cultivation types, such as sowing, growing and harvesting periods. Thus, a simplified model based on these periods is proposed. Like in the previously introduced functions, the production is considered to be growing until the end of growing season is reached; then, during the harvesting period the presence of crops in field decreases linearly (see Figure 41, the presence of crops in field is depicted with the blue line).

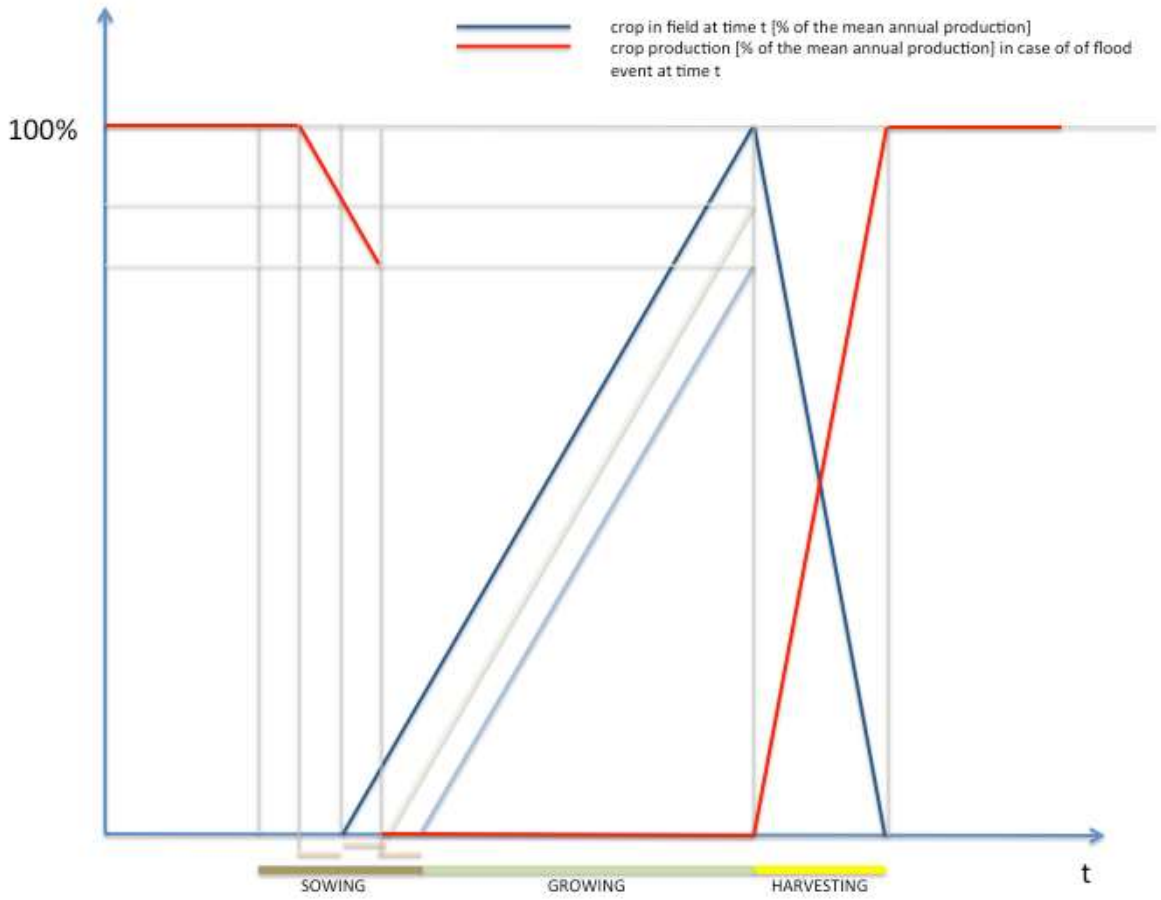

Figure 41. Percentage of crop presence in field (with respect to the mean annual production) – blue line – and crop production percentage (with respect to the same mean annual production) in case of flood event at day t of the year – red line.

If a flood occurs during the sowing period, and the soil dries before the end of such a period, crop can be planted again. Considering a growing rate equal to the one that the crop could have when planted in the middle of the sowing period, the crop will reach percentage of production

– with respect to the mean annual production – that depends on the available time till the harvesting period (see the light blue line in Figure 41).

- Then, a production function in case of flood event can be derived, based on the following assumptions:
- no production can be obtained if the flood occurs during the growing period (if this is not overlapped with the sowing period);
- considering a Δt interval in which the soil dries after a flood event, no production can be obtained if the flood occurs after the time "end of sowing-Δt");
- in the time interval between the middle of the sowing period and "end of sowing-Δt" the production decreases according to the decrease of available growing time before the harvesting time;
- outside the periods of sowing, growing and harvesting, the production is considered at its maximum value (i.e., 100%) as it is assumed that the flood event doesn't affect the production cycle.

As a result of these considerations, a general the crop production function is derived, and it is depicted in red in Figure 41.

5.8.2 Crop loss functions for Malawi

Crop loss functions for Malawi have been developed by applying the model described in paragraph 5.8.1. When possible, FAO data[4] have been preferred; in some specific cases other sources have been applied, specifically Negri and Porto (2008) for tobacco, Nsanjama, R. A.

[4] http://www.fao.org/giews/countrybrief/country.jsp?code=MWI

(1984)[5] for potatoes, MAFAP (2012)[6] for groundnuts, ICLARM – GTZ (1991)[7] for Cotton, Sweet Potato and Pigeon Peas.

As an example, the loss function for rice is reported in Figure 42.

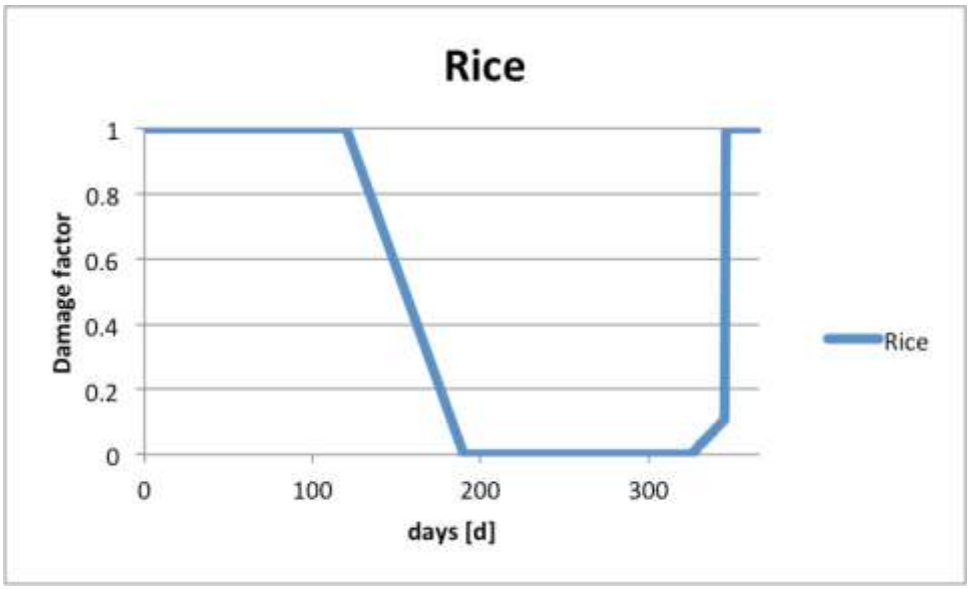

Figure 42. Rice loss function

5.8.3 Application of crop loss functions

Crop loss functions are applied whenever a water depth higher than zero is present on the cropland.

Damage factor, which measure the expected damage due to the presence of water for that specific type of crops, is a function of the period of the year in which the flood occurs. For this reason, together with hazard maps of the flooded area, also a temporal dimension should be

[5] Nsanjama, R. A. 1984. Report on Potato Production in Malawi. International Potato Course: Production, Storage, and Seed Technology. Report of Participants. International Agricultural Center, Wageningen, The Netherlands.
[6] MAFAP. Analysis of incentives and disincentives for groundnuts in Malawi. October 2012.
[7] ICLARM - GTZ. The context of small-scale integrated agriculture-acquaculture systems in Africa: a case study of Malawi. 1991.

considered. In other words it is necessary to know in which period of the year a flood can occur in the area.

This type of information can be deducted from the following picture, which shows the monthly peak discharge in different sections along the Malawian river network. Looking at the graph it is possible to deduce that December and January are the months in which it is mostly probable to have a flood.

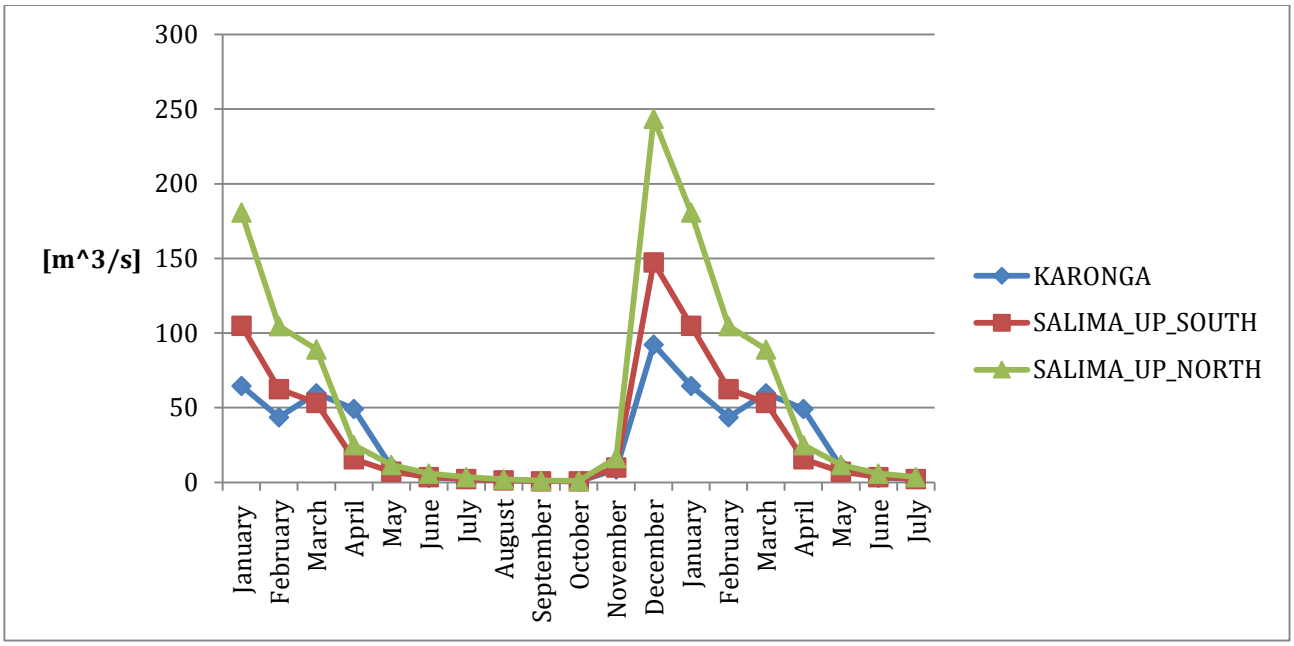

Figure 43 Monthly peak discharge recorded in different sections along the Malawian river network .

It is of course not possible to know exactly in which specific day of the year a flood can occur. As a consequence, it could happen that a certain crop loss function has a strong change in behaviour inside the considered time window (December-January), such as a curve that passes from zero to one, and it is not possible to assign a unique value of expected loss.

The criterion adopted is the one which ensures to not underestimate the total loss. The expected loss is the highest value reported on the curve in the time window which covers the months of January and December.

5.8.4 Buildings vulnerability

As previously mentioned, the 2008 Population and Housing Census of Malawi divides house types in the country into 3 categories (Lindstrom et al., 2014): permanent, semi-permanent and traditional.

In order to obtain vulnerability functions for these three typologies, the starting point has been the CAPRA[8] flood vulnerability library, and more precisely to the functions adapted to Malawi. In this collection, vulnerability functions are defined for different construction materials and for different number of stories of the considered building.

Referring to the first aspect, namely the construction material, the functions that are of interest for this study are:

- concrete;
- masonry;
- earth;
- wood.

The functions, representing the per cent damage for different water levels, are obviously different when the number of stories of the building varies. As in this study the damage assessment can't be performed at single building level, a representative building height for the considered building stock has to be chosen, and consequently the most appropriate vulnerability function to be assigned.

In order to do so, the survey on building stock carried out by GEM (see paragraph 5.7.2.4) has been considered. In this study, buildings are subdivided in categories according the construction materials. A correspondence between these categories and the building materials considered in

[8] http://www.ecapra.org

CAPRA, as well as the housing typologies, is reported in the following table. Please note that, being the number of corresponding housing negligible, the "other" typology has been omitted.

Table 6 Correspondence between the housing typologies, the building materials considered in CAPRA and the building stock materials from GEM classification for Malawi.

CAPRA - material					**Housing typologies**		
Concrete	Masonry	Earth	Wood	**Building stock material**	Traditional	Semi-permanent	Permanent
	X			Burnt bricks			X
	X	X		Unburnt bricks		X	
X				Concrete			X
		X		Mud/wattle	X		
		X		Reed/straw	X		
			X	Wood/plank	X		

Let's introduce the following indexes:

- h – generic housing typology (i.e., traditional, semi-permanent and permanent);
- r – generic region of Malawi;
- m – generic building stock material (e.g., burnt bricks, concrete, etc.);
- c – generic material for which a vulnerability function is available in the CAPRA collection, is available for Malawi and is considered in this study (i.e., concrete, masonry and earth);
- s – generic number of stories.

They can be used in order to define the following quantities:

- $y_h^r(x)$ – function expressing the per cent damage due to flood (water level x) for the generic housing typology h, in the generic region r;
- $y_c^r(x)$ – function expressing the per cent damage due to flood (water level x) for the generic material used in CAPRA collection c, in the generic region r;
- F_m^s - parameter expressing the ratio of housing that – in the overall number of housing belonging to class m – have s number of stories;
- N_m^r - parameter expressing the number of housing belonging to class m in region r;
- $w_{c,m}$ – parameter expressing the weight (importance) of the generic material used in CAPRA collection c with respect to the generic building stock material m;
- $\varphi_{m,h}^r$- parameter expressing the relevance of the generic building stock material m in region r with respect to the generic housing typology h; it assumes value in the interval [0,1], being 0 a null relevance, and 1 a complete relevance
- $\delta_{h,m}$ - binary parameter, whose value is equal to 1 if the building stock material m can be associated to the housing typology h, and 0 otherwise;

The damage due to flood for the generic housing typology can be thus expressed through the following expression:

$$y_h^r(x) = \sum_{c,m,s} y_c^s(x) \cdot w_{c,m} \cdot F_m^s \cdot \varphi_{m,h}^r \cdot$$

The parameters $w_{c,m}$ and $\delta_{h,m}$ are derived by expert judjment on the basis of the information that have been collected from the Malawian GFDRR team, whereas parameter N_m^r can be derived by the already introduced SSAHARA project. Also parameter F_m^s is derived from the same study, by considering the decomposition of each building stock material into classes corresponding to the GEM taxonomy and the average number of stories of these classes.

Finally, parameter $\varphi_{m,h}^{r}$ can be derived from the World Bank study according the following expression:

$$\varphi_{m,h}^{r} = \frac{N_m^r \cdot \delta_{h,m}}{\sum_m N_m^r \cdot \delta_{h,m}}$$

The vulnerability functions obtained according to these expressions can be then modified according to specific peculiarities of the three housing typologies. The choices and the results obtained in connection to the three considered housing classes are described in the following sub-paragraphs.

5.8.5 Derived vulnerability functions for the selected housing typologies

Vulnerability functions for the three buildings typologies of Malawi have been developed by applying the methodology described in paragraph 5.8.3.

A typical traditional house in Malawi is depicted in Figure 44:

Figure 44 Traditional House in Malawi

The vulnerability function for traditional houses in North Malawi is reported in Figure 45 together with the curves from CAPRA from which the final curve has been computed. The reduction in vulnerability determined by the fact that the traditional houses in Malawi are on

average built on an elevated level is immediately visible in the stage – damage curve specialized for Malawi.

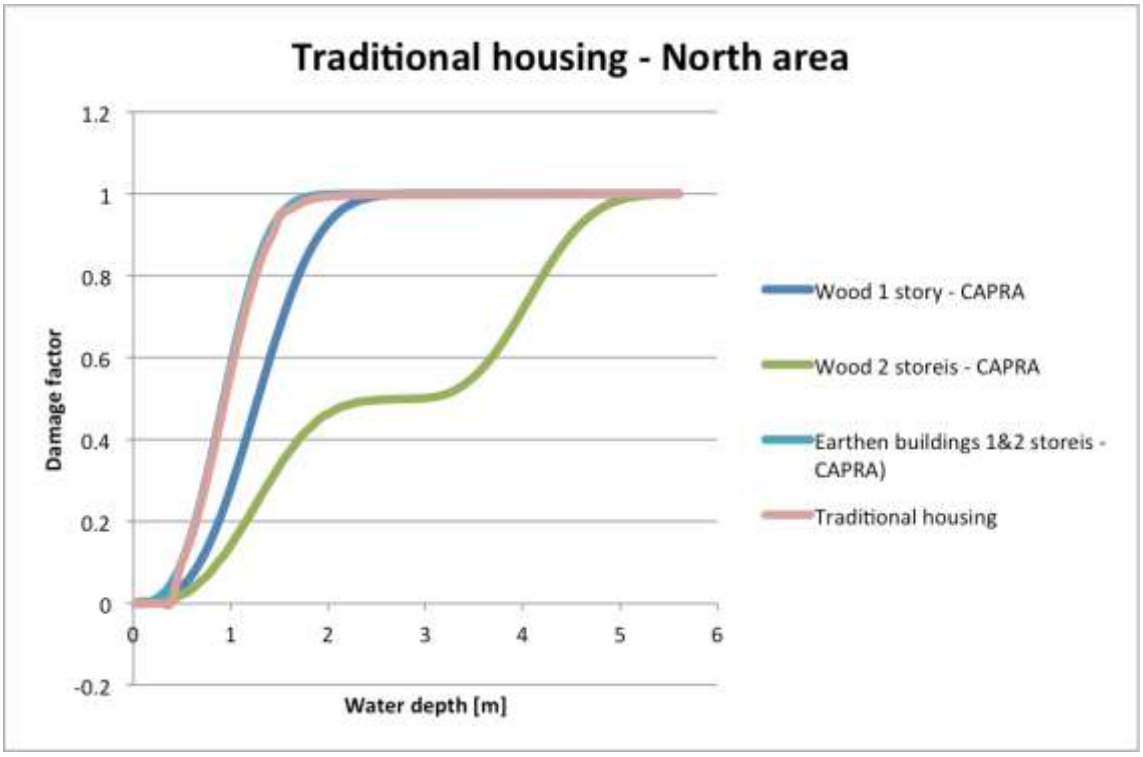

Figure 45. Vulnerability function for traditional houses in North Malawi shown together with the original CAPRA curves from which the final curve has been computed: wood 1 storey, wood 2 storeys and earthen buildings 1-2 storeys.

Similarly, Figure 46 depicts a typical semi-permanent house in Malawi and Figure 47 graphs the vulnerability function for this typology specialized for Malawi.

Figure 46 Semi-permanent House in Malawi

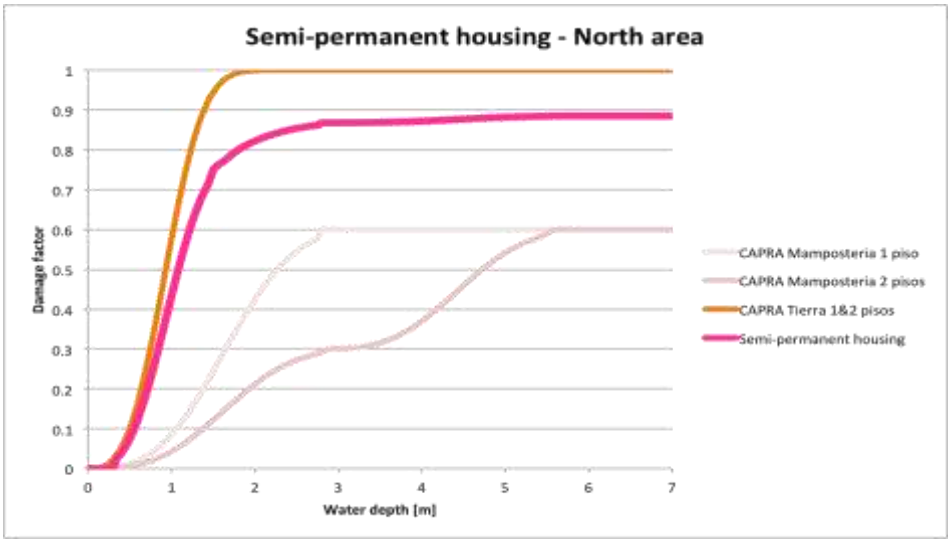

Figure 47. Vulnerability function for semi-permanent houses in North Malawi shown together with the original CAPRA curves from which the final curve has been computed.

As a last typology the permanent typology was considered that is by far the one with higher variance in construction techniques and number of storeys. Figure 48 and Figure 49 depict a typical permanent building in Malawi and it associated vulnerability curve respectively,

Figure 48 Example of-permanent House in Malawi

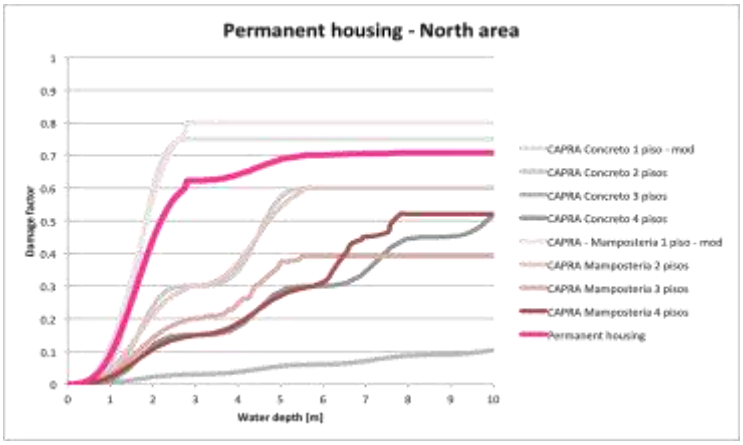

Figure 49. Vulnerability function for permanent houses in North Malawi shown together with the original CAPRA curves from which the final curve has been computed.

5.9 Risk Results

Damage is evaluated either as economic damage or in terms of affected people.

In case of economic damage evaluation, the replacement cost of the different feature typologies is obviously an essential parameter. The economic damage for each feature of each exposed

category is generally evaluated as the product of the corresponding damage factor and economic value.

When considering the built-up area, the economic damage for each pixel is composed by the sum of the corresponding economic damage of the pixel in connection to the three different housing typologies. The total damage is thus evaluated trough the following expression:

$$Total\ damage\ [\$] = \sum_{i=1}^{3} damage_i * nb_i\ *\ rc_i[\$]$$

Where:

- $i = 1, \dots, 3$ are the different building typologies present in Malawi (permanent, semi-permanent and traditional)
- $damage_i$ is the damage factor for the considered typology i, evaluated trough the damage curve, using as input the water depth [m] in the considered pixel
- nb_i is the number of buildings of the considered typology i, present in the pixel
- $rc_i[\$]$ is the replacement cost for an "average" building belonging to typology

$rc_i[\$]$ has been calculated considering an average replacement cost per square meter and an average building area for each typology.

The average building area for a given typology i has been computed through a weighted average of the areas of the building stock material classes (e.g. unburnt bricks, concrete, reed/straw…) which compose the considered typology. The relationships between typologies and building stock materials is reported in Table 6.

Damage to crops has been evaluated with an equation similar to equation ABOVE developed for buildings, in which the production cost of each crop is multiplied by a damage factor estimated through curves.

Affected population is identified counting the number of people inside the flooded area.

Results are presented in terms of Annual Average loss and losses for some reference quantiles from 2 to 1000 years return period composing a full PML curve. These parameters are presented both at the level of the administrative units (North, Centre and North+Centre, the latter including the areas around Mangochi pertaining to the south administrative area) (Table 8) and for the Hotspots of Karonga, Salima and Mangochi (*Table 9* and *Table 10*).

In the case of the hotspots a comparison between two different methodologies is presented. It is interesting to see how the two methodologies give similar results in the case of Salima where the hazard maps, although showing distinct behaviours in some areas, have a comparable footprint. On the contrary, in Karonga the impact indicators almost double in the case of the more detailed approach this mainly due to the erroneous representation of the urbanized area of Karonga in the non-processed DEM. That area is seen on the DEM as elevated due to the average quota of the buildings that is picked by the satellite sensor and in great part excluded from the exposed area. When a processed DTM is used jointly with at full 2D modelling approach that area that represent a good percentage of the asset in the area is included in the flooded area. This situation exacerbates in Mangochi where the difference in the risk indicators is one order of magnitude larger when analysed with the detailed approach. Here the main reason is actually ascribable to the flood modelling piece. Complex flow patterns are hardly reproduced by the HAND mapping method. Examples of complex flow patterns are river diversions and the blocking effect of levees or natural elevations in the landscape. In the first case, certain areas will stay dry in the fluvial flood map that are actually flooded. In the second case, the opposite happens.

All the results can be visualized trough the RASOR platform, which is available at www.rasor.eu. This platform allows to perform multi-hazard risk analyses for the full cycle of disaster management, including targeted support to critical infrastructures monitoring and climate change impact assessment.

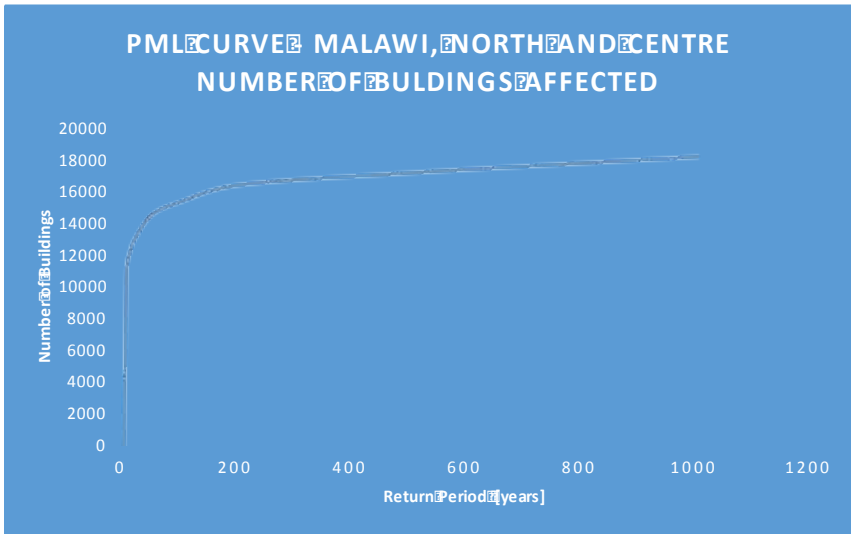

Figure 50 PML Curve for the numbers of buildings affected; the curve describes the number of buildings affected by the fluvial flooding for an event of a specific return period expressed in years.

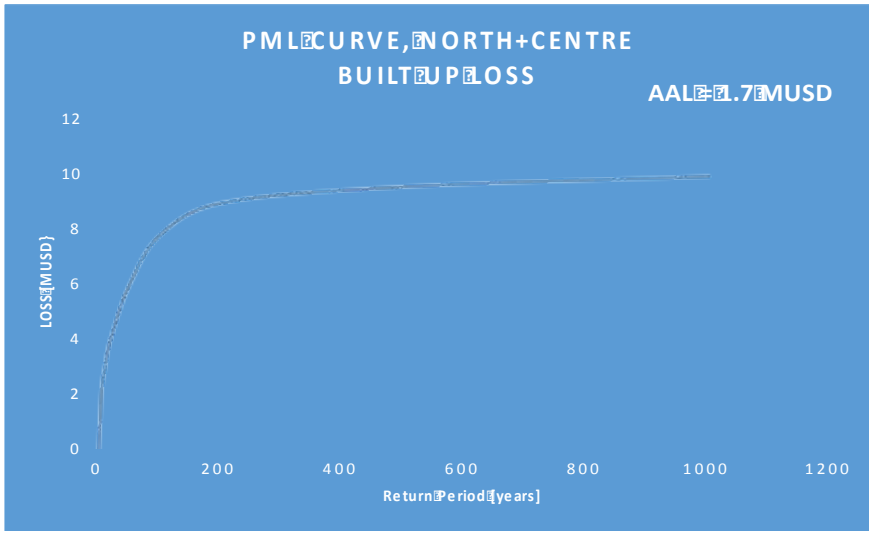

Figure 51 PML Curve for the losses of built up areas; the curve describes the losses to building by the fluvial flooding for an event of a specific return period expressed in years. The figure reports also the Average Annual Loss in MUSD for the built up area.

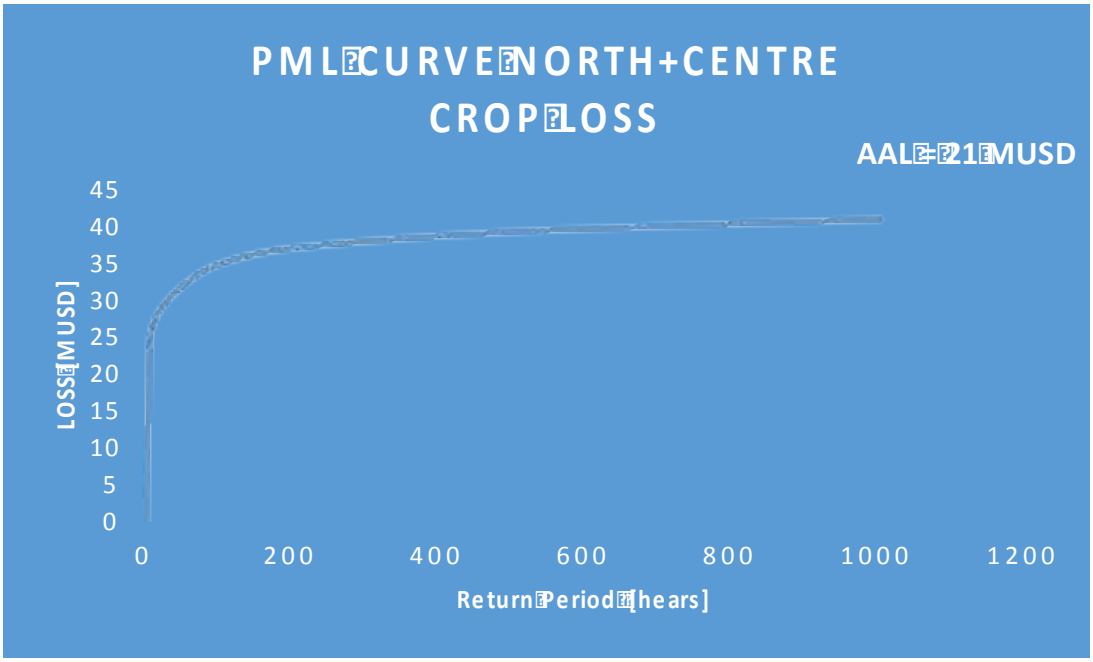

Figure 52 PML Curve for the losses of crops; the curve describes the losses to Agricultural crop by the fluvial flooding for an event of a specific return period expressed in years. The figure reports also the Average Annual Loss in MUSD for crops.

Table 7 Summary of losses for different quantiles for built-up areas and crops, Quantiles od population affected are also summarized.

LOSS BUILDINGS [M$]			
RP	North	Centre	North+Centre
5	**0.6**	**1.6**	**2.2**
10	**0.9**	**2.2**	**3.0**
20	**1.3**	**3.1**	**4.0**
50	**2.1**	**4.8**	**6.0**
100	**3.9**	**7.3**	**7.7**

200	**4.8**	**8.5**	**8.9**
500	**5.4**	**9.2**	**9.5**
1000	**5.6**	**9.3**	**9.9**
LOSS CROPS [M$]			
RP	North	Centre	North+Centre
5	**1.6**	**1.0**	**2.5**
10	**1.7**	**1.1**	**2.7**
20	**1.9**	**1.2**	**2.9**
50	**2.1**	**1.4**	**3.2**
100	**2.3**	**2.0**	**3.5**
200	**2.4**	**2.4**	**3.7**
500	**2.5**	**2.6**	**3.9**
1000	**2.7**	**2.6**	**4.1**
AFFECTED POPULATION			
RP	North	Centre	North+Centre
5	**30157**	**64764**	**89344**
10	**34813**	**73209**	**98203**
20	**35656**	**80811**	**106488**

50	**38454**	**94459**	**117372**
100	**43414**	**109924**	**131451**
200	**45531**	**119409**	**141890**
500	**46759**	**124359**	**151335**
1000	**47283**	**125590**	**155563**

Table 8 Summary of AAL and average values for different assets.

	Annual Average quantity
Affected GDP	0.6%
Affected Population	68500 people
Economic Loss (Built Up)	1.7 MUSD
Economic Loss (Crop)	21 MUSD
Roads	450 km
Railways	8 km
Schools	0
Hospitals	1

Table 9 Summary of AAL and quantiles losses for the Hotspots using the 2D detailed flood modelling.

2D MODEL				
KARONGA				
RP	Permanent	Semiperm.	Trad.	Population
AAL	**218424**	**114568**	**48051**	**5466**
2	**174395**	**62456**	**26294**	**875**
5	**267132**	**109328**	**43532**	**9305**
10	**413006**	**251538**	**102104**	**18170**
20	**633493**	**468254**	**196530**	**28099**
50	**1011742**	**834223**	**357806**	**36508**
100	**1342263**	**1133587**	**495314**	**40092**
200	**1699312**	**1438217**	**634354**	**42449**
500	**2196041**	**1835717**	**815912**	**45039**
1000	**2561783**	**2109558**	**941031**	**46732**
MANGOCHI				
RP	Permanent	Semiperm.	Trad.	Population
AAL	**9395**	**5645**	**2026**	**4850**
2	**0**	**0**	**0**	**0**
5	**3264**	**220**	**113**	**4110**
10	**12715**	**4715**	**118**	**9537**
20	**28761**	**19851**	**5708**	**11783**
50	**56542**	**45874**	**20174**	**14968**
100	**70372**	**57485**	**26021**	**16439**
200	**85440**	**72122**	**32827**	**17235**
500	**108517**	**93834**	**44417**	**18128**
1000	**122254**	**105991**	**52084**	**19477**
SALIMA				
RP	Permanent	Semiperm.	Trad.	Population
AAL	**496644**	**141816**	**66301**	**2429**
2	**419114**	**110068**	**49754**	**1072**
5	**715348**	**201031**	**93243**	**4788**
10	**1025794**	**328631**	**159654**	**7433**
20	**1349624**	**437339**	**214196**	**8256**
50	**1779401**	**549591**	**264224**	**8991**
100	**2038616**	**602671**	**285524**	**9432**
200	**2252509**	**645785**	**302532**	**9895**
500	**2471145**	**695284**	**323378**	**10492**

1000	**2601091**	**728805**	**338343**	**10903**

Table 10 Summary of AAL and quantiles losses for the Hotspots using the HAND flood modelling.

HAND COUNTOUR MAPPING				
KARONGA				
RP	Permanent	Semiperm.	Trad.	Population
AAL	**228509**	**134032**	**59047**	**2229**
2	**0**	**0**	**0**	**0**
5	**252807**	**181318**	**80627**	**3650**
10	**605018**	**362699**	**160801**	**4633**
20	**980913**	**481923**	**210233**	**5459**
50	**1454738**	**605161**	**259387**	**6419**
100	**1755919**	**683350**	**290465**	**6826**
200	**2019320**	**752868**	**318309**	**7281**
500	**2318893**	**836124**	**352046**	**7813**
1000	**2515472**	**893329**	**375595**	**8084**
MANGOCHI				
RP	Permanent	Semiperm.	Trad.	Population
AAL	**514**	**1583**	**685**	**483**
2	**0**	**0**	**0**	**0**
5	**235**	**0**	**0**	**639**
10	**950**	**386**	**59**	**1257**
20	**2290**	**1561**	**532**	**1761**
50	**5469**	**4461**	**2040**	**2336**
100	**9178**	**7742**	**3847**	**2768**
200	**14359**	**12288**	**6485**	**3155**
500	**23640**	**20270**	**10917**	**3705**
1000	**32902**	**27836**	**15318**	**4005**
SALIMA				
RP	Permanent	Semiperm.	Trad.	Population
AAL	**194930**	**71949**	**36470**	**1895**
2	**0**	**0**	**0**	**0**
5	**281815**	**109168**	**56036**	**3032**
10	**473710**	**169785**	**85115**	**4085**
20	**633394**	**216633**	**107352**	**5055**
50	**831668**	**275963**	**135639**	**6258**

100	**974000**	**318556**	**155797**	**7005**
200	**1115688**	**358837**	**174627**	**7723**
500	**1292907**	**408618**	**197537**	**8529**
1000	**1417548**	**444313**	**214315**	**8964**

A full probabilistic risk profile for Malawi has been carried out with respect to floods which are by far the most frequent hazard in the Country. The work concentrates among other things on differences obtained in hazard and risk assessment in three hotspots in the Country where two modelling approach have been applied. This with the scope of understanding how cost-beneficial it would be to invest in a more detailed DEM and modelling approach. Differences in Hazard can be important especially in areas with dense vegetation or dense urbanization where supervised post-processing of the DSM to obtain a high quality DTM delivers the highest impact. The difference in hazard reflects on the risk computations that show numbers that in some cases differ of an order of magnitude (Karonga, Mangochi), while in some other cases differences are definitely in the range of the process uncertainty (Salima). The changes in risk evaluations using both methods could justify the investment in densely populated areas where urbanization hampers the representativeness of the DEM and the full 2D modelling framework gives the biggest advantages. However, on large regions that are mainly rural the more detailed approach might not be the best option. A combined approach can be suggested as the most cost-beneficial option in the case of Malawi.

6 Dissemination of the Results in the RASOR Platform

RASOR is a web-based platform used to analyse risk. Users can examine hazard information, exposure information and vulnerability information, and simulate actual events to determine possible impacts, in terms of both direct damage and other impacts: cultural/social, environmental or systemic. Users also have access to historical records showing past events, which can be used to simulate the current impact of the same event or as a basis for new

simulations. It's the ability to change key parameters and quickly re-run simulations that enables RASOR users to model the specific impact of dedicated risk reduction measures. Previously run scenarios, as in the case of Malawi, can also be accessed in real time during an event to better estimate damage and plan response efforts. RASOR users can also work offline in QGIS to change information layers or use a RASOR mobile app to update exposure information or track the extent of a flood, and upload historical flood delineations. The mobile app was used in the Malawi workshop to map some exposed elements in a village south of Salima. The RASOR mobile app could also be used to track near real-time information during an event and can be shared with other users once uploaded to the platform.

All the results produced in the present project have been uploaded and can be consulted interactively using the RASOR platform as shown in the following figures.

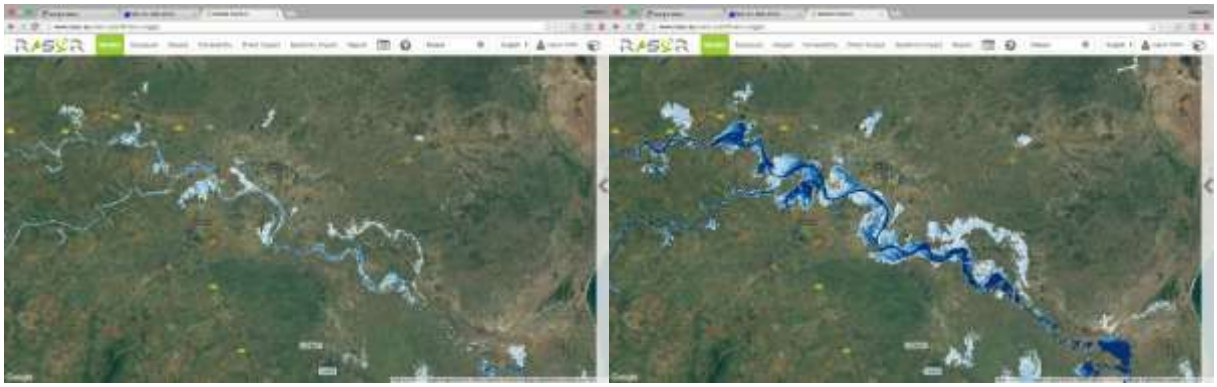

Figure 53 20 years and 500 years flood hazard maps visualized in the RASOR platform monitor section.

Figure 54 200 years flood hazard maps visualized in the RASOR platform monitor section: Detail.

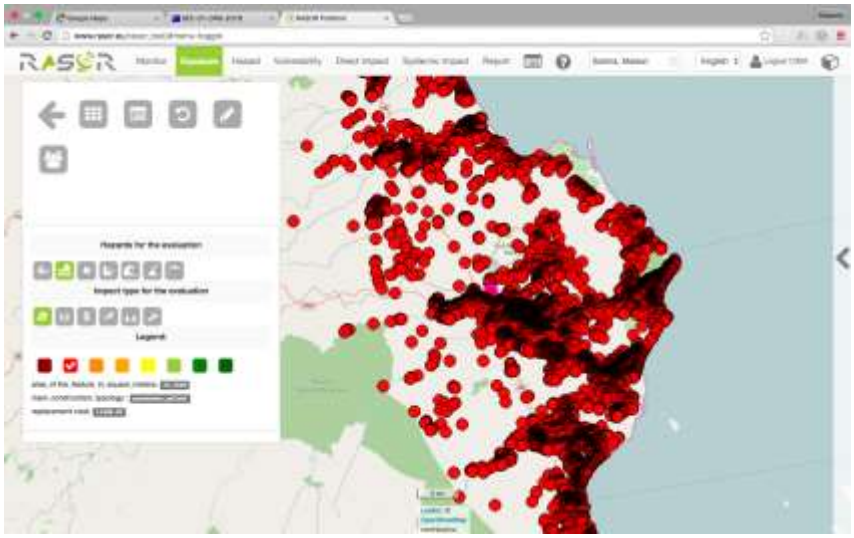

Figure 55 Built up exposure points visualized in the RASOR platform exposure section. Exposure details can be browsed and modified in this section.

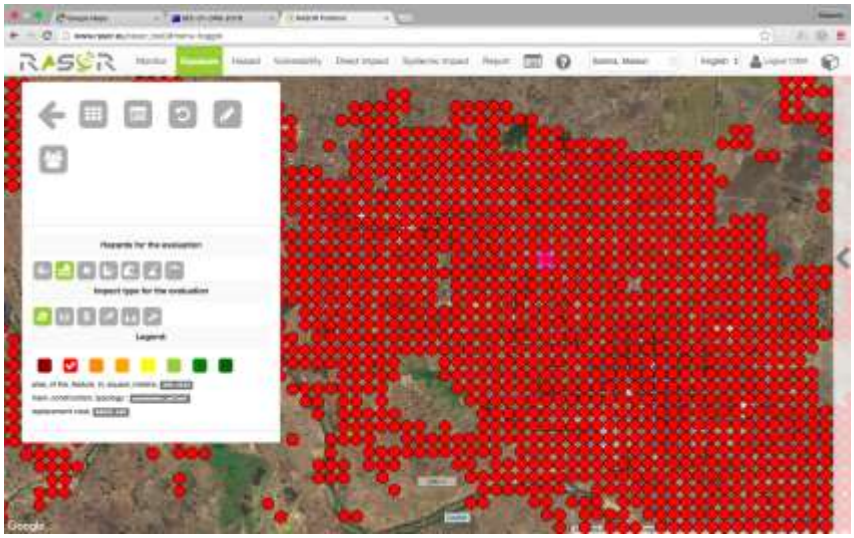

Figure 56 Built up exposure points visualized in the RASOR platform exposure section. Exposure details can be browsed and modified in this section: Detail over Salima.

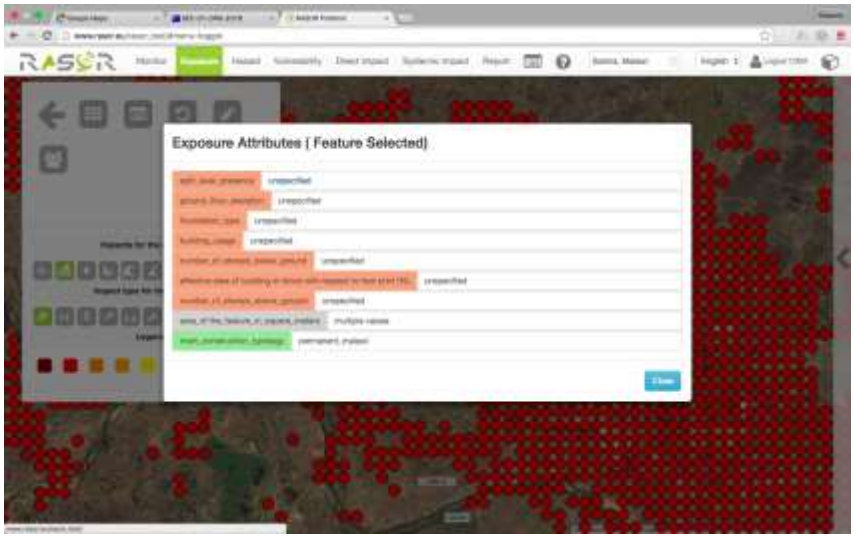

Figure 57 Built up exposure points visualized in the RASOR platform exposure section. Exposure details can be browsed and modified in this section: Exposure modification dialogue window..

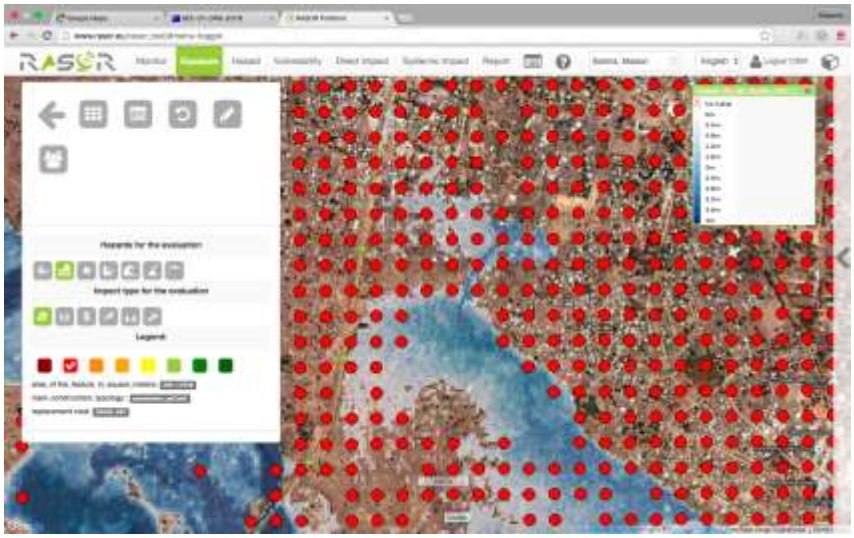

Figure 58 Built up exposure points visualized in the RASOR platform exposure section. Exposure details can be browsed and modified in this section: Characterization of the exposure points and flood overlay..

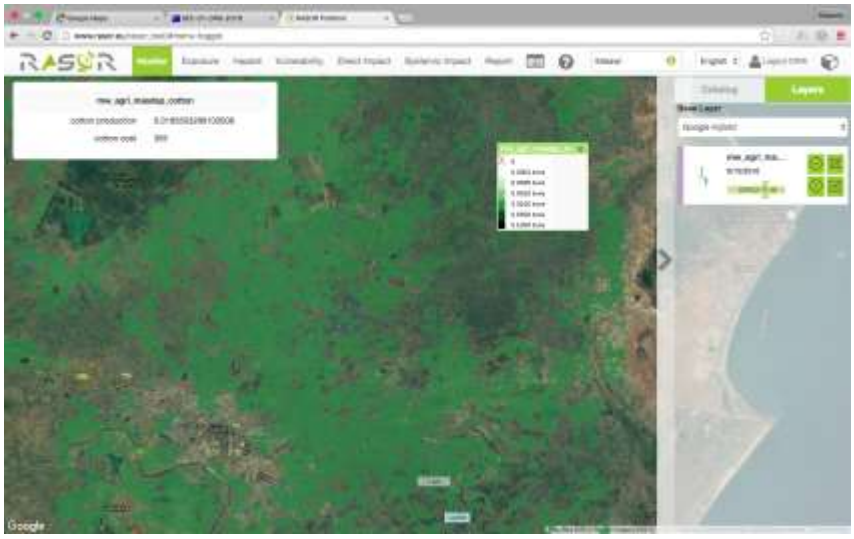

Figure 59 agricultural exposure cells visualized in the RASOR platform monitor section. Each grid cell has an estimation of the production and of the unit cost of the different cultivations.

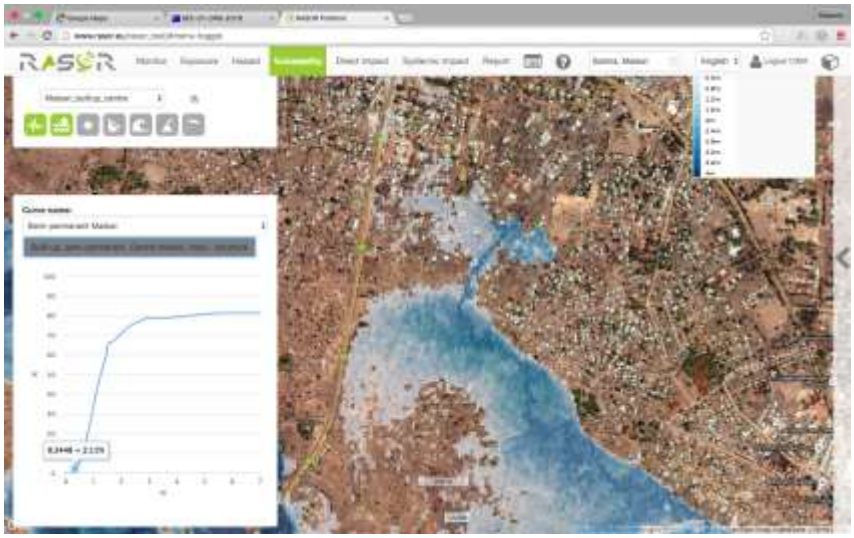

Figure 60 vulnerability curves visualized in the RASOR platform vulnerability section. Vulnerability curves can be browsed and modified in this section: semi-permanent house typology.

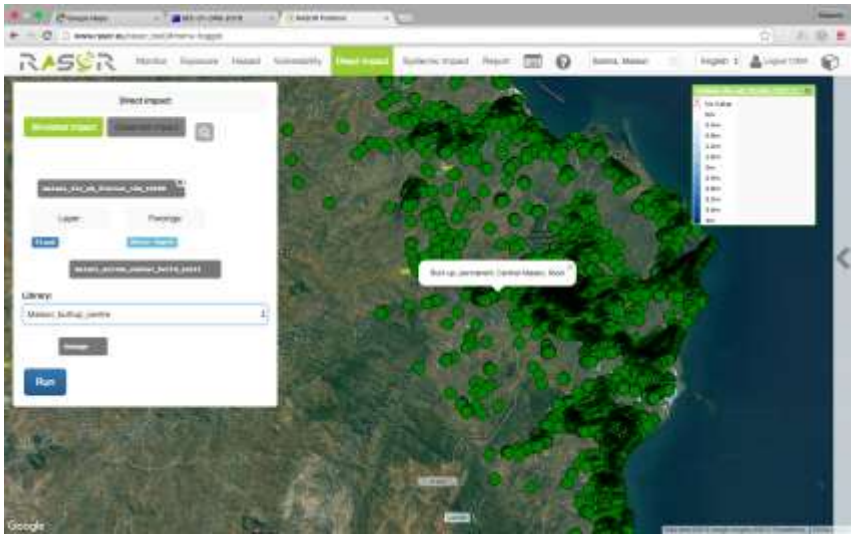

Figure 61 Direct impact can be computed within the RASOR platform in the direct impact section, exposure and forcing are connected through the available chosen vulnerability library in a dynamic way

7 Data standards, metadata and licensing

We provided all tabulated data in a CSV format. Geospatial raster data have been delivered in GeoTIFF files in EPSG:4326 WGS84 lat-lon projection. Geospatial shape data have been delivered in Shape format.

For tables and vectorized data a description of the columns or attributes have been provided. We have been using ISO metadata standards commonly used by World Bank projects as per the ToR.

For licensing, we used the following license conditions:

- Unmodified datasets and publications used as part of this effort have been attributed to the original authors of the work.
- New intellectual property published jointly by GFDRR and our consortium will have authorships determined by all contributing parties and are made available to third parties subject to the Creative Commons Attribution 3.0 License (CC-BY).

8 References

Dunne, T. and L.B. Leopold. 1978. Water in Environmental Planning. W.H. Freeman and Company, New York.

You, L., U. Wood-Sichra, S. Fritz, Z. Guo, L. See, and J. Koo. 2014. Spatial Production Allocation Model (SPAM) 2005 v2.0. April 29, 2015. Available from http://mapspam.info

Herold, C. and Rudari R., Improvement of the Global Flood Model for the GAR 2013 and 2015. Geneva, Switzerland: UNISDR, Back Ground paper for the Global Risk Assessment, http://www.preventionweb.net/english/hyogo/gar/2013/en/home/documents.html, 2013

Kernkamp, H. W. J., Dam, A., Stelling, G. S. & Goede, E. D. (2011). Efficient scheme for the shallow water equations on unstructured grids with application to the Continental Shelf. Ocean Dynamics, 61(8), 1175–1188. doi:10.1007/s10236-011-0423-6

Melchers, R.E., 1999. Structural reliability analysis and prediction. 2nd ed. Chichester: John Wiley & Sons, 437 pp.

Ngongondo, C., Chong-Yu, X., Tallaksen, L.M., Alemaw, B. (2015), Observed and simulated changes in the water balance components over Malawi, during 1971-2000. Quaternary International 369, 7-16. http://dx.doi.org/10.1016/j.quaint.2014.06.028

Nobre, A.D., Cuartas, L.A., Hodnett, M., Rennó, C.D., Rodrigues, G., Silveira, A., Waterloo, M., Saleska S. (2011), Height above the Nearest Drainage, a hydrologically relevant new terrain model, J. of Hydrol., doi: 10.1016/j.jhydrol.2011.03.051

Rudari, R., Silvestro F., Campo L., Rebora N., Boni G., Improvement of the global flood model for the GAR 2015, Back Ground paper for the Global Risk Assessment, http://www.preventionweb.net/english/hyogo/gar/2015/en/home/documents.html, 2015

Silvestro, F, Gabellani S., Delogu F., Rudari R., and Boni G., Exploiting remote sensing land surface temperature in distributed hydrological modelling: the example of the Continuum model, Hydrol. Earth Syst. Sci., 17, 39-62, doi:10.5194/hess-17-39-2013, 2013

Silvestro, F., Gabellani, S., Rudari, R., Delogu, F., Laiolo, P., and Boni, G., Uncertainty reduction and parameter estimation of a distributed hydrological model with ground and remote-sensing data, Hydrol. Earth Syst. Sci., 19, 1727-1751, doi:10.5194/hess-19-1727-2015. http://www.hydrol-earth-syst-sci.net/19/1727/2015/hess-19-1727-2015.htm, 2015

Veldkamp, T. I. E., Wada, Y., de Moel, H., Kummu, M., Eisner, S., Aerts, J. C. J. H. and Ward, P. J.: Changing mechanism of global water scarcity events: Impacts of socioeconomic changes and inter-annual hydro-climatic variability, Glob. Environ. Chang., 32, 18–29, doi:10.1016/j.gloenvcha.2015.02.011, 2015.

Verwey, A., Kernkamp, H. W. J., Stelling, G. S., Tse, M. L. & Leung, W. C. (2011). Potential And Application Of Hydrodynamic Modelling On Unstructured Grids. In Proceedings of the Sixth International Conference on Asian and Pacific Coasts (APAC 2011) (pp. 1–8).

Ward, P. J., Jongman, B., Weiland, F. S., Bouwman, A., van Beek, R., Bierkens, M. F. P., Ligtvoet, W. and Winsemius, H. C.: Assessing flood risk at the global scale: model setup,

results, and sensitivity, Environ. Res. Lett., 8(4), 044019, doi:10.1088/1748-9326/8/4/044019, 2013.

Winsemius, H. C., Aerts, J. C. J. H., Van Beek, L. P. H., Bierkens, M. F. P., Bouwman, A., Jongman, B., Kwadijk, J. C. J., Ligtvoet, W., Lucas, P. L., Van Vuuren, D. P. and Ward, P. J.: Global Drivers of Future River Flood Risk, Nat. Clim. Chang., Under revi, 2015.

Winsemius, H. C., Van Beek, L. P. H., Jongman, B., Ward, P. J. and Bouwman, A.: A framework for global river flood risk assessments, Hydrol. Earth Syst. Sci., 17(5), 1871–1892, doi:10.5194/hess-17-1871-2013, 2013.

ANNEX 1: Example of information contained in the file header of the agricultural production layer

```
Files: malawi_agri_rice_production30m.tif

Size is 12299, 29346

Coordinate System is:

PROJCS["WGS 84 / UTM zone 36S",

    GEOGCS["WGS 84",

        DATUM["WGS_1984",

            SPHEROID["WGS 84",6378137,298.257223563,

                AUTHORITY["EPSG","7030"]],

            AUTHORITY["EPSG","6326"]],

        PRIMEM["Greenwich",0],

        UNIT["degree",0.0174532925199433],

        AUTHORITY["EPSG","4326"]],

    PROJECTION["Transverse_Mercator"],

    PARAMETER["latitude_of_origin",0],

    PARAMETER["central_meridian",33],

    PARAMETER["scale_factor",0.9996],

    PARAMETER["false_easting",500000],
```

```
    PARAMETER["false_northing",10000000],
    UNIT["metre",1,
        AUTHORITY["EPSG","9001"]],
    AUTHORITY["EPSG","32736"]]
Origin = (454995.000000000000000,8974765.000000000000000)
Pixel Size = (30.000000000000000,-30.000000000000000)
Metadata:
  AREA_OR_POINT=Area
  Crop_type=rice
Image Structure Metadata:
  COMPRESSION=DEFLATE
  INTERLEAVE=PIXEL
Corner Coordinates:
Upper Left    (   454995.000,  8974765.000)  (  32d35'24.84"E,
9d16'28.48"S)
Lower Left    (  454995.000, 8094385.000) ( 32d34'35.99"E, 17d14'
6.44"S)
Upper Right   (   823965.000,  8974765.000)  (  35d56'54.08"E,
9d15'45.61"S)
Lower Right   (   823965.000,  8094385.000)  (  36d  2'44.92"E,
```

17d12'45.07"S)

Center (639480.000, 8534575.000) (34d17'14.79"E, 13d15'9.22"S)

Band 1 Block=12299x1 Type=Float32, ColorInterp=Gray

Min=0.000 Max=0.508

Minimum=0.000, Maximum=0.508, Mean=0.000, StdDev=0.002

Metadata:

STATISTICS_MAXIMUM=0.50805914402008

STATISTICS_MEAN=0.00015098891077448

STATISTICS_MINIMUM=0

STATISTICS_STDDEV=0.0021539232894011

unit=tons

Band 2 Block=12299x1 Type=Float32, ColorInterp=Undefined

Min=0.000 Max=144.000

Minimum=0.000, Maximum=144.000, Mean=15.240, StdDev=44.297

Metadata:

STATISTICS_MAXIMUM=144

STATISTICS_MEAN=15.239673484515

STATISTICS_MINIMUM=0

STATISTICS_STDDEV=44.297464192158

```
unit=USD/tons
```

ANNEX 2 Northern Malawi Flood Workshop Report Salima, 20-22 July, 2016

A consortium of companies led by CIMA Research Foundation and including Deltares and Athena Global completed a study on flood modeling in the northern and central regions of Malawi. The study objectives were:

- **Inform flood DRM planning, preparedness and investment decisions** in Northern Regions/Lake Malawi through improved availability of risk information
- Apply TanDEM-X **12m** Digital Elevation Model over project area to develop a **comprehensive flood modeling framework** visualized in the RASOR risk assessment tool to generate potential impact:
    - Population affected (number of people);
    - Physical property damage for government assets, ($US or other metric e.g., number of structures)
    - Agricultural crop and livestock losses, ($US or other metric e.g., area and type of asset affected)
    - Estimate reliable return periods for both **fluvial** (baseline) and **pluvial** (if possible) **flooding**

The study results include comprehensive flood hazard maps at return periods ranging from 5 to 1000 years, for north and central Malawi, including both fluvial and pluvial flooding.

The consortium came to Malawi to present results of this study and build capacity through training on the RASOR platform and RASOR mobile app, in order to increase the ability of local users to access and effectively use study results.

The workshop included representation from a range of different national organizations and representation from the three districts where the report included hotspot analysis: Karonga, Salima, and Mangochi. In all, approximately 20 participants joined the event. The day before the workshop, a meeting of national organizations was convened to review the objectives of the event and the presentation materials. The detailed list of participants includes:

1. Frederick Kapute – Water Department - dwomangochi@gmail.com
2. Peter Kadewere – Water Resources Department - kadewere@yahoo.co.uk
3. Lucy Mtilatila – Climate Change and Met Services – lucyngombe@yahoo.com
4. Walusunga Mwafulima – Disaster Office - walusungu.mwafulirwa@gmail.com
5. Victor Phiri– Met for Karonga – phirivictor62@gmail.com
6. Aaron Chaponda – Water Development – Salima – am.chaponda@yahoo.com
7. Waki Chungwa – Water Development – wchungwa@gmail.com
8. Blessings Kantema– Dodma – Salima- bblssins@gmail.com
9. Lasteen Kalumbo – Met – kalambo.lasteen@gmail.com
10. Newton Chirambo – Met – maheberichirambo@yahoo.com

11. Carlo Chabwiga - Disaster risk management– carlolync@gmail.com
12. Chikondi Mbemba – Water Resources Department - chikondimbemba@gmail.com
13. Tanazio Kwenda – Surveys – tanaziokwenda@gmail.com
14. Gumbi Gumbi – Surveys – gumbiwagumbi@gmail.com
15. Silence Chirwa Surveys – chirwasilence@gmail.com
16. Marcef Kaunda – Dept. of Water Resources - marckaunda@outlook.com
17. Francis Nkoka – GFDRR/World Bank
18. Emma Phillips – GFDRR
19. Roberto Rudari – CIMA Foundation/RASOR
20. Andrew Eddy – Athena Global/RASOR

The workshop began with welcoming remarks from the DRM expert from the district of Salima, Blessings Kantema. Workshop convener Emma Phillips, GFDRR DRM expert, presented the objectives for the two-day event, which were to share the results of the study and build capacity at the national and district level to support use of the results for future risk reduction work.

The first part of the workshop was dedicated to presenting the results of the study, including detailed explanations of study methodology and work undertaken to obtain the results. This was divided into three sections: hazard, exposure, and vulnerability. A final section was dedicated to the purposes of such information, including its use for calculating Annual Average Loss (AAL) and Possible Maximum Loss (PML).

Under the Hazard component, participants were shown how the consortium calculated both fluvial and pluvial return periods based on modeled results, and this for both short and long return periods. These hazard layers can be used s a reference as a stand alone layer, or can be merged with exposure layers to calculate impact.

Exposure layers were also developed using a statistical approach to redistribute population based on a 100 m grid across urban and rural areas. Separate data were used to calculate

exposure in terms of agricultural crops, to estimate damages by area in relation to affected crops. This methodology is statistical rather than empirical, but can be validated in the field through observed damages.

Vulnerability is calculated using a dedicated library of vulnerability values that were developed in the project specifically for Malawi. One example of modifications made for the library was the small riser used in traditional Malawi housing in flood prone areas, raising the level of the house by 30 to 50 cm. This architectural specificity results in significantly reduced flooding from ponding and minor fluvial flooding.

Finally, the participants were shown how these results can be integrated into planning by calculating the Average Annual Loss (AAL) and Possible Maximum Loss (PML). AAL is the amount of loss per year averaged out over the complete return period. The PML is the largest loss that might occur at any point in the considered period. Understanding these two notions and how they work together is important for planning risk reduction expenditure.

Day two, participants downloaded the RASOR mobile app and went into the field to characterize buildings in a flood zone so that they could be used in an exposure layer that helps calculate possible impacts of flooding, using the hazard maps developed in the study. In the afternoon, participants we shown the RASOR (Rapid Analysis and Spatialisation of Risk) Platform, a free and open tool developed by a CIMA-led consortium to better analyze risk and support risk reduction decisions.

The field exercise using the RASOR app began with a visit to a zone prone to flooding according to the hazard maps and local knowledge. The zone was selected by the Salima DRM expert, Surveys, and the RASOR team. Participants travelled to the zone and the mobile app was explained to everyone. People formed groups and went out to map various buildings in the centre of the village. The results were taken back to the meeting room and uploaded to the

RASOR platform, where damage impact was calculated using the hazard maps and a newly-generated exposure layer.

Back in the conference centre, participants were shown other scenarios within RASOR, and were given an opportunity to ask questions about how the platform worked. Explanations of how to use the platform in conjunction with InaSAFE for offline functionality (or QGIS), and with the mobile app were given.

At the end of the workshop, participants provided feedback on the results, the RASOR tool and mobile app as possible means of accessing and using these results, and the way forward.

Questions & Answers

1. Can you use the model for early warning purposes?

Yes, it is possible but need additional work, which are mainly operational in nature. The model for hazard can be used for early warning purposes. What is difficult is adding the real time information (forecasting) and management of that data.

2. Can you access the data as shape files?

Hazard maps are available in the raster GeoTiff format. Exposure data are available in shape files. All files available on the web and freely accessible. To download the files on RASOR all you need is a user name and password.

3. Are there any hazard maps for landslides?

This project focuses on pluvial and fluvial hazard. However, this is a multi-hazard framework and the platform can be used for other perils if you have the data and upload it.

REQUEST: study on earthquake and landslide analysis for Malawi.

This have been covered by the European Union - Africa, Caribbean and Pacific (EU ACP) Africa Disaster Risk Financing Program, implemented by GFDRR and the World Bank, which is in the pipeline for Malawi.

4. Has the model taken into account future changes in the environment that could trigger the extent of the flooding? There is environmental degradation in Karonga.

The scenarios of this study provide a full spectrum of what happens in the future based on the current scenario. But this relates to present climate, and doesn't take into account changes in climate. This is a starting point for planning. This information needs to be constantly updated.

This can be done on the exposure level – i.e. through community mapping can update the changes in the assets in an area.

In the next iteration of work for Malawi, we will be providing future climate scenarios.

5. Can you use the tool as a quick assessment of the impact of floods? How often is EU Watch updated? Did you validate the Hand Contour and Hydrological mapping – compared to the actual situation on the ground?

Yes you can use the framework, but EU Watch data are not updated fast enough to do a quick assessment of the impacts of flood. But what you can do is upload flood delineation maps from satellite, if available, and upload to the RASOR tool and do a quick assessment of population affected, etc. or compare the flood extend to one of the historical or statistical scenarios developed and select the one that is more similar and do the economic evaluation. Some satellite validation was performed in the project, but not on a quantatative basis. Through earth observation flood delineation maps we did a quick validation of the products, but additional information coming from the districts including for example field surveys of flooded areas or information coming from PDNA's can be used for further validation. In particular, for the crop work, if drought input data is shared, we can better validate.

6. Has this study taken into account rising moisture in Mzuzu where houses collapsed because of the water table collapse for vulnerability?

The study did not study groundwater flooding, as it was outside the scope of the terms of reference. This type of flooding is difficult to estimate. It is not fluvial or pluvial – it is ground water flooding that is caused by rising water tables and it behaves very differently in different soil types. It is essentially a local phenomenon and varies a lot from village to village. We should look at this not only for vulnerability, but also for the hazard maps. Coastal (along the lake) and ground water flooding would both be important for the Malawi context. This was outside the scope of the first study, but could be done.

Comments on Exposure Data:

· Gumbi mentioned the need to use the national statistics office (NSO) data. There is a census in Malawi next year. The idea would be to link the district shape files using data from the census and also use world pop raster file. This should be discussed further by the team.

· Gumbi suggested looking at the pattern of the settlements in Malawi by using pattern recognition for the disaggregation of the exposure dataset. Rural settlements have a distinct pattern in Malawi. The model can be improved by the exposure disaggregation by using pattern recognition algorithms. The team will look into this.

Annex A Fluvial flood maps Karonga

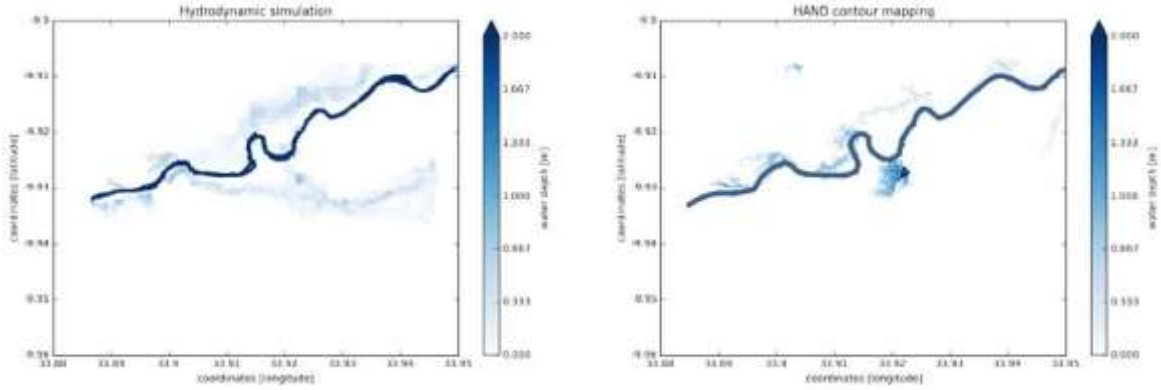

Figure A.1: Karonga flood maps for 5 yr return period. 2D hydraulic model (left) vs HAND contour mapping (right).

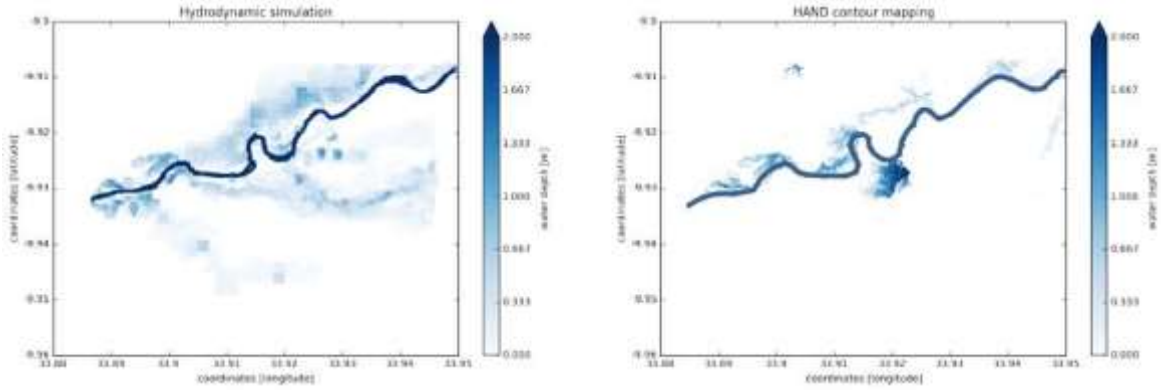

Figure A.2: Karonga flood maps for 10 yr return period. 2D hydraulic model (left) vs HAND contour mapping (right).

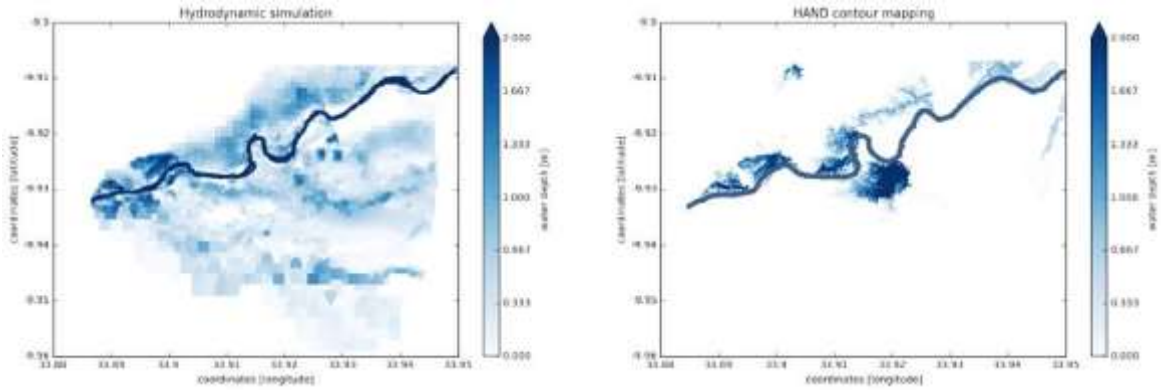

Figure A.3: Karonga flood maps for 100 yr return period. 2D hydraulic model (left) vs HAND contour mapping (right).

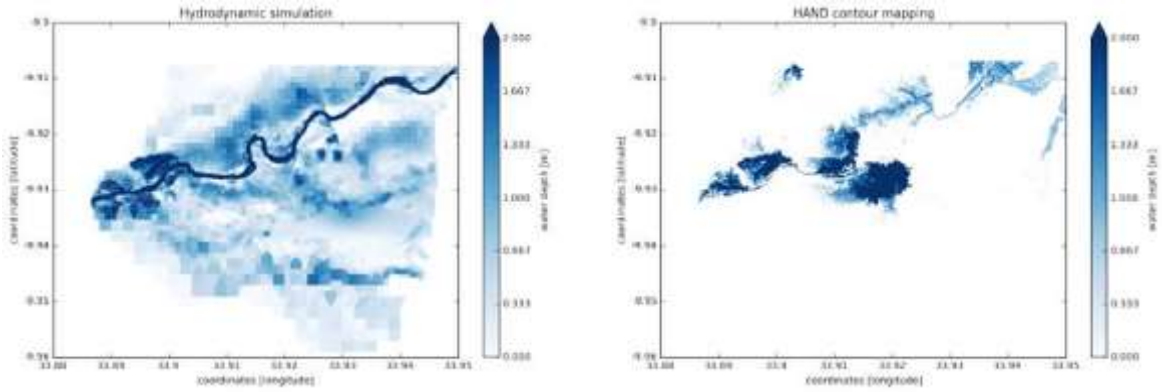

Figure A.4: Karonga flood maps for 1000 yr return period. 2D hydraulic model (left) vs HAND contour mapping (right).

Annex B Fluvial flood maps Salima

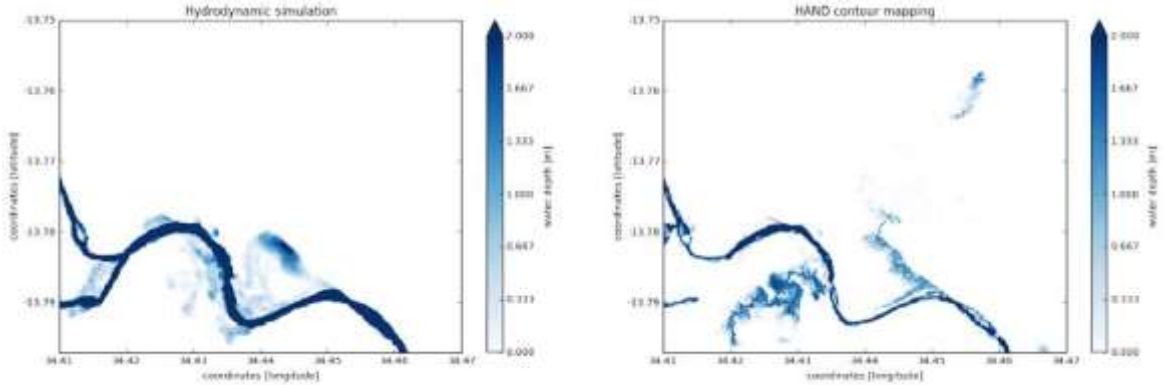

Figure B.1: Salima flood maps for 5 yr return period. 2D hydraulic model (left) vs HAND contour mapping (right).

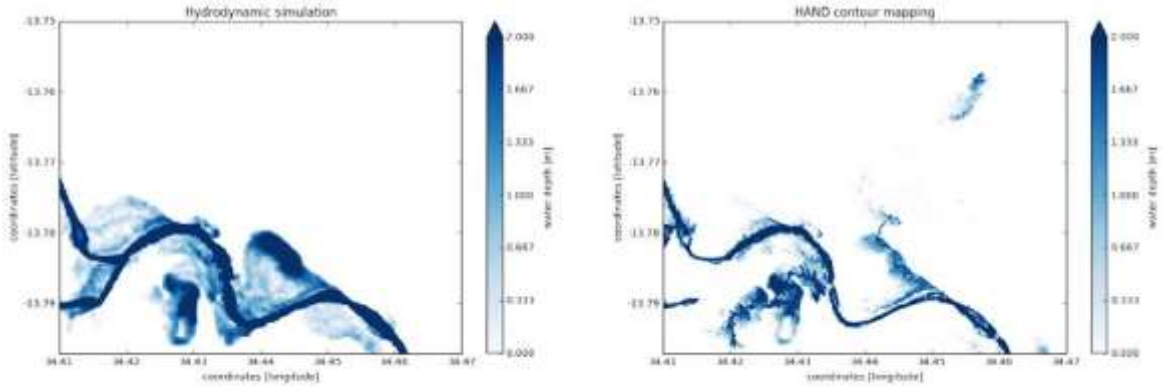

Figure B.2: Salima flood maps for 10 yr return period. 2D hydraulic model (left) vs HAND contour mapping (right).

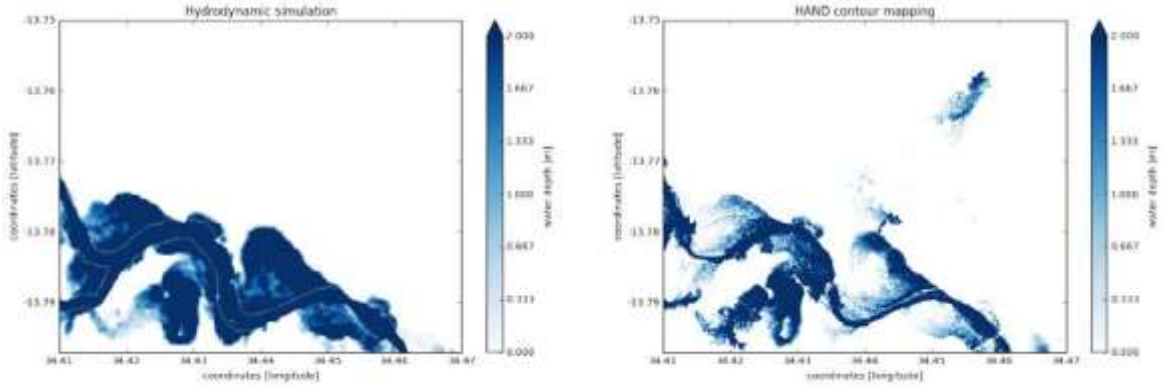

Figure B.3: Salima flood maps for 100 yr return period. 2D hydraulic model (left) vs HAND contour mapping (right).

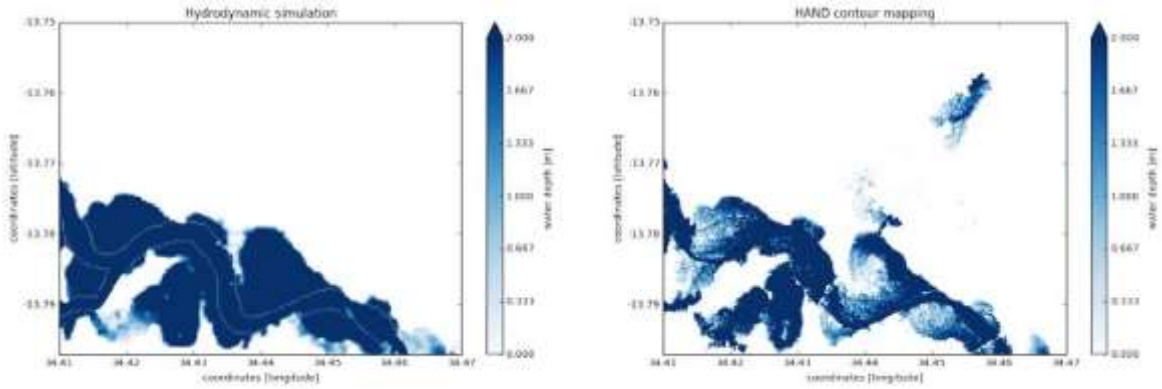

Figure B.4: Salima flood maps for 1000 yr return period. 2D hydraulic model (left) vs HAND contour mapping (right).

Annex C Pluvial flood maps Mangochi

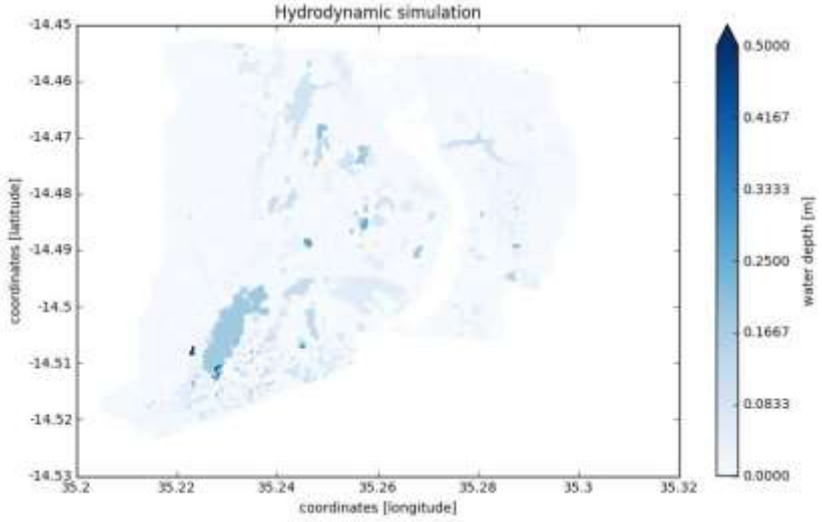

Figure C.1: Mangochi flood map for 5 yr return period, from 2D hydraulic model.

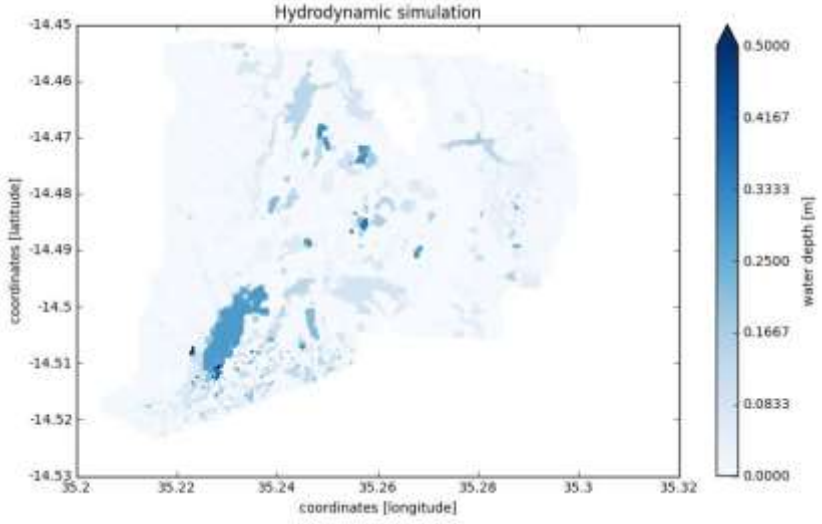

Figure C.2: Mangochi flood map for 10 yr return period, from 2D hydraulic model.

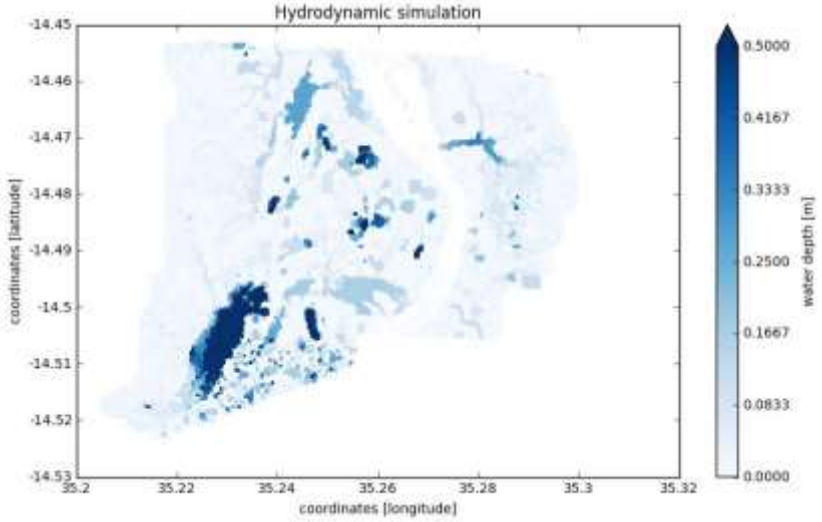

Figure C.3: Mangochi flood map for 100 yr return period, from 2D hydraulic model.

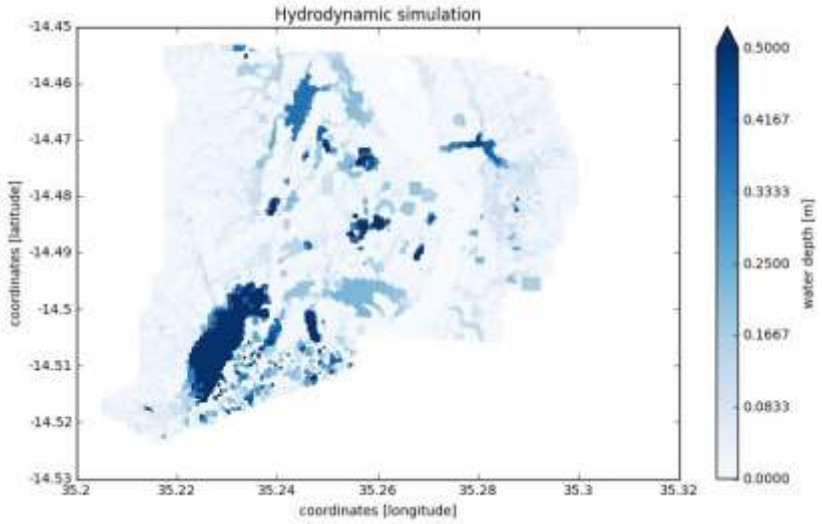

Figure C.4: Mangochi flood map for 1000 yr return period, from 2D hydraulic model.

Annex D Where do I find the data?

All deliverables of the project have been shared with GFDRR trough a Box folder at the address https://app.box.com/files/0/f/6083249142/Malawi. An access to the deliverables folder can be granted by GFDRR upon request.

In addition, all geographical layers produced have been put on the RASOR Geonode (http://www.rasor.eu/catalog) and can be consulted and downloaded. A user an passwords can be requested to access the catalog and the platform at the address http://www.rasor-project.eu/rasor-platform/ .

All layers can be consulted and used to produce additional risk information using the RASOR Platform (www.rasor.eu).

For guidance on how to use the platform please consult the wiki manual here: http://www.rasor.eu/wiki/index.php/Main_Page.

Some of the data have been already transferred into the local Malawi Geonode installation and can be found at http://www.masdap.mw.